Uncloaking globular clusters in the inner Galaxy[1]

Javier Alonso-García

Departamento de Astronomía y Astrofísica, Pontificia Universidad Católica de Chile, 782-0436 Macul, Santiago, Chile

Department of Astronomy, University of Michigan, Ann Arbor, MI 48109-1090

jalonso@astro.puc.cl

Mario Mateo

Department of Astronomy, University of Michigan, Ann Arbor, MI 48109-1090

mmateo@umich.edu

Bodhisattva Sen

Department of Statistics, Columbia University, New York, NY 10027

bodhi@stat.columbia.edu

Moulinath Banerjee

Department of Statistics, University of Michigan, Ann Arbor, MI 48109-1107

moulib@umich.edu

Márcio Catelan

Departamento de Astronomía y Astrofísica, Pontificia Universidad Católica de Chile, 782-0436 Macul, Santiago, Chile

Dante Minniti

Departamento de Astronomía y Astrofísica, Pontificia Universidad Católica de Chile, 782-0436 Macul, Santiago, Chile

Kaspar von Braun

NASA Exoplanet Science Institute, California Institute of Technology, Pasadena, CA 91125-2200

kaspar@caltech.edu

Received _____; accepted _____

ABSTRACT

Extensive photometric studies of the globular clusters located towards the center of the Milky Way have been historically neglected. The presence of patchy differential reddening in front of these clusters has proven to be a significant obstacle to their detailed study. We present here a well-defined and reasonably homogeneous photometric database for 25 of the brightest Galactic globular clusters located in the direction of the inner Galaxy. These data were obtained in the B, V, and I bands using the Magellan 6.5m telescope and the *Hubble Space Telescope*. A new technique is extensively used in this paper to map the differential reddening in the individual cluster fields, and to produce cleaner, dereddened color-magnitude diagrams for all the clusters in the database. Subsequent papers will detail the astrophysical analysis of the cluster populations, and the properties of the obscuring material along the clusters' lines of sight.

Subject headings: Globular clusters: general – catalogs – Galaxy: bulge – Galaxy: evolution – HertzsprungRussell (HR) diagram – Globular Clusters: individual (NGC 6121 - M 4, NGC 6144, NGC 6218 - M 12, NGC 6235, NGC 6254 - M 10, NGC 6266 - M 62, NGC 6273 - M 19, NGC 6287, NGC 6304, NGC 6333 - M 9, NGC 6342, NGC 6352, NGC 6355, NGC 6397, NGC 6522, NGC 6541, NGC 6553, NGC 6558, NGC 6624, NGC 6626 - M 28, NGC 6637 - M 69, NGC 6642, NGC 6656 - M 22, NGC 6681 - M 70, NGC 6809 - M 55)

1. Introduction

The globular cluster system of the Milky Way has long been used to learn about the evolution of the Galaxy. As the Galactic globular clusters (GGCs) constitute some of the oldest systems in the Milky Way, the study of the stellar populations of these *fossils* can give us important clues of the early stages of the Galaxy's formation. The tool most extensively used in this task has been the analysis of the color-magnitude diagrams (CMDs) (de Angeli et al. 2005; Marín-Franch et al. 2009). However, the presence of significant differential extinction in low-latitude fields, particularly near the Galactic center, greatly complicates traditional CMD analyses. As a result, the study of many GGCs located towards the inner Galaxy has been historically neglected.

Various recent studies have tried to overcome the difficulties associated with the study of inner GGCs to better exploit them as probes of the stellar populations near the Galactic Center. One obvious approach is to use near-infrared photometry to study these clusters (e.g.,Davidge (2000); Valenti et al. (2007)) to take advantage of the smaller extinction in these bands. But to extract precise information about the ages of the GGCs, an accurate location of the main sequence turn-off (MSTO) point is crucial in most methods of cluster dating (Stetson et al. 1996; Sarajedini et al. 1997; Gratton et al. 2003). Infrared photometry sufficiently deep to reach the main sequence (MS) with enough precision to accurately locate the turn-off (TO) point is difficult to achieve, and only now are we starting to see the first results after the careful application of new adaptive optics techniques on big

---

[1]Based partly on observations with the NASA/ESA *Hubble Space Telescope*, obtained at the Space Telescope Science Institute, which is operated by the Association of Universities for Research in Astronomy, Inc., under NASA contract NAS 5-26555. This paper also includes data gathered with the 6.5 meter Magellan Telescopes located at Las Campanas Observatory, Chile.

telescopes (Moretti et al. 2009). Deep photometry for non-highly reddened GGCs is much more easily obtained in the optical, but at the cost of increased extinction. A number of techniques have been developed to produce extinction maps for individual clusters as a means of dealing with this issue (e.g., Melbourne & Guhathakurta (2004); von Braun & Mateo (2001)). In general, the resolution and accuracy of optical extinction maps are not adequate to fully eliminate the effects of differential reddening at a level of precision to produce deep optical CMDs of similar high quality now typical for high-latitude clusters with little or no differential extinction (e.g.,Rosenberg et al. (2000a); Piotto et al. (2002)).

In this paper we present a new optical photometric database consisting of a sample of 25 GGCs located towards the Galactic Center. We use a new dereddening technique (Alonso-García et al. (2011), from now on referred to as Paper I) to map the differential extinction along their fields, and produce new, cleaner, differentially dereddened CMDs of the clusters. In section 2, we give the criteria used to define our sample of GGCs. Section 3 summarizes the steps that we followed to obtain precise astrometry and optical photometry of the stars in these clusters suitable for our analyses. In section 4 we apply the dereddening technique described in Paper I, and provide an overview of the differentially dereddened CMDs of the clusters in our sample, along with extinction maps along their fields. We also describe the characteristic features of the environments in which they are located, and briefly summarize previous optical and infrared photometric studies where appropriate. Finally, in section 5, we provide a summary of our results.

2. Selection of our sample members

The cluster sample presented in this study consists of 25 GGCs in the direction of the inner Galaxy, all located within 30 deg of the Galactic Center. Because the precision of our dereddening technique (Paper I) requires good sampling and photometry down to a

few magnitudes below the MSTO, and also depends on the density of stars and the spatial variations in the extinction, the clusters in our sample were chosen to also satisfy the following criteria:

- Exhibit moderate mean extinction, implying that they may suffer from extinction variations. We explicitly restricted our sample to clusters with a mean reddening of $E(B-V) \geq 0.07$ mag.

- Be sufficiently luminous to possess a well-defined MS. Our analysis requires a significant number of stars (at least a few hundreds) to calculate the extinction in a region. We therefore chose clusters with a luminosity satisfying $M_{\rm V} \leq -6$.

- Be relatively nearby. With our dereddening technique, the stars that provide most of the information about the differential extinction are those located in the CMD sequences most nearly orthogonal to the reddening vector (subgiant branch (SGB) and upper MS). Since one of the goals of this project is to accurately calculate the relative ages of these clusters, we must also reach the MS with good photometric precision at the TO in order to carry out a reliable age/metallicity analysis. Hence, we chose clusters with an apparent distance modulus of $(m-M)_{\rm V} \leq 16.6$.

- Be sufficiently extended so that we can define maps that cover a significant solid angle around the clusters. We therefore chose clusters with a tidal radius $r_t \geq 7.5$ arcmin.

We were able to observe 25 of the 31 GGCs that fulfill these requirements, according to the 2003 version of the Harris (1996) catalog. Their positions are shown in Figure 1 along with the rest of the clusters located in the inner Galaxy. Their characteristics, according to

the most recent (December 2010) version[2] of the Harris catalog, are given in Table 1.

3. Observations and data reduction

We obtained optical photometric data for our sample of GGCs using the Magellan 6.5m Baade Telescope located at the Las Campanas Observatory (LCO) in Chile, and the *Hubble Space Telescope* (*HST*). In this section we provide a complete summary of these observations and explain in detail the steps followed for the reduction and calibration of the data. The final photometry has an absolute precision with respect to the calibrating stars of $\sigma \sim 0.02 - 0.03$ magnitudes in most cases. The internal precision among the stars observed in each field is around $\sigma \sim 0.01 - 0.02$ magnitudes, sufficient to achieve the precise extinction maps that will allow us to produce clean CMDs. From these we will aim to derive the cluster parameters with an accuracy similar to those derived from high-Galactic latitude clusters CMDs that suffer little or no differential extinction.

3.1. Observations

The GGCs in our sample were observed over four nights, May, 30th to June, 2nd 2005, with the LCO 6.5 m Magellan Baade Telescope, using the Inamori Magellan Areal Camera and Spectrograph (IMACS) in imaging mode. We used the f/4 camera to image a

[2]According to this updated version of the catalog, two of the clusters in our sample, NGC 6287 and NGC 6355, do not fulfill anymore the apparent distance modulus requirement to belong to our sample. However, we have still kept these clusters in our studied sample, since previous studies of these objects have been very scarce, and their published parameters are accordingly quite uncertain.

field of view (FOV) of $15.46' \times 15.46'$, with a pixel size of $0.11''$. All fields were observed using standard Johnson-Cousins B,V, and I filters (Bessell 1979). Two sets of observations with different exposure times (short and long) were taken in the B and V filters, and three (extra-short, short, and long) in I, for every cluster. Although the nights during our observing run were not all completely photometric, the seeing conditions were very good, with average values of $\sim 0.6''$ in V for the whole run. Table 2 lists the details of these ground-based photometry observations.

In order to obtain useful photometry of the inner regions of the more centrally crowded clusters, we supplemented our Magellan images with images taken with the Advanced Camera for Surveys (ACS) aboard *HST*. These data were obtained in by our group's Snapshot program 10573. The ACS has a FOV of $3.37' \times 3.37'$, with a pixel size of $0.05''$. Five clusters of our sample were observed using the $f435w(B_{435})$, $f555w(V_{555})$, and $f814w(I_{814})$ filters. Table 3 lists the details of these new *HST* observations.

To better calibrate our photometry, we also used images available through the *HST* data archive for all the clusters in our sample. The data taken from the *HST* data archive are comprised of $f439w(B_{439})$, $f555w(V_{555})$, $f606w(V_{606})$, and $f814w(I_{814})$ images obtained with the Wide Field Planetary Camera 2 (WFC2), and of $f435w(B_{435})$, $f606w(V_{606})$, and $f814w(I_{814})$ images taken with the ACS. Table 4 lists the different *HST* programs that we use data from.

3.2. Data reduction and photometry derivation

For the ground-based data, the initial processing of the raw CCD images was done with the routines in the *ccdred* package of the Image Reduction and Analysis Facility (IRAF). The images were first corrected for bias, then flatfielded using a combination of dome and

twilight flats. Afterward, since different frames for every cluster were taken with different exposure times in the B, V, and I filters (see Table 2), and they had small spatial offsets between them, the frames of every individual cluster were aligned, using the IRAF task *imalign*, and average-combined for every exposure time and filter, with the IRAF task *imcombine*.

Stellar photometry was carried out on the ground-based processed images using an updated version of DoPHOT (Schechter et al. 1993). This version works on any platform and accepts images consisting of real data values. It also provides better aperture corrections than previous versions, allowing for variations in aperture corrections as a function of field position and stellar magnitude (see Appendix A).

We also carried out an astrometric analysis of the cluster fields in our sample. We derived coordinates (Right Ascension α and Declination δ) for all stars detected in our photometric study by comparison with bright stars obtained in each field from the Two Micron All Sky Survey (2MASS) catalog stars available through the Infrared Processing and Analysis Center (IPAC) website. In practice, more than 100 stars were available as astrometric references within the fields of every chip of our CCD camera. A third order polynomial fit, done with the IRAF task *mscpeak*, produced dispersions of $\sigma \sim 0.25''$, consistent with the catalog precision. Using the astrometric information of the images we could also calculate if there were variations in the pixel area coverage accross the images, which could lead to miscalculations in the measured fluxes. But the pixel area changed by less than 1% across any of the chips of the camera, and therefore we did not need to apply any corrections to the measured photometry.

To calibrate our ground-based data, we first transformed the photometry from each of the individual eight CCDs in the camera in IMACS to a common zero point, and then transformed this system to a standard system–in our case, the Johnson-Cousins system

(Bessell 1979). We arbitrarily chose one of the CCDs, chip 2, as the one defining the instrumental system and brought the photometry from the other chips to this system (see Appendix B). After this was done, we placed our photometry in the Johnson-Cousins photometric system by observing Landolt (1992) fields over a range of airmasses during the nights of our 2005 observing run (see Appendix C). Since these nights were not completely photometric we used Stetson (2000) photometric standard stars and the photometry from the clusters obtained with the *HST* to fine-tune the calibration of our ground-based data (see Appendix C).

The photometry of the data from the *HST* observations was obtained using the programs HSTPHOT for the WFPC2 data (Dolphin 2000) and DolPHOT for the ACS data (Dolphin 2000). These programs have been specifically tailored to analyze data from these cameras. They take the images for every cluster retrieved from the the *HST* in the different filters, and analyze them all at the same time. The programs align the images, combine them and provide the final combined-frame and individual-frame photometry, both in the *HST* filter system and in the Johnson-Cousins system. We follow the author's prescriptions to give the input parameters for the analysis to both programs. Photometric goodness-of-fit parameters were employed to select only objects with high-quality measurements. Only measurements for which an object was classified as stellar (HSTPHOT and DolPHOT types 1 and 2), and for which $-0.1 \leq sharpness \leq 0.1$, $crowding \leq 0.5$, and errors in all measured magnitudes $\sigma \leq 0.1$ were retained.

4. Dereddened color-magnitude diagrams and extinction maps

In this section we present the results of applying the dereddening method described in Paper I to all the clusters in our sample of inner GGCs. We provide the CMDs of these clusters before and after correcting for differential extinction and describe any

improvements. We also provide the extinction maps that the dereddening technique generates, and compare them with the extinction maps supplied by Schlegel et al. (1998), from now on referred as the SFD extinction maps. For each cluster, we provide references to its more recent – but not necessarily all– optical and infrared photometric studies. We also report studies that explore the presence of different stellar populations in the observed GGCs, and speculate on the possibility of several stellar populations in some of the sampled clusters from the presence of a color-extended HB, as suggested in some recent studies (D'Antona & Caloi 2008; Gratton et al. 2010; Caloi & D'Antona 2011).

A detailed explanation of the dereddening method is provided in Paper I, but we summarize here the different steps that we follow to apply the method, along with the results from every step, to obtain the final extinction maps and dereddened CMDs. The technique is applied independently to the two available colors ($B-V$ and $V-I$), and it is only at the end of the process that the extinction maps obtained from both analyses are averaged.

The first step of our dereddening method is to calculate the probabilities for the observed stars to belong to the cluster. In order to do that, we first calculate the surface density of the stars as functions of distance r to the cluster center, as explained in Paper I, and by a fit with an empirical King (1962) profile plus constant field model (see Figure 2 and Table 6) obtain, using Equation 12 from Paper I, the cluster membership probabilities as a function of position in the sky $P(X=1|r)$ (see Figure 3). Then we calculate, following Paper I, the probability densities of the observed stars as a function of r, color c, and magnitude m, and the probability density of being field members as function of c and m by comparison with a Besançon model (Robin et al. 2003) (see table 7). Finally, applying Equation 20 from Paper I, we are able to find $P(X=1|r,c,m)$, the probabilities of the individual stars to be members of the cluster as a function of position in the sky and in the

CMD (see Figure 4 in this paper, and Figure 4 from Paper I as examples of the method). We restrict our analysis to stars down to the completeness limit of our observations, and areas in which the probability $P(X = 1|r) > 0.1$ (see Table 5), as calculated in Equation 13 in Paper I. There are a few cases in which we do not calculate $P(X = 1|r, c, m)$ for one of the colors, since the observed CMD of the cluster is not calibrated in that color (NGC 6558 in $B - V$, and NGC 6235, NGC 6342 and NGC 6355 in $V - I$), and a comparison with the Besançon models can lead to mistakes. In those cases, we equal the total probability to just $P(X = 1|r)$ (see Equation 13 in Paper I), and proceed with the next steps of the analysis, which are not affected by any constant offset in the color calibration.

Once the cluster membership probabilities have been calculated, we need to build the ridgeline for the CMDs of every cluster in our sample. We follow the three-step recipe described in Paper I to obtain the ridgelines[3] for both available colors (see Figures 5 and 6).

After that, we move the stars along the reddening vector (Cardelli et al. 1989) until they intersect the ridgeline and smooth the resulting individual color excesses, obtaining an extinction map[4]. From this map, we take the relative extinction that corresponds to every star observed. We then plot the CMD of the stars in our observation after having been

[3]For some clusters the ridgelines were better calculated if we used only stars where the membership probability as a function of distance was $P(X = 1|r) > 0.5$, instead of $P(X = 1|r) > 0.1$ as in Paper I. For homegeneity on the process through the sample, we apply this more severe cut to calculate the ridgelines of all the observed clusters.

[4]For some clusters the reddening maps were better obtained when, in the iterative process described in section 2.4 of Paper I, we use stars with extinctions at most 2σ away from the extinction value calculated in the previous iteration, as opposed to the 3σ threshold mentioned in Paper I. Again for homegeneity on the process through the sample, we apply this more severe cut to calculate the extinction maps of all the observed clusters.

corrected for the differential reddening and use it as the input for the next iteration.

Finally, after the process converges for both colors, we average the extinction maps obtained from both colors, generating a final extinction map and the dereddened CMDs (see Figures 7 to 31).

We now describe in more detail the individual cases of the different clusters in the sample. We display their $B-V$ vs. V and $V-I$ vs. V CMDs, before and after being differentially dereddened (see Figures 7 to 31), and describe any improvements in the photometry. The CMDs are plotted using the merged space and ground data, whenever space-based observations deeper than ground-based observations exist, or the ground photometry in the rest of the cases. To quantify improvements in the photometry, we have measured the definition of the evolutionary sequences in the CMD by fitting Gaussian functions to different magnitude cuts in the different sequences (1.5 mag above and 0.5 mag below the TO, this is, RGB and upper MS), similar to what we did in Figure 9 of Paper I. To give an idea of the importance of the field star contamination, we compare the total number of observed stars in every FOV with the number of stars provided by the Besançon model of the Galaxy for the same pointing and FOV.

We also present the extinction maps across the field of the clusters, along with their resolution and precision (see Figures 7 to 31). We compare these maps with the SFD extinction maps (see Figure 32). The extinction maps provided by our dereddening technique give the differential extinction in the field referred to the unknown absolute extinction where our ridgelines lie. The comparison with the SFD maps allows us to establish these absolute extinction zero points. In order to make the comparison, we need to bring down our extinction maps to the lower resolution of the SFD maps. Since our extinction maps are described by non-parametric continuous functions, we evaluate these functions in $\sim$ 1600 different points in every pixel of the SFD maps and average the

obtained values using our precision maps to calculate a weighted average that provides us with one extinction value per SFD pixel. We observe that both our maps and the SFD maps generally agree in identifying the same regions of higher and lower extinction, although our maps usually show higher variation (reaching sometimes a factor of 2) in the extinction values than the SFD maps. Notice also that the SFD maps give the extinction integrated along the line of sight (i.e., extinction in the foreground, but also in the background of the observed clusters), while the extinction maps provided by our technique show the extinction just in the foreground of the observed clusters.

NGC 6121 - M 4 (Figure 7).

The changes in the extinction across the field are significant ($\Delta E(B-V) = 0.15$). The highest extinction is located in the northwestern region of the field, while the northeastern region of the field shows the lowest. There is a small blob of higher extinction ($\Delta E(B-V) \sim 0.05$) $\sim 0.02\,$deg south of the center of the cluster, which the SFD map fails to show (see Figure 32). The absolute extinction zero point of our reddening map is $E(B-V) = 0.50$ from comparing our map with the SFD map. These significant values of extinction, both absolute and differential, are a consequence of the cluster being located behind the Ophiucus dust complex, about 120 pc away from us.

M 4 is likely the closest GC to the Sun. Because of this, stars in the upper RGB are saturated in our images, even in the shortest exposures, and they do not appear in our CMDs of this cluster. The region studied for this cluster encompasses the whole FOV of our CCD, since the number of field stars present is small ($< 20\%$ of the stars in our CMD). Due to the proximity of M 4 to the Sun, most of the field stars are located behind the cluster. They are generally dimmer than the cluster stars, and the evolutionary sequences of the field stars are easily differentiable from the cluster sequences. The definition of the different branches in the CMD of the cluster are improved after the dereddening process, especially

in the $V, V-I$ CMD. The evolutionary sequences get $\sim 35\%$ tighter there. A noticeable feature in the CMDs of this cluster is the presence of a bimodal HB, with both red and blue components, though the blue HB (BHB) is not very extended. This bimodality of the HB suggests the presence of several stellar populations in this cluster.

Some recent ground-based optical photometric studies of this cluster include Rosenberg et al. (2000a) in VI, Mochejska et al. (2002) in UBV, and Anderson et al. (2006) in BV. Recent deep optical *HST* CMDs of this cluster have been presented in $U_{336}V_{555}I_{814}$ by Bassa et al. (2004), in $V_{555}I_{814}$ by Richer et al. (2004), and in $V_{606}I_{814}$ by Ferdman et al. (2004) and Hansen et al. (2004). This cluster is also a member of the ACS survey of GGCs obtained in the $V_{606}I_{814}$ bands (Anderson et al. 2008a). Recent infrared photometric studies of this cluster are by Cho & Lee (2002) in JK, and by Ferraro et al. (2000) in VJK. Pulone et al. (1999) also used the *HST* for an optical and infrared study of the stellar mass function of this cluster in $V_{555}I_{814}J_{110}H_{160}$. The presence of significant differential reddening in this cluster has been pointed out in many studies, and a map of the differential extinction was provided by Mochejska et al. (2002) (see Figure 33). Recently, the presence of distinct populations has been suggested from spectroscopic studies of stars in the RGB (Marino et al. 2008; Carretta et al. 2010) and in the HB (Marino et al. 2011a).

NGC 6144 (Figure 8).

NGC 6144 is also located behind the ρ Ophiuchi dust cloud and very close ($\sim 40'$ northeast) to NGC 6121 (M 4). Unsurprisingly, NGC 6144 also suffers from high and differential reddening. The variation of the extinction across the field is one of the highest shown in our sample ($\Delta E(B-V) = 0.5$). Extinction is higher in the northern region of the observed field, ~ 0.1 deg from the center of the cluster, and peaks in the northeastern area. The absolute extinction zero point of our reddening map is $E(B-V) = 0.75$ from comparing our map with the SFD map. This is one of the few cases in which the differential

extinction variation across the field is more important (by a factor of 2) in the SFD maps than in ours.

The region studied for this cluster encompasses the whole FOV of our CCD, since there is only a moderate field star contamination ($\sim$ 50% of the stars in our CMD). Also the field stars are redder on average than the stars in the cluster whose different evolutionary sequences are clearly distinguishable in the CMD. The different evolutionary sequences are better defined ($\sim$ 25% tighter) in the CMD of the cluster after applying the dereddening process. This cluster shows a short BHB, which suggests the presence of a single population, or the dominance of one population.

The most recent ground-based optical photometric study of this cluster we found was done in BVI by Neely et al. (2000) for the RGB and HB stars. From *HST* data, the first CMD of this cluster was published by Sarajedini et al. (2007) as a part of their $V_{606}I_{814}$ ACS survey of GGCs. Lan et al. (2010) provide also CMDs in $U_{336}V_{606}H\alpha_{656}R_{675}I_{814}$ using HST data. Infrared upper RGB photometry has been presented for this cluster by Davidge (2000) in JHK, and by Minniti et al. (1995) in JK.

NGC 6218 - M 12 (Figure 9).

The differential extinction across the field of this cluster is very mild ($\Delta E(B-V) \sim$ 0.04). Extinction is higher in the northern region ($\sim$ 0.1 deg of the cluster center). The absolute extinction zero point of our reddening map is $E(B-V) = 0.18$ from comparing with the SFD map.

The region studied for this cluster encompasses the whole FOV of our CCD, since the number of field stars present is small ($<$ 10% of the stars in our CMD). The mild differential extinction produces only a small improvement in the CMD of the cluster after being dereddened. The evolutionary sequences get $\sim$ 10% tighter in $V, V-I$, a little less in

$V, B-V$. Some of the CMD features, like the RGB (Thompson) bump, are more clearly visible now. A significant feature of this cluster is its extended BHB, which suggests the presence of several populations of stars.

Ground-based VI photometric data on M12 down to a few magnitudes under the TO have most recently been presented by von Braun et al. (2002) and Rosenberg et al. (2000b), BV data by Brocato et al. (1996), BVI data by Hargis et al. (2004) and deeper VR data by de Marchi et al. (2006). *HST* $B_{439}V_{555}$ data on M12 were published by Piotto et al. (2002) using the WFPC2. This cluster is also a member of the ACS survey of GGCs in $V_{606}I_{814}$ (Anderson et al. 2008a). We have found no infrared photometrical study of this cluster. von Braun et al. (2002) mapped the extinction in this location, finding little differential reddening in the field (see Figure 33). Recently, Carretta et al. (2007) have suggested the presence of two distinct populations with different helium content from a spectroscopic study of RGB stars. Carretta et al. (2010) also find evidence for different populations from a spectroscopic study of stars in the RGB.

NGC 6235 (Figure 10).

The changes in extinction across the field are moderate ($\Delta E(B-V) \sim 0.1$), being the southeastern area of the field the region of highest extinction. The absolute extinction zero point of our reddening map is $E(B-V) = 0.39$ from comparing our map with the SFD map. These moderately high values of extinction, both absolute and differential, are a consequence of the cluster's projected position, close to the Ophiucus dust complex.

The region studied for this cluster includes only stars located less than $5.37'$ away from the cluster center, due to the high number of field stars relative to the GC stars ($\sim 85\%$ of the stars when we look at the whole FOV of IMACS). As with NGC 6144, the field stars are redder on average than the cluster stars. This allow us to easily differentiate the cluster and field evolutionary sequences. These sequences in the cluster get $\sim 15\%$ tighter after being

differentially dereddened. This cluster shows a BHB, not very extended, which suggests the presence of a single population, or the dominance of one population.

The most recent ground-based optical photometric study of this cluster we found was done in BV for RGB and HB stars by Howland et al. (2003), who found a differential extinction relation along the X axis of their data and used it to correct their photometry. This cluster has also been observed with the WFPC2 aboard the *HST* and its $B_{439}V_{555}$ CMD has been published in the GGC survey by Piotto et al. (2002). Infrared upper RGB photometry has been presented for this cluster by Davidge (2000) in JHK and by Minniti et al. (1995) in JK. Deeper JHK RGB near-infrared photometry was presented by Chun et al. (2010).

NGC 6254 - M 10 (Figure 11).

The extinction variation across the field of this cluster is mild ($\Delta E(B-V) \sim 0.1$). Extinction is higher towards the west, peaking close ($\sim 0.02\,\mathrm{deg}$) to the cluster center. The absolute extinction zero point of our reddening map is $E(B-V) = 0.28$ from comparing our map with the SFD map.

The region studied for this cluster encompasses the whole FOV of our CCD, since the number of field stars present is small ($< 10\%$ of the stars in our CMD). The CMD of this cluster, with an extended BHB, and its distance to the center of the Galaxy are very similar to those of M 12. The evolutionary sequences get $\sim 25\%$ tighter after being differentially dereddened, and features like the the RGB bump are more clearly visible now. The extended blue horizontal branch (EBHB) suggests the presence of several stellar populations.

NGC 6254 has previously been studied using ground-based facilities by Rosenberg et al. (2000b) and von Braun et al. (2002) in VI and by Pollard et al. (2005) in BVI. Piotto

& Zoccali (1999) used both ground-based facilities and *HST* for their study of this cluster in the VI bands. Beccari et al. (2010) used also the *HST* for their mass segregation study of this cluster in the $V_{606}I_{814}$ bands. This cluster is also a member of the ACS survey of GGCs in $V_{606}I_{814}$ (Anderson et al. 2008a). Valenti et al. (2004a) studied this cluster in the infrared JK bands. The presence of differential reddening has been previously noted, and von Braun et al. (2002) mapped the extinction in the cluster field, finding a higher differential extinction than in M 12 (see Figure 33). Carretta et al. (2010) find evidence for different populations from a spectroscopic study of stars in the RGB.

NGC 6266 - M 62 (Figure 12).

A band of material causing a significant increase in extinction ($\Delta E(B-V) \sim 0.25$) crosses the field in the east-west direction less than 0.02 deg south from the cluster center. The absolute extinction zero point of our reddening map is $E(B-V) = 0.47$ from comparing our map with the SFD map. In the SFD map the presence of this band of extinction is not so clear.

The area studied for this cluster is restricted to the inner $6.84'$ of the cluster, due to the number of field stars ($\sim 50\%$ of the stars when we look at the whole FOV of IMACS) and the relatively small tidal radius ($r_t = 11.28'$). The definition of the different branches in the CMD of the cluster is highly improved, approximately by a factor of 2, after the dereddening process. Also now the presence of an EBHB is clearly visible and the location of the RGB bump is more easily identifiable. A striking feature in the CMD of this cluster is the presence of an extended and well populated HB, with both red and blue components. The BHB in particular is very extended. The shape of the HB and the fact that this is one of the most massive clusters in the Milky Way make this cluster a clear candidate to have several stellar populations.

Previous work using ground-based data includes that of Rosenberg et al. (2000a) in

VI, and Gerashchenko & Kadla (2004), Contreras et al. (2005) and Contreras et al. (2010) in BV. Beccari et al. (2006) studied this cluster using a combination of BVI (ground) and $U_{255}U_{336}V_{555}$ (space) bands. Cocozza et al. (2008) studied a pulsar in M 62 and used their *HST* data to show the $B-R$ vs. R CMD of the cluster. NGC 6266 is also included in the *HST* GGCs survey in $B_{439}V_{555}$ published by Piotto et al. (2002). Valenti et al. (2007) and Chun et al. (2010) studied this cluster in the infrared JHK bands. The presence of differential reddening has been previously noted, and Gerashchenko & Kadla (2004) mapped the extinction towards the central region of the cluster (see Figure 33).

NGC 6273 - M 19 (Figure 13).

The changes in the extinction across the field are significant ($\Delta E(B-V) \sim 0.3$). Extinction is higher towards the east, and peaks in a small region located very close, less than 0.02 deg, of the center of the cluster. The absolute extinction zero point of our reddening map is $E(B-V) = 0.32$ from comparing our map with the SFD map.

The area studied for this cluster is restricted to the inner $8.26'$ of the cluster, due to the number of field stars ($\sim 40\%$ of the stars when we look at the whole FOV of IMACS). The definition of the different branches in the CMD of the cluster is highly improved after the dereddening process. The different sequences get tighter by approximately a factor of 2 after being differentially dereddened, and now the presence of an EBHB is clearly visible and the location of the RGB bump is more easily identifiable. The EBHB suggests the presence of several stellar populations in this cluster.

The most recent optical photometric study of this cluster we found was done by Piotto et al. (1999) in $B_{439}V_{555}$ from *HST* images. As part of their study, they obtained a map of the differential reddening of the central region of the cluster. Piotto et al. (2002) included the CMD from this work in their *HST* GGCs survey in $B_{439}V_{555}$. In the infrared this cluster was studied in JHK by Chun et al. (2010), by Davidge (2001) and by Valenti et al. (2007).

NGC 6287 (Figure 14).

The variation of the extinction across the field is one of the highest shown in our sample ($\Delta E(B-V) = 0.75$). Extinction is higher in the northern region. A narrow band of material causing the highest extinction in the field crosses it in the east-west direction less than 0.02 deg from the cluster center. The absolute extinction zero point of our reddening map is $E(B-V) = 0.67$ from comparing our map with the SFD map. These significant values of extinction, both absolute and differential, are a consequence of the cluster's projected proximity to the Ophiucus dust complex.

The area studied for this cluster is restricted to the inner $4.13'$ of the cluster due to the number of field stars ($\sim 75\%$ of the stars when we look at the whole FOV of IMACS). The definition of the different branches in the CMD of the cluster is highly improved, approximately by a factor of 2, after the dereddening process. Now the RGB and SGB are easily identifiable, which was not the case before applying the dereddening technique. A short BHB is observed in the CMD, suggesting the presence of a single population, or the dominance of one population.

Previous photometric studies in the optical were done in BV by Stetson & West (1994) from ground-based observations and in VI by Fullton et al. (1999) from space-based observations. NGC 6287 is included in the *HST* GGCs survey in $B_{439}V_{555}$ published by Piotto et al. (2002). In the infrared, Chun et al. (2010) and Davidge (2001) studied this cluster in JHK, and Lee et al. (2001) in $J_{110}H_{160}$ using the *HST*.

NGC 6304 (Figure 15).

The variation of the extinction across the field is moderate ($\Delta E(B-V) = 0.15$). The area located ~ 0.05 deg east of the center of the cluster is the region of highest extinction. The absolute extinction zero point of our reddening map is $E(B-V) = 0.49$

from comparing our map with the SFD map.

The area studied for this cluster only includes stars with distances less than 3.65′ away from the cluster center, due to the high number of field stars relative to the GC stars ($> 90\%$ of the stars when we look at the whole FOV of IMACS). The improvement of the CMD of this cluster is only marginal. The CMD of this cluster shows a very short, red HB (RHB).

This cluster has been previously observed and studied using ground-based facilities by Ortolani et al. (2000) in BV and Rosenberg et al. (2000a) in VI. It is one of the clusters in the GGCs survey by Piotto et al. (2002) in $B_{439}V_{555}$ and in the ACS GGCs survey in $V_{606}I_{814}$ (Anderson et al. 2008a) done using *HST* data. Valenti et al. (2005) studied this cluster in the infrared JHK bands. Valenti et al. (2007) include results from this study in their infrared compilation of bulge GGCs.

NGC 6333 - M 9 (Figure 16).

The changes in the extinction across the field are significant ($\Delta E(B-V) \sim 0.25$). The area located ~ 0.1 deg southwest of the cluster center is the region of highest extinction. The absolute extinction zero point of our reddening map is $E(B-V) = 0.43$ from comparing our map with the SFD map.

The area studied for this cluster is restricted to the inner 5.59′ of the cluster due to the number of field stars ($\sim 45\%$ of the stars when we look at the whole FOV of IMACS) and the relatively small tidal radius ($r_t = 8.16'$). The evolutionary sequences of M 9 get $\sim 35\%$ tighter after being differentially dereddened. This cluster posseses an EBHB, which suggests the presence of several stellar populations in this cluster.

The most recent optical photometric study of this cluster we found is that of Janes & Heasley (1991) in BV for stars brighter than the TO point. Although this cluster has been

previously observed with the *HST* (see Table 4), the first CMD of M 9 using space data is published in this paper in BVI. In the infrared Davidge (2001) and Chun et al. (2010) studied this cluster in JHK.

NGC 6342 (Figure 17).

The changes in the extinction across the field are significant ($\Delta E(B-V) \sim 0.4$). The northwestern quadrant of the field, reaching the projected position of the center of the cluster, is the region of highest extinction. The absolute extinction zero point of our reddening map is $E(B-V) = 0.59$ from comparing our map with the SFD map.

The area studied for this cluster reaches only stars with distances less than $4.21'$ away from the cluster center, due to the significant number of field stars relative to GC stars ($\sim$ 70% of the stars when we look at the whole FOV of IMACS). The definition of the different branches in the CMD of the cluster is highly improved after the dereddening process, getting tighter by a factor of 2. Now the RGB and SGB are easily identifiable, along with a RHB, which was not the case before applying the dereddening technique.

The only recent optical photometric studies found for this cluster are those of Heitsch & Richtler (1999) in VI using ground-based facilities and that of Piotto et al. (2002) in $B_{439}V_{555}$ using the *HST*. In the infrared Valenti et al. (2004b) studied this cluster in $VJHK$. Valenti et al. (2007) include results from this study in their infrared compilation of bulge GGCs. A map of the differential reddening was produced by Heitsch & Richtler (1999) (see Figure 33).

NGC 6352 (Figure 18).

The differential extinction variation across the field of this cluster is only moderate ($\Delta E(B-V) \sim 0.15$). Extinction is higher in the northern region of the analyzed field. The absolute extinction zero point of our reddening map is $E(B-V) = 0.34$ from comparing

our map with the SFD map.

The area studied for this cluster is restricted to the inner $5.61'$ of the cluster, due to the high number of field stars relative to the GC stars ($> 90\%$ of the stars when we look at all the available FOV). The evolutionary sequences get $\sim 30\%$ tighter after being differentially dereddened. The cluster shows a RHB.

This cluster was studied by Sarajedini & Norris (1994) in BV and Rosenberg et al. (2000a) and Pancino et al. (2010) in VI from the ground, and from space by Fullton et al. (1995) in VI_C, using pre-COSTAR data, and by Faria & Feltzing (2002) in $V_{555}I_{814}$ and by Pulone et al. (2003) in $V_{606}I_{814}$. It is also a member of the ACS survey of GGCs in $V_{606}I_{814}$ (Anderson et al. 2008a). We have found no infrared photometrical study of this cluster. Pancino et al. (2010) show the presence of two populations of stars with anticorrelated CN and CH band strengths.

NGC 6355 (Figure 19).

The changes in the extinction across the field are significant ($\Delta E(B-V) \sim 0.3$). The southwestern area of the cluster is the region of highest extinction. The absolute extinction zero point of our reddening map is $E(B-V) = 1.20$ from comparing our map with the SFD map.

The area studied for this cluster is restricted to the inner $2.36'$ of the cluster, due to the high number of field stars relative to the GC stars ($> 90\%$ of the stars when we look at all the available FOV). The evolutionary sequences get $\sim 10\%$ tighter after being differentially dereddened. This cluster posseses a BHB, although the small number of stars in the HB, due to the small studied field, makes it difficult to infer any information about different populations in this cluster.

The only previous recent optical photometric studies found are those by Ortolani et al.

(2003) in BVI using ground-based facilities, and that by Piotto et al. (2002) in $B_{439}V_{555}$ using the *HST*. In the infrared Chun et al. (2010), Davidge (2001), and Valenti et al. (2007) studied this cluster in JHK.

NGC 6397 (Figure 20).

The differential extinction in this cluster is only mild ($\Delta E(B-V) \sim 0.05$). Extinction is not especially concentrated in any area of the field. The absolute extinction zero point of our reddening map is $E(B-V) = 0.18$ from comparing our map with the SFD map.

This is the cluster with the smallest apparent distance modulus, though it is not the one closest to the Sun. As for M 4, stars in the upper RGB are saturated in our images, even in the shortest exposures, and they do not appear in our CMDs of this cluster. The contamination from field stars is moderate ($\sim$ 30% of the stars when we look at all the available FOV), mainly affecting MS stars in the cluster. This moderate contamination allows us to study almost all the available FOV, up to $8.18'$ from the cluster center. The sequences of NGC 6397 get $\sim$ 10% tighter after being differentially dereddened. This cluster shows a short BHB, which suggests the presence of a single population, or the dominance of one population.

Some of the most recent studies of this cluster done with ground-based facilities are those by Rosenberg et al. (2000a) in VI, Anderson et al. (2006) in $UBVI$, and Kaluzny et al. (2006) in BV. This cluster has also been observed with the *HST*. A series of papers has been published dedicated to the study of the characteristics of this cluster using very deep photometry obtained with the ACS (Anderson et al. 2008b; Hurley et al. 2008; Richer et al. 2008; Davis et al. 2008). NGC 6397 is also included in the GGC survey from Piotto et al. (2002) in $B_{439}V_{555}$ and of the ACS GGC survey in $V_{606}I_{814}$ (Anderson et al. 2008a). de Marchi et al. (2000) also used the *HST* for an optical and infrared study of the stellar mass function of this cluster in $V_{606}I_{814}J_{110}H_{160}$. Recent spectroscopic studies of this cluster

have found different chemistry among its stars: Carretta et al. (2010) show some O-Na anti-correlation is present, although the number statistics is small (only 16 stars studied, the smallest in their sample of GCs); Lind et al. (2011) claim the presence of two different stellar populations that have different chemical compositions of N, O, Na, Mg, and probably Al, and note that the cluster is clearly dominated (75%) by the second generation.

NGC 6522 (Figure 21).

The differential extinction variation in this cluster is moderate ($\Delta E(B-V) = 0.1$), although we should realize that the studied region is also small (see next paragraph). Extinction is higher in the southwestern region of the analyzed field. The absolute extinction zero point of our reddening map is $E(B-V) = 0.58$ from comparing our map with SFD map.

This cluster is located in Baade's Window. The high number of non-cluster member stars ($> 90\%$ of the stars when we look at all the available FOV) restricts the study in this region to stars closer than $2.33'$ from the cluster center. The improvement of the CMD of this cluster after being dereddened is only marginal. It shows an EBHB, which suggests the presence of several stellar populations in this cluster.

The most recent optical photometric studies found, done with ground-based data, are those by Barbuy et al. (1994) in BV, and Terndrup & Walker (1994) in BVI. Terndrup et al. (1998) show a differential extinction relation with respect to the center of the cluster and use it to correct their previous photometry. Using the *HST*, the cluster was studied by Shara et al. (1998) in the $U_{336}B_{439}$ bands using pre-COSTAR data. It is also one of the clusters in the Piotto et al. (2002) GCs survey in $B_{439}V_{555}$. In the infrared, Davidge (2001) and Valenti et al. (2010) studied this cluster in JHK.

NGC 6541 (Figure 22).

The differential extinction in this cluster is moderate ($\Delta E(B-V) \sim 0.1$). Extinction is not especially concentrated in any area of the field, although there seems to be an increase towards the southeast area of the observed field. The absolute extinction zero point of our reddening map is $E(B-V) = 0.16$ from comparing our map with the SFD map.

The region studied for this cluster encompasses most of the FOV of our CCD, up to $8.63'$ from the cluster center, since there is only a moderate field star contamination ($\sim 40\%$ of the stars in our CMD). Also the field stars are redder on average than the stars in the cluster, which lets us distinguish NGC 6541 evolutionary sequences unambiguosly. The sequences in the cluster get $\sim 10\%$ tighter after being differentially dereddened. This cluster possesses an EBHB, which suggests the presence of several stellar populations.

Ground-based studies of this cluster were presented by Alcaino et al. (1997) in $BVRI$ and by Rosenberg et al. (2000a) in VI. It has also been studied using *HST* WFPC2 data by Lee & Carney (2006) in VI, and it is one of the clusters in the ACS GGC survey observed in $V_{606}I_{814}$ (Anderson et al. 2008a). In the infrared Kim et al. (2006) studied this cluster in JHK.

NGC 6553 (Figure 23).

There are significant changes in the extinction across the field ($\Delta E(B-V) \sim 0.25$). In our maps, the highest extinction is located in the northern region of the field, while the southwestern region of the field shows the lowest, which is not the trend shown in the SFD maps, but it does agree well with the trend of the map provided by Heitsch & Richtler (1999) (see Figure 33). The absolute extinction zero point of our reddening map is $E(B-V) = 1.35$ from comparing our map with the SFD map.

The area studied for this cluster is restricted to the inner $3.91'$ of the cluster, due to the high number of field stars relative to GC stars ($> 90\%$ of the stars when we look at all

the available FOV). The upper MS and RGB get $\sim 30\%$ tighter after being differentially dereddened, and the RGB bump now is more clearly identifiable. The well-populated bump, the very extended upper RGB and a RHB, suggest that this is a metal-rich GGCs.

Some of the most recent optical photometric studies of this cluster are that by Sagar et al. (1999) in VI using ground-based data and those by Beaulieu et al. (2001) and Zoccali et al. (2001) in $V_{555}I_{814}$ using *HST* data. Zoccali et al. (2001) calculated the extinction map, not shown in their paper, and applied it to get a clean CMD. Heitsch & Richtler (1999) show an extinction map (see Figure 33) calculated with data from Sagar et al. (1999). Guarnieri et al. (1998) in $VIJK$, and Ferraro et al. (2000) in VJK studied this cluster in the optical and in the infrared. Valenti et al. (2007) includes results from this last study in their infrared compilation of bulge GGCs.

NGC 6558 (Figure 24).

The extinction variations in this cluster are significant ($\Delta E(B-V) \sim 0.15$), especially when we consider the small size of the studied field (see next paragraph). The absolute extinction zero point of our reddening map is $E(B-V) = 0.51$ from comparing our map with SFD map.

The high number of non-cluster member stars ($> 90\%$ of the stars when we look at the whole FOV of IMACS) restrict the study of this region to stars closer than $1.81'$ from the cluster center. The improvement of the CMD is only marginal. This cluster shows a BHB, although the low definition of the HB due to the small number of stars in this region caused by the small field FOV studied makes it difficult to infer any information about different populations in this cluster.

We found only two previous optical photometric studies using ground-based data, those by Rich et al. (1998) and by Barbuy et al. (2007), both in VI. Although this cluster

has been previously observed with the *HST*, the first CMD of the deep MS stars using space-based data is published in this paper in VI. In the infrared Chun et al. (2010) studied this cluster in JHK.

NGC 6624 (Figure 25).

The differential extinction across the field is moderate ($\Delta E(B-V) \sim 0.15$). Extinction is higher in the southeastern region of the analyzed field. The absolute extinction zero point of our reddening map is $E(B-V) = 0.25$ from comparing our map with the SFD map.

The area studied for this cluster is restricted to the inner $3.92'$ of the cluster, due to the high number of field stars relative to the GC stars ($> 90\%$ of the stars when we look at all the available FOV). There are also some dim blue field stars in our CMD that belong to the Sagittarius dwarf galaxy. Stars from this galaxy's MS are easily observed in the CMD at magnitudes dimmer than $V \sim 21$ and colors bluer than the cluster MS. The improvement of the CMD of the cluster after being dereddened is only marginal. This cluster possesses a RHB.

This cluster has been studied using ground-based data by Sarajedini & Norris (1994), who presented a photometric study of the RGB and HB stars in BV. Richtler et al. (1994) and Rosenberg et al. (2000a) obtained deeper photometry, reaching a few magnitudes below the TO in BV and VI, respectively. Using *HST*, studies of this cluster were published by Sosin & King (1995) in BV using pre-COSTAR data, and by Guhathakurta et al. (1996) in $U_{336}B_{439}V_{555}$ and Heasley et al. (2000) in VI. This cluster is also a member of the Piotto et al. (2002) $B_{439}V_{555}$ GGCs survey, and of the $V_{606}I_{814}$ ACS GGCs survey (Anderson et al. 2008a). In the infrared Valenti et al. (2004b) studied this cluster in $VJHK$. Valenti et al. (2007) include results from this study in their infrared compilation of bulge GGCs.

NGC 6626 - M 28 (Figure 26).

The extinction variations across the field of this cluster are significant ($\Delta E(B-V) \sim 0.2$). Extinction is lower at the projected center and southwestern region of the observed field, which is not the trend observed in the SFD maps. The absolute extinction zero point of our reddening map is $E(B-V) = 0.46$ from comparing our map with the SFD map.

The area studied for this cluster is restricted to the inner $4.95'$ of the cluster, due to the high number of field stars relative to the GC stars ($> 90\%$ of the stars when we look at all the available FOV). Due to its proximity, the cluster's brightest stars are brighter on average than the field's, and we can identify without much difficulty stars from the RGB. The evolutionary sequences of M28 get $\sim 35\%$ tighter after being differentially dereddened. This cluster shows an EBHB, which suggests the presence of several stellar populations.

This cluster has been studied in the optical using ground-based data by Rosenberg et al. (2000a) in VI, and using *HST* data by Testa et al. (2001) and by Golden et al. (2001) in VI. Davidge et al. (1996) used a combination of optical and infrared bands ($BVJK$) to study this cluster. In the infrared Chun et al. (2010) studied this cluster in JHK.

NGC 6637 - M 69 (Figure 27).

The differential extinction across most of the observed field is moderate ($\Delta E(B-V) \sim 0.1$). Extinction is not especially concentrated in any area of the field. The absolute extinction zero point of our reddening map is $E(B-V) = 0.17$ from comparing our map with the SFD map.

The area studied for this cluster is restricted to the inner $4.39'$ of the cluster, due to the high number of field stars relative to the GC stars ($> 90\%$ of the stars when we look at all the available FOV). There are also some dim blue field stars in our CMD that belong to the Sagittarius dwarf galaxy. Stars from this galaxy's MS are easily observed in the CMD at magnitudes dimmer than $V \sim 21$ and colors bluer than the cluster MS. The improvement

of the CMD of this cluster is only marginal. This cluster posseses a RHB.

This cluster has been the subject of several studies, usually along with the also metal-rich NGC 6624. Using ground-based data Ferraro et al. (1994), in $BVJK$, and Sarajedini & Norris (1994), in BV, present a photometric study of the RGB and HB stars of this cluster, and Richtler et al. (1994) and Rosenberg et al. (2000a) got deeper photometry, reaching a few magnitudes below the TO, in BV and VI respectively. Using *HST* data, Heasley et al. (2000) studied this cluster in VI. This cluster is also a member of the Piotto et al. (2002) $B_{439}V_{555}$ GGCs survey, and of the $V_{606}I_{814}$ ACS GGCs survey (Anderson et al. 2008a). In the infrared this cluster was studied by Ferraro et al. (2000) in VJK and by Valenti et al. (2005) in JHK. Valenti et al. (2007) include results from these studies in their infrared compilation of bulge GGCs.

NGC 6642 (Figure 28).

The differential extinction in this cluster is high ($\Delta E(B-V) \sim 0.2$). The absolute extinction zero point of our reddening map is $E(B-V) = 0.36$ from comparing our map with the SFD map.

During the observation of this cluster with the Magellan telescope, we had the least photometric conditions of our run (see Table 10). This resulted in the shallowest CMD of our study, reaching only stars down to the very upper parts of the MS. The high number of non-cluster member stars ($> 90\%$ of the stars when we look to all the available FOV) restricts the study in this area to stars closer than $2.22'$ from the cluster center. The improvement of the CMD of this cluster after being dereddened is only marginal. A prominent feature in the CMDs of this cluster is the presence of a bimodal HB, with both red and blue components, though the blue BHB is not very extended. This bimodality of the HB can suggest the presence of several stellar populations.

The most recent optical photometric study of NGC 6642 using ground-based data was done by Barbuy et al. (2006) in BVI. Using *HST*, Balbinot et al. (2009) studied this cluster in $V_{606}I_{814}$. NGC 6642 is also a member of the Piotto et al. (2002) $B_{439}V_{555}$ GGCs survey. In the infrared Davidge (2001), Kim et al. (2006), and Valenti et al. (2007) studied this cluster in JHK.

NGC 6656 - M 22 (Figure 29).

The extinction variation across the field of this cluster is moderate ($\Delta E(B-V) \sim 0.1$). Extinction is lower in the southern area of the field. The absolute extinction zero point of our reddening map is $E(B-V) = 0.33$ from comparing our map with the SFD map.

The relative proximity of M22 explains why the upper RGB stars are saturated in our observations and are excluded from the CMDs of this cluster. The region studied for this cluster encompasses the whole FOV of our CCD, since there is only a moderate field star contamination ($\sim 40\%$ of the stars in our CMD). Due to the proximity of M 22, most of the field stars are located behind the cluster. They are generally dimmer than the cluster stars, and the evolutionary sequences of the field stars are easily differentiable from the brighter sequences of the cluster. After being dereddened, the sequences of the cluster get $\sim 25\%$ tighter in $V, V-I$, a little less in $V, B-V$. An EBHB suggests the presence of several stellar populations in this cluster.

There are several optical photometric studies for this cluster. Using ground-based data, it was studied by Monaco et al. (2004) in BVI, by Webb et al. (2004) in UV, by Kaluzny & Thompson (2001) in BV, by Rosenberg et al. (2000a) in VI, and by Anthony-Twarog et al. (1995), by Richter et al. (1999) and by Lee et al. (2009) in Strömgrem *uvbyCa*, *vby* and *VbyCa* bands, respectively. Piotto & Zoccali (1999) used both ground facilies and the *HST* for their study of this cluster in VI, and Anderson et al. (2003) show CMDs for the cluster in $B_{435}V_{606}R_{675}I_{814}$ bands. This cluster is also a member of the ACS survey of GGCs in

$V_{606}I_{814}$ (Anderson et al. 2008a). Piotto (2009) shows a double SGB in his study of M 22 using $V_{606}I_{814}$. In the infrared Minniti et al. (1995), Davidge & Harris (1996) and Cho & Lee (2002) studied this cluster in JK. The presence of a metallicity spread in this cluster has been the subject of a long debate, complicated by the presence of insterstellar reddening (see Pancino et al. (2010) for a brief historic review). Some recent studies seem to confirm the presence of at least two stellar populations with different chemical compositions, both photometrically (Piotto 2009) and spectroscopically (Marino et al. 2009; Da Costa et al. 2009; Carretta et al. 2010; Marino et al. 2011b), although the studies by Kayser et al. (2008) and by Pancino et al. (2010) do not find clear CH and CN anti-correlations or bimodalities for the stars in their sample.

NGC 6681 - M 70 (Figure 30).

The differential extinction across most of the observed field is mild ($\Delta E(B-V) \sim 0.05$). Extinction is not especially concentrated in any area of the field. The absolute extinction zero point of our reddening map is $E(B-V) = 0.09$ from comparing our map with the SFD map.

The area studied for this cluster is restricted to the inner $5.21'$ of the cluster, due to the high number of Galactic field stars relative to the GC stars ($\sim 70\%$ of the stars when we look to all the available FOV). The field stars are redder on average than the cluster stars, which allows us to easily distinguish the different evolutionary sequences. There are also some dim blue field stars in our CMD that belong to the Sagittarius dwarf galaxy. Stars from this galaxy's MS are easily observed in the CMD at magnitudes dimmer than $V \sim 21$ and colors bluer than the cluster MS. The improvement of the CMD of this cluster is only marginal. M 70 posseses an extended BHB, suggesting the presence of several stellar populations in this cluster.

The most recent optical photometric studies we found, using ground-based data, are

those by Brocato et al. (1996) in BV, and by Rosenberg et al. (2000a) in VI. Using *HST* data, Piotto et al. (2002) included it in their GGCs survey in $B_{435}V_{555}$. This cluster is also a member of the $V_{606}I_{814}$ ACS survey of GGCs (Anderson et al. 2008a). In the infrared Kim et al. (2006) studied this cluster in JHK.

NGC 6809 - M55 (Figure 31).

The extinction variation across the field of this cluster is only mild ($\Delta E(B-V) \sim 0.05$). Extinction is higher in the northwestern area of the observed field. The improvement of the CMD of this cluster is only marginal. The absolute extinction zero point of our reddening map is $E(B-V) = 0.14$ from comparing our map with the SFD map.

The region studied for this cluster encompasses the whole FOV of our CCD, since the number of field stars present is small ($< 10\%$ of the stars in our CMD), though there is clear contamination from stars in the background Sagittarius dwarf galaxy. Stars from its MS are easily observed in the CMD at magnitudes dimmer than $V \sim 21$ and colors bluer than the cluster MS. The tip of the RGB is saturated in our CMDs of this cluster, due to the small apparent distance modulus of M 55. The improvement of the CMD of this cluster is only marginal. The cluster shows a BHB, not very extended, suggesting the presence of a single population, or the dominance of one population.

The latest optical photometric studies of this cluster done using ground-based data are by Kaluzny et al. (2005) in $UBVI$, by Pych et al. (2001) and by Zloczewski et al. (2011) in BV, and by Rosenberg et al. (2000a) in VI. Using a combination of ground-based and *HST* data, this cluster was studied by Lanzoni et al. (2007) in BVI, and by Bassa et al. (2008) in $BVRIH_{\alpha}$. The ACS VI photometry used by Bassa et al. (2008) comes from Anderson et al. (2008a), since this cluster is one of the members of the ACS GGC survey. In the infrared this cluster was studied by Ferraro et al. (2000) in VJK. The presence of more than one stellar population has been suggested by Carretta et al. (2010) based on the

Na-O anti-correlation found in their study, but the studies by Kayser et al. (2008) and by Pancino et al. (2010) do not find a clear CH and CN anti-correlations or bimodalities on the stars in their sample.

5. Summary

This article is the second of a series devoted to the study of the inner GGCs. High and patchy differential extintion in the line of sight makes difficult to extract accurate and meaningful information about the physical parameters of the GCs located in the Galactic bulge and inner disk and halo. In this article we present a highly homogeneous and complete optical sample of the brightest GCs located towards the center of the Milky Way. We produce some of the deepest CMDs of the 25 inner GGCs that comprise our sample, using Magellan 6.5m telescope and *HST* observations. We apply a new dereddening technique to map the differential extinction in front of these GCs and eliminate their effects in the CMDs[5]. The GGCs in our sample show tighter evolutionary sequences, up to a factor of 2 in some cases, in the CMDs built after applying the dereddening method. These cleaned CMDs will be used in subsequent papers to analyse the astrophysical parameters of the GCs and their stellar populations. The high-definition extinction maps will be also used in future papers to study the properties of the obscuring material along the GGCs' lines of sight.

This study was supported by grants 0206081 from NSF and GO10573.01-A from STScI. STcI is operated by NASA under contract to AURA. Support was also provided

[5]We are working on making this photometric database easily accesible to the community through a webpage

by MIDEPLAN's Programa Inicativa Científica Milenio through grant P07-021-F, awarded to The Milky Way Millennium Nucleus, by Proyecto Fondecyt Regular 1110326, by Basal PFB-06, FONDAP 15010003, and Anillos ACT-86. This publication makes use of data products from the Two Micron All Sky Survey, which is a joint project of the University of Massachusetts and the Infrared Processing and Analysis Center/California Institute of Technology, funded by the National Aeronautics and Space Administration and the National Science Foundation. This research used the facilities of the Canadian Astronomy Data Centre operated by the National Research Council of Canada with the support of the Canadian Space Agency.

A. DoPHOT

In this work, we have obtained the photometry using a new version of DoPHOT. DoPHOT is a software created to extract PSF photometry from astronomical images. A complete and deep explanation of its main characteristics, and a description of how it works, is given by Schechter et al. (1993)

The main new characteristics of the distribution of DoPHOT we developed for this work are:

- All the program subroutines and functions have been rewritten to make them compatible with the standards of Fortran90.
- We have tried to make the subroutines and functions more easily readable. To achieve this, we have eliminated all the common statements present in previous versions and named all the variables used by the subroutine and function in the call statement. Also with the same spirit of making the program more understandable we have created, combined or eliminated some of the subroutines, and included, at the

beginning of each file, a brief explanation of what every function and subroutine does.

- The program works now with real values for the pixel values, so there is no need to worry about conversions to integers as in previous distributions.

- The stars are masked, obliterated, added, and subtracted across the different subroutines of the program in circular sections, and not in rectangular sections as before. This way fewer usable pixels are obliterated, and fewer pixels outside an interesting radius are dealt with.

In addition to this, this distribution shares some of the characteristics of the program that were present in previous distributions, but that were not mentioned in the original paper:

- DoPHOT allows for a variable PSF model in the image.

- DoPHOT can perform an aperture correction to the magnitudes obtained, according to their positions and magnitudes. The program checks for variations in the aperture correction in magnitude and in position in the image, and corrects the fitted magnitude accordingly.

This new version of DoPHOT is publicly available through:
http://www.astro.puc.cl/ jalonso/dophot.tar

B. Instrumental calibration

The camera in IMACS consists of eight chips, each with its own slightly different mean quantum efficiency and color sensitivity. To calibrate our data, we must first transform the photometry from each of the individual chips to a common zero point, then transform

this system to a standard system–in our case, the Johnson-Cousins system (Bessell 1979). In this appendix, we shall focus on the first step of transforming the individual chips to a common instrumental system.

For this purpose, we arbitrarily chose one of the chips, chip 2 (see Figure 34), as the one defining the instrumental system. The goal was to tie all the other chips to this chip's photometric zero point. We attempted to do this in two ways. First, we observed one Landolt (1992) field (PG 1047+003) in every one of the chips and in all three filters (BVI) in rapid succession on every night of our run. There were very few stars in this field, and the scatter we found in the mean photometric offsets – about 0.05 mag between chips – was too large given our need to bring all our photometry to a common system to 1-2% precision. We surmise that the relatively poor results from this approach reflects the quality of the nights during the 2005 run, and also possible flat-field variations at the 2-3% level for this run.

We tried a second approach during a sequence of observations during a 2006 Magellan run (see Table 2) in which we tried to auto-calibrate the IMACS chip array using stars from the cluster NGC 6397. The basic idea was to obtain a minimal number of exposures in each filter so that at least part of all chips overlapped with chip 2, the chip defining our instrumental photometric system. We found that a sequence of three exposures could achieve the desired overlap. Figure 34 illustrates the approach. In the left panel, the darker outline of the IMACS chip shows the location of a first exposure, in this case at the same location as the actual field we observed in 2005 for the cluster NGC 6397. The second exposure, shown as a lighter (red) outline is offset in both RA and Dec so that four of its chips (1, 2, 5 and 6) overlap with the position of chip 2 in the first exposure. The right panel again shows the initial pointing in the darker outline, with a third pointing as a lighter (green) outline. Now, chips 3, 4, 7 and 8 of the last exposure overlap with chip 2

from the first exposure. This sequence, repeated for each filter, generated a large list of stars that have been observed on chip2 *and* on every other chip in the array. Because only three exposures were required and because we took these in rapid succession, we can safely ignore airmass variations as we calculate the offsets from a given chip to the system defined by chip 2. In addition, we have exposures from the 2005 and 2006 runs of the *same* fields (the dark outlines in Figure 34) that allow us to determine any possible variations in chip sensitivities between runs.

The model we used to transform each chip to the chip 2 system has the form

$$m_2 = m_i + Z_i + \gamma_i c_i, \tag{B1}$$

where m_i is the instrumental magnitude of chip i (excluding $i = 2$), Z_i is the zero-point offset from chip i to chip 2, and γ_i is the color coefficient for instrumental color c_i. In practice, we carried out this analysis separately for each filter, B, V, and I, with the colors defined appropriately for each filter ($(B-V)$ for the B-band transformation and $(V-I)$ for the V and I-band transformations). We found that the color terms are all negligibly small in the chip-to-chip transformations for each filter, so the final model adopts $\gamma_i = 0$ for all chips and all colors. Thus we only had to detemine the mean values of the Z_i coefficients as the weighted mean of the differences of the instrumental magnitudes, $m_i - m_2$, for all stars in common between chip i and chip 2. Weights for each measurement were assigned according to the photometric errors and the dispersion in the offset ditribution. A first application of this approach, to the calibration sequence of NGC 6397 obtained in 2006 (Figure 34), allowed us to place all the data from that run on the 2006 chip 2 instrumental system.

Since the relative sensitivities of the chips might have changed between the 2005 and 2006 runs, we then took an additional step to define the chip-to-chip offsets for the 2005 run from which all our ground-based cluster photometry is defined. This process involves the observations of NGC 6397 from our 2006 run (described above) and the observations of

the same field for the same cluster obtained in 2005.

For this purpose we adopted the following transformation:

$$m_{i,06} = m_{i,05} + Y_i + \delta_i c_i + k_{05} X_{05} - k_{06} X_{06}. \quad \text{(B2)}$$

The zero-point offset from the 2005 observations required to place them on the 2006 system for chip i is given by Y_i (this now includes the case $i = 2$), for a color term δ_i, and an instrumental color on the 2005 system of c_i. The final two terms account for the different airmasses and possibly different extinction coefficients for each run and each observation. We do not know this product (extinction coefficient k times airmass X) for the 2006 run, because we did not observe standard stars on that run. But we know that the sum of these products is constant when comparing the 2005 and 2006 NGC 6397 observations. Thus, we can rewrite the equation above as

$$m_{i,06} = m_{i,05} + Y'_i + \delta_i c_i, \quad \text{(B3)}$$

in close analogy to Equation B1. Note that the new zero point offset now implicitly includes the airmass terms:

$$Y'_i = Y_i + k_{05} X_{05} - k_{06} X_{06}. \quad \text{(B4)}$$

We can simplify this due to the fact that we found that the color terms in Equation B3 are all negligibly small. Thus we only had to detemine the mean values of the Y'_i coefficients as the weighted mean of the differences of the instrumental magnitudes, $m_{i,06} - m_{i,05}$, for all stars from chip i. As before, weights for each measurement were assigned according to the photometric errors and the dispersion in the offsets distribution.

At this stage, we can transform the 2005 NGC 6397 data to a common instrumental system defined by chip 2 from the 2006 observations of this same cluster. But what we really require are the offsets in the 2005 system that bring all data from the IMACS chips

obtained in 2005 to a common system. That is, the final chip-to-chip offsets for the 2005 data are simply

$$\Delta Y'_i = Y'_i - Y'_2. \tag{B5}$$

The values of Z and $\Delta Y'$ required to tie the various chips systems to a common system defined by chip 2 are listed in Table 8. The errors in the values of Z and $\Delta Y'$ are $\sigma \sim 0.001$, the error of the mean of the distributions used to obtain them (see Figure 35). The dispersions of the distributions from which these Z and $\Delta Y'$ are derived, a measure of the internal precision of our photometry, are $\sigma \sim 0.01$.

C. Absolute calibration

We placed our photometry in the Johnson-Cousins photometric system by observing Landolt (1992) fields over a range of airmasses during the nights of our 2005 observing run. Since the first two nights were the most photometric of our run, we only used the standard fields observed those two nights to obtain the following transformations:

$$B = 3.417 + b - 0.283X + 0.130(b - v), \tag{C1}$$

$$V = 3.706 + v - 0.166X - 0.017(b - v), \tag{C2}$$

$$I = 3.065 + i - 0.049X - 0.020(v - i), \tag{C3}$$

where X is the airmass, b, v, and i are the instrumental magnitudes in the instrumental system and B, V, and I the corresponding magnitudes in the Johnson-Cousins photometric system.

To fine-tune our calibration we decided to compare our photometry with Stetson (2000) photometric standard stars. We found in some cases significant absolute offsets between Stetson's and our photometry. These zero points could be easily calculated (see Table 9

and Figure 36). However, only thirteen of our clusters had stars in common with Stetson's catalog, and only twelve had stars calibrated in all three filters.

To extend the comparison to more clusters, we looked for members of our sample already observed with at least one of the two *HST*'s optical wide-field imaging instruments, WFPC2 and ACS. We found that all of the clusters have already been observed at least in two of our filters, and most of them in all three (see Table 9). We retrieved the available data from the *HST* archive and derived photometry from the stars in these data using the programs HSTPHOT for the WFPC2 data (Dolphin 2000) and DolPHOT for the ACS data (Dolphin 2000). These programs have been specifically tailored to analyze data from these cameras.

The comparison between the *HST* and ground-based data is complicated by the large resolution difference in the datasets and the highly crowded fields. When the offsets in the photometries of individual stars of a cluster are plotted, there is a clear, asymmetric spread in the data (see Figure 37). Due to the higher resolution of the *HST*, individual stars in the *HST* data are blends in the ground-based data. To obtain the absolute offset between the two systems eliminating the blended stars effect we calculated a weighted mean of the offsets of the stars in common (see Figure 37), where the weights were assigned according to the photometric errors and the dispersion in the offset distribution. The weighted mean was iteratively calculated, ignoring stars 2σ away from the mean value at each iteration. Whenever we have zero points calculated separately from independent WFPC2 and ACS data, a mean value was adopted.

The results were then compared with the ones we found from the Stetson comparison, since our aim is to put all the photometry in the Stetson system (see Figure 38). A small offset for each filter was found and added to the individual cluster zero points ($\Delta B = -0.045 \pm 0.012$ mag, $\Delta V = -0.056 \pm 0.007$ mag, and $\Delta I = -0.025 \pm 0.008$ mag).

These offsets may be due to the fact that the *HST* observations used in our absolute calibration are located closer to the center of the cluster than the Stetson stars used, or they may reflect small system zero point differences. The final offsets applied to the individual clusters can be seen in Table 10.

REFERENCES

Alcaino, G., Liller, W., Alvarado, F., Kravtsov, V., Ipatov, A., & Samus, N. 1997, AJ, 114, 2638

Alonso-García, J., Mateo, M., Sen, B., Banerjee, M., & von Braun, K. 2011, AJ, 141, 146

Anderson, J., Bedin, L. R., Piotto, G., Yadav, R. S., & Bellini, A. 2006, A&A, 454, 1029

Anderson, J., Cool, A. M., & King, I. R. 2003, ApJ, 597, L137

Anderson, J., et al. 2008a, AJ, 135, 2055

Anderson, J., et al. 2008b, AJ, 135, 2114

Anthony-Twarog, B. J., Twarog, B. A., & Craig, J. 1995, PASP, 107, 32

Balbinot, E., Santiago, B. X., Bica, E. & Bonatto, C. 2009, MNRAS, 396, 1596

Barbuy, B., Bica, E., Ortolani, S., & Bonatto, C. 2006, A&A, 449, 1019

Barbuy, B., Ortolani, S., & Bica, E. 1994, A&A, 285, 871

Barbuy, B., Zoccali, M., Ortolani, S., Minniti, D., Hill, V., Renzini, A., Bica, E., & Gómez, A. 2007, AJ, 134, 1613

Bassa, C. G., Pooley, D., Verbunt, F., Homer, L., Anderson, S. F., & Lewin, W. H. G. 2008, A&A, 488, 921

Bassa, C., et al. 2004, ApJ, 609, 755

Beaulieu, S. F., Gilmore, G., Elson, R. A. W., Johnson, R. A., Santiago, B., Sigurdsson, S., & Tanvir, N. 2001, AJ, 121, 2618

Beccari, G., Ferraro, F. R., Possenti, A., Valenti, E., Origlia, L., & Rood, R. T. 2006, AJ, 131, 2551

Beccari, G., Pasquato, M., De Marchi, G., Dalessandro, E., Trenti, M., & Gill, M. 2010, ApJ, 713, 194

Bessell, M. S. 1979 PASP, 91, 589

Brocato, E., Buonanno, R., Malakhova, Y., & Piersimoni, A. M. 1996, A&A, 311, 778

Caloi, V. & D'Antona, F. 2011, arXiv1106.0810C

Cardelli, J. A., Clayton, G. C. & Mathis, J. S. 1989, ApJ, 345, 245

Carretta, E., et al. 2007, A&A, 464, 939

Carretta, E., Bragaglia, A., Gratton, R. G., Recio-Blanco, A., Lucatello, S., D'Orazi, V. & Cassisi, S. 2010, A&A, 516, A55

Cho, D.-H., & Lee, S.-G. 2002, AJ, 124, 977

Chun, S.-H., et al. 2010, A&A, 518, A15

Cocozza, G., Ferraro, F.R., Possenti, A., Beccari, G., Lanzoni, B., Ransom, S., Rood, R.T., & D'Amico, N. 2008, ApJ, 679, L105

Contreras, R., Catelan, M., Smith, H. A., Pritzl, B. J., & Borissova, J. 2005, ApJ, 623, L117

Contreras, R., Catelan, M., Smith, H. A., Pritzl, B. J., Borissova, J. & Kuehn, C. A. 2010, AJ, 140, 1766

Da Costa, G. S., Held, E. V., Saviane, I., & Gullieuszik, M. 2009, ApJ, 705, 1481

D'Antona, F. & Caloi, V. 2008, MNRAS, 390,693

Davidge, T. J. 2000, AJ, 120, 1853

Davidge, T. J. 2001, AJ, 121, 3100

Davidge, T. J., & Harris, W. E. 1996, ApJ, 462, 255

Davidge, T. J., Côté, P. & Harris, W. E. 1996, ApJ, 468, 641

Davis, D. S., Richer, H. B., Anderson, J., Brewer, J., Hurley, J., Kalirai, J. S., Rich, R. M., & Stetson, P. B. 2008, AJ, 135, 2155

de Angeli, F., Piotto, G., Cassisi, S., Busso, G., Recio-Blanco, A., Salaris, M., Aparicio, A., & Rosenberg, A. 2005, AJ, 130, 116

de Marchi, G., Paresce, F., & Pulone, L. 2000, ApJ, 530, 342

de Marchi, G., Pulone, L., & Paresce, F. 2006, A&A, 449, 161

Dolphin, A. E. 2000, PASP, 112, 1383

Faria, D., & Feltzing, S., 2002, in ASP Conf. Ser. 274, Observed HR Diagrams and Stellar Evolution, ed. T. Lejeune & J. Fernandes (San Francisco: ASP), 373

Ferdman, R. D., et al. 2004, AJ, 127, 380

Ferraro, F. R., Fusi-Pecci, F., Guarnieri, M. D., Moneti, A., Origlia, L., & Testa, V. 1994, MNRAS, 266, 829

Ferraro, F. R., Montegriffo, P., Origlia, L., & Fusi Pecci, F. 2000, AJ, 119, 1282

Fullton, L. K., Carney, B. W., Olszewski, E. W., Zinn, R., Demarque, P., Janes, K. A., Da Costa, G. S., & Seitzer, P. 1995, AJ, 110, 652

Fullton, L. K., Stetson, P. B., & Carney, B. W. 1999, Ap&SS, 265, 361

Gerashchenko, A. N., & Kadla, Z. 2004, A&AT, 23, 35

Gratton, R. G., Bragaglia, A., Carretta, E., Clementini, G., Desidera, S., Grundahl, F., & Lucatello, S. 2003, A&A, 408, 529

Gratton, R. G., Carretta, E., Bragaglia, A., Lucatello, S. & D'Orazi, V. 2010, A&A, 517, A81

Golden, A., Butler, R. F., & Shearer, A. 2001, A&A, 371, 198

Guarnieri, M. D., Ortolani, S., Montegriffo, P., Renzini, A., Barbuy, B., Bica, E., & Moneti, A. 1998, A&A, 331, 70

Guhathakurta, P., Yanny, B., Bahcall, J. N., & Schneider, D. P. 1996, in IAU Symp. 174, Dynamical Evolution of Star Clusters: Confrontation of Theory and Observations, ed. P. Hut & J. Makino (Dordrecht: Kluwer), 333

Hansen, B. M. S., et al. 2004, ApJS, 155, 551

Hargis, J. R., Sandquist, E. L., & Bolte, M. 2004, ApJ, 608, 243

Harris, W.E. 1996, AJ, 112, 1487

Heasley, J. N., Janes, K. A., Zinn, R., Demarque, P., Da Costa, G. S., & Christian, C. A. 2000, AJ, 120, 879

Heitsch, F., & Richtler, T. 1999, A&A, 347, 455

Howland, R., Sarajedini, A., Tiede, G. P., Gokas, T., Djagalov, R. & Martins, D. H. 2003, AJ, 125, 801

Hurley, J. R., et al. 2008, AJ, 135, 2129

Janes, K. A. & Heasley, J. N. 1991, AJ, 101, 2097

Kaluzny, J., Pietrukowicz, P., Thompson, I. B., Krzeminski, W., Schwarzenberg-Czerny, A., Pych, W., & Stachowski, G. 2005, MNRAS, 359, 677

Kaluzny, J., & Thompson, I. B. 2001, A&A, 373, 899

Kaluzny, J., Thompson, I. B., Krzeminski, W., & Schwarzenberg-Czerny, A. 2006, MNRAS, 365, 548

Kayser, A., Hilker, M., Grebel, E. K., & Willemsen, P. G. 2008, A&A, 486, 437

Kim, J.-W., et al. 2006, A&A, 459, 499

King, I. 1962, AJ, 67, 471

Lan, S-H., Kong, A. K. H., Verbunt, F., Lewin, W. H. G., Bassa, C., Anderson, S. F., & Pooley, D. 2010, ApJ, 712, 380

Landolt, A. U. 1992, AJ, 104, 340

Lanzoni, B., Dalessandro, E., Perina, S., Ferraro, F. R., Rood, R. T., & Sollima, A. 2007, ApJ, 670,1065

Lee, J.-W., & Carney, B. W. 2006, AJ, 132, 2171

Lee, J.-W., Carney, B. W., Fullton, L. K. & Stetson, P. B. 2001, AJ, 122, 3136

Lee, J.-W., Kang, Y.-W., Lee, J. & Lee, Y.-W. 2009, Nature, 462, 480

Lind, K., Charbonnel, C., Decressin, T., Primas, F., Grundahl, F. & Asplund, M. 2011, A&A, 527, A148

Marín-Franch, A., et al. 2009, ApJ, 694, 1498

Marino, A. F., Milone, A. P., Piotto, G., Villanova, S., Bedin, L. R., Bellini, A., & Renzini, A. 2009, A&A, 505, 1099

Marino, A. F., Villanova, S., Piotto, G., Milone, A. P., Momany, Y., Bedin, L. R., & Medling, A. M. 2008, A&A, 490, 625

Marino, A. F., Villanova, S., Milone, A. P., Piotto, G., Lind, K., Geisler, D. & Stetson, P. B. 2011, ApJ, 730, L16

Marino, A. F., et al. 2011, A&A, 532, A8

Melbourne, J., & Guhathakurta, P. 2004, AJ, 128, 271

Minniti, D., Olszewski, E. W., & Rieke, M. 1995, AJ, 110, 1686

Mochejska, B. J., Kaluzny, J., Thompson, I., & Pych, W. 2002, AJ, 124,1486

Monaco, L., Pancino, E., Ferraro, F. R., & Bellazzini, M. 2004, MNRAS, 349, 1278

Moretti, A., et al. 2009, A&A, 493, 539

Neely, R. K., Sarajedini, A., Martins, D. H. 2000, AJ, 119, 1793

Ortolani, S., Momany, Y., Bica, E., & Barbuy, B. 2000, A&A, 357, 495

Ortolani, S., Bica, E., & Barbuy, B. 2003, A&A, 402, 565

Pancino, E., Rejkuba, M, Zoccali, M., & Carrera, R. A&A, 524, A44

Piotto, G. 2009, IAU Symp., 258, 233

Piotto, G., & Zoccali, M. 1999, A&A, 345, 485

Piotto, G., Zoccali, M., King, I. R., Djorgovski, S. G., Sosin, C., Rich, R. M., & Meylan, G. 1999, AJ, 118, 1727

Piotto, G., et al. 2002, A&A, 391, 945

Pollard, D. L., Sandquist, E. L., Hargis, J. R., & Bolte, M. 2005, ApJ, 628, 729

Pulone, L., de Marchi, G., Covino, S., & Paresce, F. 2003, A&A, 399, 121

Pulone, L., de Marchi, G., & Paresce, F. 1999, A&A, 342, 440

Pych, W., Kaluzny, J., Krzeminski, W., Schwarzenberg-Czerny, A., & Thompson, I. B. 2001, A&A, 367, 148

Rich, R. M., Ortolani, S., Bica, E., & Barbuy, B. 1998, AJ, 116, 1295

Richer, H. B., et al. 2004, AJ, 127, 2771

Richer, H. B., et al. 2008, AJ, 135, 2141

Richter, P., Hilker, M., & Richtler, T. 1999, A&A, 350, 476

Richtler, T., Grebel, E. K., & Seggewiss, W. 1994, A&A, 290, 412

Robin, A. C., Reylé, C., Derrière, S., & Picaud, S. 2003, A&A, 409, 523

Rosenberg, A., Aparicio, A., Saviane, I., & Piotto, G. 2000a, A&AS, 144, 5

Rosenberg, A., Aparicio, A., Saviane, I., & Piotto, G. 2000b, A&AS, 145, 451

Sagar, R., Subramaniam, A., Richtler, T., & Grebel, E. K. 1999, A&AS, 135, 391

Salaris, M., Held, E. V., Ortolani, S., Gullieuszik, M., & Momany, Y. 2007, A&A, 476, 243

Sarajedini, A., Chaboyer, B., & Demarque, P. 1997, PASP, 109, 1321

Sarajedini, A., & Norris, J. E. 1994, ApJS, 93, 161

Sarajedini, A., et al. 2007, AJ, 133, 1658

Schechter, P., Mateo, M., & Saha, A. 1993, PASP, 105, 1342

Schlegel, D., Finkbeiner, D., & Davis, M. 1998, ApJ, 500, 525

Shara, M. M., Drissen, L., Rich, R. M., Paresce, F., King, I. R., & Meylan, G. 1998, ApJ, 495, 796

Sosin, C., & King, I. R. 1995, AJ, 109, 639

Stetson, P. B. 2000, PASP, 112, 925

Stetson, P. B., Vandenberg, D. A., & Bolte, M. 1996, PASP, 108, 560

Stetson, P. B., & West, M. J. 1994, PASP, 106, 726

Terndrup, D. M., Popowski, P., Gould, A., Rich, R. M., & Sadler, E. M. 1998, AJ, 115, 1476

Terndrup, D. M., & Walker, A. R. 1994, AJ, 107, 1786

Testa, V., Corsi, C. E., Andreuzzi, G., Iannicola, G., Marconi, G., Piersimoni, A. M., & Buonanno, R. 2001, AJ, 121, 916

Valenti, E., Ferraro, F. R., Perina, S., & Origlia, L. 2004a, A&A, 419, 139

Valenti, E., Ferraro, F. R., & Origlia, L. 2004b, MNRAS, 351, 1204

Valenti, E., Ferraro, F. R., & Origlia, L. 2007, AJ, 133, 1287

Valenti, E., Ferraro, F. R., & Origlia, L. 2010, MNRAS, 402, 1729

Valenti, E., Origlia, L., & Ferraro, F. R. 2005, MNRAS, 361, 272

von Braun, K., & Mateo, M. 2001 AJ, 121, 1522

von Braun, K., Mateo, M., Chiboucas, K., Athey, A., & Hurley-Keller, D. 2002, AJ, 124, 2067

Webb, N. A., Serre, D., Gendre, B., Barret, D., Lasota, J.-P., & Rizzi, L. 2004, A&A, 424, 133

Zloczewski, K., Kaluzny, J., & Thompson, I. B. 2011, MNRAS, 414, 3711

Zoccali, M., Renzini, A., Ortolani, S., Bica, E., & Barbuy, B. 2001, AJ, 121, 2638

Table 1. Characteristics of the GCs in our sample according to the 2010 version of the Harris (1996) GGC catalog.

Cluster name	l[1]	b[2]	R_{GC}[3]	$R_{\odot}$[4]	$[Fe/H]$	$E(B-V)$	$(m-M)_V$	V	r_t[5]
NGC 6121 (M 4)	350.97	15.97	5.9	2.2	-1.16	0.35	12.82	-7.19	51.82
NGC 6144	351.93	15.70	2.7	8.9	-1.76	0.36	15.86	-6.85	33.35
NGC 6218 (M 12)	15.72	26.31	4.5	4.8	-1.37	0.19	14.01	-7.31	17.28
NGC 6235	358.92	13.52	4.2	11.5	-1.28	0.31	16.26	-6.29	11.18
NGC 6254 (M 10)	15.14	23.08	4.6	4.4	-1.56	0.28	14.08	-7.48	18.47
NGC 6266 (M 62)	353.57	7.32	1.7	6.8	-1.18	0.47	15.63	-9.18	11.28
NGC 6273 (M 19)	356.87	9.38	1.7	8.8	-1.74	0.38	15.90	-9.13	14.57
NGC 6287	0.13	11.02	2.1	9.4	-2.10	0.60	16.72	-7.36	6.96
NGC 6304	355.83	5.38	2.3	5.9	-0.45	0.54	15.52	-7.30	13.25
NGC 6333 (M 9)	5.54	10.71	1.7	7.9	-1.77	0.38	15.67	-7.95	8.00
NGC 6342	4.90	9.72	1.7	8.5	-0.55	0.46	16.08	-6.42	15.81
NGC 6352	341.42	-7.17	3.3	5.6	-0.64	0.22	14.43	-6.47	10.44
NGC 6355	359.59	5.43	1.4	9.2	-1.37	0.77	17.21	-8.07	15.81
NGC 6397	338.17	-11.96	6.0	2.3	-2.02	0.18	12.37	-6.64	15.81
NGC 6522	1.02	-3.93	0.6	7.7	-1.34	0.48	15.92	-7.65	15.81
NGC 6541	349.29	-11.19	2.1	7.5	-1.81	0.14	14.82	-8.52	13.04
NGC 6553	5.26	-3.03	2.2	6.0	-0.18	0.63	15.83	-7.77	7.66
NGC 6558	0.20	-6.02	1.0	7.4	-1.32	0.44	15.70	-6.44	9.49
NGC 6624	2.79	-7.91	1.2	7.9	-0.44	0.28	15.36	-7.49	18.97
NGC 6626 (M 28)	7.80	-5.58	2.7	5.5	-1.32	0.40	14.95	-8.16	11.23
NGC 6637 (M 69)	1.72	-10.27	1.7	8.8	-0.64	0.18	15.28	-7.64	7.92

Table 1—Continued

Cluster name	l[1]	b[2]	R_{GC}[3]	$R_{\odot}$[4]	$[Fe/H]$	$E(B-V)$	$(m-M)_V$	V	r_t[5]
NGC 6642	9.81	-6.44	1.7	8.1	-1.26	0.40	15.79	-6.66	9.77
NGC 6656 (M 22)	9.89	-7.55	4.9	3.2	-1.70	0.34	13.60	-8.50	31.90
NGC 6681 (M 70)	2.85	-12.51	2.2	9.0	-1.62	0.07	14.99	-7.12	9.49
NGC 6809 (M 55)	8.79	-23.27	3.9	5.4	-1.94	0.08	13.89	-7.57	15.32

[1]Galactic longitude, in degrees.

[2]Galactic latitude, in degrees.

[3]Galactocentric distance, in kiloparsecs.

[4]Distance from the Sun, in kiloparsecs.

[5]Tidal radius, in arcminutes.

Table 2. Summary of the observations with the Magellan telescope.

Cluster	RA_{2000}[1]	Dec_{2000}[2]	UT Date	Filter	Exp. Time[3]	Airmass
NGC6121	16 23 40.0	-26 30 29.8	2005 Jun 2	B	$3\times1, 3\times25$	1.37-1.42
···	···	···	···	V	$3\times1, 3\times20$	1.43-1.48
···	···	···	···	I	$3\times1, 3\times15$	1.50-1.57
NGC6144	16 27 18.7	-26 00 28.4	2005 May 31	B	$3\times5, 3\times120$	1.38-1.52
···	···	···	···	V	$3\times5, 3\times120$	1.55-1.65
···	···	···	···	I	$1\times1, 3\times3, 3\times75$	1.77-1.92
NGC6218	16 47 18.6	-01 55 51.6	2005 Jun 1	B	$3\times5, 3\times120$	1.34-1.44
···	···	···	···	V	$3\times5, 3\times120$	1.46-1.55
···	···	···	···	I	$1\times1, 3\times3, 3\times75$	1.56-1.66
NGC6235	16 53 29.8	-22 09 37.8	2005 May 31	B	$3\times5, 3\times120$	1.19-1.27
···	···	···	···	V	$3\times5, 3\times120$	1.28-1.34
···	···	···	···	I	$1\times1, 3\times3, 3\times75$	1.36-1.44
NGC6254	16 57 13.0	-04 04 58.3	2005 Jun 1	B	$3\times5, 3\times120$	1.14-1.16
···	···	···	···	V	$3\times5, 3\times120$	1.17-1.20
···	···	···	···	I	$1\times1, 3\times3, 3\times75$	1.21-1.25
NGC6266	17 01 17.2	-30 05 42.8	2005 May 30	B	$3\times5, 3\times120$	1.01-1.02
···	···	···	···	V	$3\times5, 3\times120$	1.02-1.03
···	···	···	···	I	$1\times1, 3\times3, 3\times75$	1.03-1.04
NGC6273	17 02 41.5	-26 15 17.8	2005 May 30	B	$3\times5, 3\times120$	1.00
···	···	···	···	V	$3\times5, 3\times120$	1.00-1.01
···	···	···	···	I	$1\times1, 3\times3, 3\times75$	1.01

Table 2—Continued

Cluster	RA_{2000}[1]	Dec_{2000}[2]	UT Date	Filter	Exp. Time[3]	Airmass
NGC6287	17 05 13.8	-22 41 28.2	2005 Jun 2	B	$3\times5, 3\times120$	1.24-1.32
···	···	···	···	V	$3\times5, 3\times120$	1.33-1.42
···	···	···	···	I	$1\times1, 3\times3, 3\times75$	1.44-1.53
NGC6304	17 14 37.1	-29 26 43.2	2005 May 31	B	$3\times5, 3\times120$	1.06-1.08
···	···	···	···	V	$3\times5, 3\times120$	1.09-1.11
···	···	···	···	I	$1\times1, 3\times3, 3\times75$	1.12-1.15
NGC6333	17 19 16.1	-18 30 00.0	2005 Jun 2	B	$3\times5, 3\times120$	1.02-1.03
···	···	···	···	V	$3\times5, 3\times120$	1.02
···	···	···	···	I	$1\times1, 3\times3, 3\times75$	1.02
NGC6342	17 21 14.5	-19 34 13.1	2005 May 31	B	$3\times5, 3\times120$	1.04-1.06
···	···	···	···	V	$3\times5, 3\times120$	1.02-1.04
···	···	···	···	I	$1\times1, 3\times3, 3\times75$	1.02
NGC6355	17 24 03.1	-26 20 12.2	2005 Jun 2	B	$3\times5, 3\times120$	1.03-1.06
···	···	···	···	V	$3\times5, 3\times120$	1.06-1.09
···	···	···	···	I	$1\times1, 3\times3, 3\times75$	1.09-1.12
NGC6352	17 25 35.1	-48 24 20.40	2005 Jun 1	B	$3\times5, 3\times120$	1.06
···	···	···	···	V	$3\times5, 3\times120$	1.06-1.07
···	···	···	···	I	$1\times1, 3\times3, 3\times75$	1.08
NGC6397	17 40 48.2	-53 39 23.4	2005 May 31	B	$3\times1, 3\times25$	1.11
···	···	···	···	V	$3\times1, 3\times20$	1.10
···	···	···	···	I	$3\times1, 3\times15$	1.10

Table 2—Continued

Cluster	RA_{2000}[1]	Dec_{2000}[2]	UT Date	Filter	Exp. Time[3]	Airmass
···	···	···	2006 Apr 20	B	3×15	1.10
···	···	···	···	V	3×15	1.10
···	···	···	···	I	3×15	1.10
NGC6522	18 03 38.5	-30 00 59.6	2005 May 30	B	$3 \times 5, 3 \times 120$	1.01-1.02
···	···	···	···	V	$3 \times 5, 3 \times 120$	1.02-1.03
···	···	···	···	I	$1 \times 1, 3 \times 3, 3 \times 75$	1.04-1.05
NGC6541	18 08 07.8	-43 41 20.7	2005 May 31	B	$3 \times 5, 3 \times 120$	1.15-1.18
···	···	···	···	V	$3 \times 5, 3 \times 120$	1.18-1.22
···	···	···	···	I	$1 \times 1, 3 \times 3, 3 \times 75$	1.23-1.26
NGC6553	18 09 20.1	-25 53 26.6	2005 May 31	B	$3 \times 5, 3 \times 120$	1.02-1.03
···	···	···	···	V	$3 \times 5, 3 \times 120$	1.03-1.06
···	···	···	···	I	$1 \times 1, 3 \times 3, 3 \times 75$	1.07-1.09
NGC6558	18 10 23.1	-31 44 48.0	2005 May 30	B	$3 \times 5, 3 \times 120$	1.07-1.10
···	···	···	···	V	$3 \times 5, 3 \times 120$	1.11-1.13
···	···	···	···	I	$1 \times 1, 3 \times 3, 3 \times 75$	1.14-1.18
NGC6624	18 23 45.2	-30 20 39.7	2005 May 30	B	$3 \times 5, 3 \times 100$	1.21-1.24
···	···	···	···	V	$3 \times 5, 3 \times 100$	1.25-1.30
···	···	···	···	I	$1 \times 1, 3 \times 3, 3 \times 60$	1.31-1.36
NGC6626	18 24 37.3	-24 51 10.8	2005 Jun 2	B	$3 \times 5, 3 \times 120$	1.02-1.04
···	···	···	···	V	$3 \times 5, 3 \times 120$	1.04-1.05
···	···	···	···	I	$1 \times 1, 3 \times 3, 3 \times 75$	1.06-1.07

Table 2—Continued

Cluster	RA_{2000}[1]	Dec_{2000}[2]	UT Date	Filter	Exp. Time[3]	Airmass
NGC6637	18 31 28.0	-32 19 55.6	2005 Jun 2	B	$3 \times 5, 3 \times 120$	1.20-1.24
···	···	···	···	V	$3 \times 5, 3 \times 120$	1.25-1.30
···	···	···	···	I	$1 \times 1, 3 \times 3, 3 \times 75$	1.17-1.19
NGC6642	18 31 58.7	-23 27 36.0	2005 Jun 2	B	$3 \times 5, 3 \times 120$	1.36-1.43
···	···	···	···	V	$3 \times 5, 3 \times 120$	1.45-1.53
···	···	···	···	I	$1 \times 1, 3 \times 3, 3 \times 75$	1.56-1.67
NGC6656	18 36 28.6	-23 53 13.5	2005 May 31	B	$3 \times 1, 3 \times 35$	1.52-1.58
···	···	···	···	V	$3 \times 1, 3 \times 30$	1.45-1.51
···	···	···	···	I	$3 \times 1, 3 \times 20$	1.38-1.43
NGC6681	18 43 17.4	-32 16 29.7	2005 Jun 2	B	$3 \times 5, 3 \times 120$	1.00-1.01
···	···	···	···	V	$3 \times 5, 3 \times 120$	1.01-1.02
···	···	···	···	I	$1 \times 1, 3 \times 3, 3 \times 75$	1.02-1.03
NGC6809	19 40 04.1	-30 56 43.8	2005 May 31	B	$3 \times 1, 3 \times 35$	1.07-1.08
···	···	···	···	V	$3 \times 1, 3 \times 30$	1.09-1.10
···	···	···	···	I	$3 \times 1, 3 \times 20$	1.11-1.12

[1]Units of right ascension are hours, minutes, and seconds.

[2]Units of declination are degrees, arcminutes, and arcseconds.

[3]Number of exposures × exposure time, in seconds.

Table 3. Summary of ACS observations from Snapshot program 10573.

Cluster	α_{2000}[1]	δ_{2000}[2]	UT Date	Filter	Exp. Time[3]
NGC6218	16 47 14.50	-01 56 52.0	2006 Feb 1	B_{435}	120
...	...	...	...	V_{555}	50
...	...	...	...	I_{814}	20
NGC6333	17 19 11.80	-18 30 59.0	2006 May 31	B_{435}	2×340
...	...	...	...	V_{555}	240
...	...	...	...	I_{814}	90
NGC6553	18 09 17.50	-25 54 28.0	2006 Apr 4	B_{435}	3×340
...	...	...	...	V_{555}	300
...	...	...	...	I_{814}	60
NGC6624	18 23 40.70	-30 21 39.0	2006 Jun 5	B_{435}	360
...	...	...	...	V_{555}	160
...	...	...	...	I_{814}	65
NGC6637	18 31 23.20	-32 20 53.0	2006 Jun 6	B_{435}	300
...	...	...	...	V_{555}	120
...	...	...	...	I_{814}	50

[1]Units of right ascension are hours, minutes, and seconds.

[2]Units of declination are degrees, arcminutes, and arcseconds.

[3]Number of exposures $\times$ exposure time, in seconds.

Table 4. Summary of *HST* programs whose archival data have been used in our analysis.

Cluster	Camera	Program	Filters
NGC6121	WFPC2	6116	V_{555}, I_{814}
···	ACS	10775	V_{606}, I_{814}
NGC6144	WFPC2	11014	B_{439}, R_{675}
···	ACS	10775	V_{606}, I_{814}
NGC6218	WFPC2	8118	B_{439}, V_{555}
···	ACS	10775	V_{606}, I_{814}
NGC6235	WFPC2	7470	B_{439}, V_{555}
···	ACS	···	···
NGC6254	WFPC2	6113	V_{606}, I_{814}
···	ACS	10775	V_{606}, I_{814}
NGC6266	WFPC2	8118	B_{439}, V_{555}
···	WFPC2	8709	V_{555}, I_{814}
···	ACS	···	···
NGC6273	WFPC2	7470	B_{439}, V_{555}
···	ACS	···	···
NGC6287	WFPC2	6561	$B_{439}, V_{555}, I_{814}$
···	ACS	···	···
NGC6304	WFPC2	7470	B_{439}, V_{555}
···	ACS	10775	V_{606}, I_{814}
NGC6333	WFPC2	5366	V_{555}, I_{814}
···	ACS	···	···

Table 4—Continued

Cluster	Camera	Program	Filters
NGC6342	WFPC2	7470	B_{439}, V_{555}
···	ACS	···	···
NGC6352	WFPC2	5366	V_{555}, I_{814}
···	ACS	10775	V_{606}, I_{814}
NGC6355	WFPC2	7470	B_{439}, V_{555}
···	ACS	···	···
NGC6397	WFPC2	5929	B_{439}, V_{555}
···	WFPC2	7335	V_{555}, I_{814}
···	ACS	10775	V_{606}, I_{814}
NGC6522	WFPC2	6095	B_{439}, V_{555}
···	ACS	···	···
NGC6541	WFPC2	5366	V_{555}, I_{814}
···	ACS	10775	V_{606}, I_{814}
NGC6553	WFPC2	7307	V_{555}, I_{814}
···	ACS	···	···
NGC6558	WFPC2	···	···
···	ACS	9799	V_{606}, I_{814}
NGC6624	WFPC2	5324	B_{439}, V_{555}
···	WFPC2	5366	V_{555}, I_{814}
···	ACS	10775	V_{606}, I_{814}
NGC6626	WFPC2	6779	V_{555}, I_{814}

Table 4—Continued

Cluster	Camera	Program	Filters
···	ACS	···	···
NGC6637	WFPC2	8118	B_{439}, V_{555}
···	WFPC2	5366	V_{555}, I_{814}
···	ACS	10775	V_{606}, I_{814}
NGC6642	WFPC2	8118	B_{439}, V_{555}
···	ACS	9799	V_{606}, I_{814}
NGC6656	WFPC2	5344	B_{439}, R_{675}
···	WFPC2	7615	V_{606}, I_{814}
···	ACS	10775	V_{606}, I_{814}
NGC6681	WFPC2	8723	B_{439}, V_{555}
···	ACS	10775	V_{606}, I_{814}
NGC6809	WFPC2	···	···
···	ACS	10775	V_{606}, I_{814}

Table 5. Limits for the stars used in our analysis.

Cluster	V_{CL}[a]	ΔV_{CL}[b]	$R_{0.1}$[c]
NGC 6121	20.70	1.9	···
NGC 6144	22.33	1.7	···
NGC 6218	21.72	1.8	···
NGC 6235	22.65	2.1	5.37
NGC 6254	22.07	1.9	···
NGC 6266	21.51	2.2	6.84
NGC 6273	21.80	2.3	8.26
NGC 6287	21.90	2.2	4.13
NGC 6304	21.70	2.9	3.65
NGC 6333	22.29	2.2	5.59
NGC 6342	22.42	2.3	4.21
NGC 6352	21.86	2.3	5.61
NGC 6355	21.99	2.2	2.36
NGC 6397	20.80	2.1	8.18
NGC 6522	21.04	3.4	2.33
NGC 6541	22.30	2.0	8.63
NGC 6553	21.35	2.4	3.91
NGC 6558	21.48	3.1	1.81
NGC 6624	21.54	2.7	3.92
NGC 6626	21.04	2.7	4.95
NGC 6637	20.98	2.2	4.39

Table 5—Continued

Cluster	V_{CL}[a]	ΔV_{CL}[b]	$R_{0.1}$[c]
NGC 6642	19.99	1.9	2.22
NGC 6656	20.76	2.4	···
NGC 6681	21.98	2.2	5.21
NGC 6809	21.89	2.0	···

[a]V magnitude where the completeness limit is reached.

[b]ΔV between the completeness limit and our dimmest observation for that cluster.

[c]Distance, in arcmin, from the center of the cluster where $P(X = 1|r) = 0.1$. No distance given if the limit of the camera FOV is reached.

Table 6. Paremeters used to obtain and fit the empirical King (1962) models.

Cluster	r_c[a]	r_t[b]	k[c]	c_f[d]	c_B[e]
NGC 6121	1.16	51.82	1069.8	22.4	14.2
NGC 6144	0.94	33.35	1067.8	11.9	36.5
NGC 6218	0.79	17.28	5336.6	4.4	8.1
NGC 6235	0.33	11.18	6140.2	56.2	82.3
NGC 6254	0.77	18.47	8905.6	13.0	13.3
NGC 6266	0.22	11.28	153639.3	221.3	222.8
NGC 6273	0.43	14.57	35673.5	162.9	154.8
NGC 6287	0.29	6.96	8549.7	62.8	66.1
NGC 6304	0.21	13.25	37443.9	586.8	548.4
NGC 6333	0.45	8.00	27214.7	143.0	125.8
NGC 6342	0.05	15.81	241666.3	165.2	145.6
NGC 6352	0.83	10.44	3042.5	123.7	177.5
NGC 6355	0.05	15.81	127282.0	374.7	650.0
NGC 6397	0.05	15.81	771500.0	60.4	40.5
NGC 6522	0.05	15.81	321899.2	972.0	1277.3
NGC 6541	0.18	13.04	190598.4	85.3	119.5
NGC 6553	0.53	7.66	11152.9	428.5	681.1
NGC 6558	0.03	9.49	376029.8	609.4	903.8
NGC 6624	0.06	18.97	232671.2	310.2	415.1
NGC 6626	0.24	11.23	57055.1	377.1	414.6
NGC 6637	0.33	7.92	11542.9	115.4	146.5

Table 6—Continued

Cluster	r_c[a]	r_t[b]	k[c]	c_f[d]	c_B[e]
NGC 6642	0.10	9.77	4603.9	111.9	152.4
NGC 6656	1.33	31.90	4607.3	159.8	134.6
NGC 6681	0.03	9.49	1660360.2	101.5	118.6
NGC 6809	1.80	15.32	3253.0	17.9	17.0

[a]Core radius, in arcminutes, according to 2010 version of Harris (1996) catalog.

[b]Tidal radius, in arcminutes, according to 2010 version of Harris (1996) catalog.

[c]k constant from the fitted King (1962) profile.

[c]Density of non-member field stars from the fit.

[c]Density of non-member field stars according to the Besançon model.

Table 7. Parameters used to obtain the Besançon model for the non-cluster stars in the observed fields.

NGC 6121	
Field of view	
Field	Small field
	l=350.97°; b=15.97°
	Solid angle=2.100 square degree
Extinction law	
Diffuse extinction	0.0 mag/kpc
Discrete clouds	A_v=1.30; Distance=0pc
Selection on	
Intervals of magnitude	$15.04 \leq B \leq 24.48$
	$14.56 \leq V \leq 22.58$
	$13.18 \leq I \leq 22.53$
Photometric errors	Error function: Exponential
	Band=B; A=0.006, B=21.75, C=0.861
	Band=V; A=0.006, B=22.24, C=0.901
	Band=I; A=0.007, B=23.66, C=0.997
NGC 6144	
Field of view	
Field	Small field
	l=351.93°; b=15.70°
	Solid angle=1.350 square degree

Table 7—Continued

Extinction law	
Diffuse extinction	0.0 mag/kpc
Discrete clouds	A_v=1.88; Distance=0pc
Selection on	
Intervals of magnitude	$16.59 \leq B \leq 25.64$
	$16.05 \leq V \leq 24.13$
	$14.73 \leq I \leq 23.54$
Photometric errors	Error function: Exponential
	Band=B; A=0.005, B=23.11, C=0.864
	Band=V; A=0.005, B=24,35, C=0.938
	Band=I; A=0.009, B=25.36, C=1.043
NGC 6218	
Field of view	
Field	Small field
	l=15.72°; b=26.31°
	Solid angle=6.108 square degree
Extinction law	
Diffuse extinction	0.0 mag/kpc
Discrete clouds	A_v=0.67; Distance=0pc
Selection on	
Intervals of magnitude	$14.99 \leq B \leq 25.03$

Table 7—Continued

	$14.75 \leq V \leq 23.52$
	$14.04 \leq I \leq 22.80$
Photometric errors	Error function: Exponential
	Band=B; A=0.004, B=22.20, C=0.838
	Band=V; A=0.003, B=21.25, C=0.803
	Band=I; A=0.004, B=23.20, C=0.940
NGC 6235	
Field of view	
Field	Small field
	l=358.92°; b=13.52°
	Solid angle=0.610 square degree
Extinction law	
Diffuse extinction	0.0 mag/kpc
Discrete clouds	A_v=1.31; Distance=0pc
Selection on	
Intervals of magnitude	$17.14 \leq B \leq 26.09$
	$16.79 \leq V \leq 24.74$
	$15.70 \leq I \leq 24.05$
Photometric errors	Error function: Exponential
	Band=B; A=0.008, B=24.42, C=0.904
	Band=V; A=0.010, B=26.45, C=1.000

Table 7—Continued

	Band=I; A=0.012, B=26,95, C=1.068
NGC 6254	
Field of view	
Field	Small field
	l=15.14°; b=23.08°
	Solid angle=3.910 square degree
Extinction law	
Diffuse extinction	0.0 mag/kpc
Discrete clouds	A_v=0.77; Distance=0pc
Selection on	
Intervals of magnitude	$15.50 \leq B \leq 25.29$
	$15.54 \leq V \leq 23.97$
	$14.78 \leq I \leq 23.37$
Photometric errors	Error function: Exponential
	Band=B; A=0.005, B=22.33, C=0.839
	Band=V; A=0.004, B=22.32, C=0.840
	Band=I; A=0.005, B=24.38, C=0.969
NGC 6266	
Field of view	
Field	Small field
	l=353.57°; b=7.32°

Table 7—Continued

	Solid angle=0.190 square degree
Extinction law	
Diffuse extinction	0.0 mag/kpc
Discrete clouds	A_v=1.38; Distance=0pc
Selection on	
Intervals of magnitude	$15.75 \leq B \leq 25.14$
	$15.56 \leq V \leq 23.71$
	$14.75 \leq I \leq 22.44$
Photometric errors	Error function: Exponential
	Band=B; A=0.006, B=22.68, C=0.866
	Band=V; A=0.005, B=23.22, C=0.899
	Band=I; A=0.009, B=30.12, C=1.238
NGC 6273	
Field of view	
Field	Small field
	l=356.87°; b=9.38°
	Solid angle=0.280 square degree
Extinction law	
Diffuse extinction	0.0 mag/kpc
Discrete clouds	A_v=1.22; Distance=0pc
Selection on	

Table 7—Continued

Intervals of magnitude	$16.38 \leq B \leq 25.59$
	$16.09 \leq V \leq 24.08$
	$15.46 \leq I \leq 23.09$
Photometric errors	Error function: Exponential
	Band=B; A=0.007, B=21.67, C=0.820
	Band=V; A=0.007, B=22.70, C=0.873
	Band=I; A=0.010, B=24.54, C=1.002
NGC 6287	
Field of view	
Field	Small field
	l=0.13°; b=11.02°
	Solid angle=0.600 square degree
Extinction law	
Diffuse extinction	0.0 mag/kpc
Discrete clouds	A_v=2.08; Distance=0pc
Selection on	
Intervals of magnitude	$16.77 \leq B \leq 25.46$
	$16.05 \leq V \leq 24.11$
	$14.66 \leq I \leq 23.37$
Photometric errors	Error function: Exponential
	Band=B; A=0.004, B=23.65, C=0.890

Table 7—Continued

	Band=V; A=0.007, B=25.91, C=0.998
	Band=I; A=0.007, B=26.72, C=1.088
NGC 6304	
Field of view	
Field	Small field
	l=355.83°; b=5.38°
	Solid angle=0.064 square degree
Extinction law	
Diffuse extinction	0.0 mag/kpc
Discrete clouds	A_v=1.80; Distance=0pc
Selection on	
Intervals of magnitude	$17.45 \leq B \leq 25.87$
	$16.78 \leq V \leq 24.56$
	$15.34 \leq I \leq 23.80$
Photometric errors	Error function: Exponential
	Band=B; A=0.005, B=22.25, C=0.826
	Band=V; A=0.010, B=26.91, C=1.019
	Band=I; A=0.010, B=26.82, C=1.084
NGC 6333	
Field of view	
Field	Small field

Table 7—Continued

	l=5.54°; b=10.70°
	Solid angle=0.380 square degree
Extinction law	
Diffuse extinction	0.0 mag/kpc
Discrete clouds	A_v=1.18; Distance=0pc
Selection on	
Intervals of magnitude	$16.04 \leq B \leq 26.11$
	$15.41 \leq V \leq 24.50$
	$14.50 \leq I \leq 23.54$
Photometric errors	Error function: Exponential
	Band=B; A=0.006, B=22.93, C=0.844
	Band=V; A=0.006, B=23.22, C=0.882
	Band=I; A=0.015, B=29.32, C=1.192
NGC 6342	
Field of view	
Field	Small field
	l=4.90°; b=9.73°
	Solid angle=0.290 square degree
Extinction law	
Diffuse extinction	0.0 mag/kpc
Discrete clouds	A_v=1.64; Distance=0pc

Table 7—Continued

Selection on	
Intervals of magnitude	$16.95 \leq B \leq 26.11$
	$16.31 \leq V \leq 24.73$
	$15.12 \leq I \leq 23.44$
Photometric errors	Error function: Exponential
	Band=B; A=0.006, B=24.15, C=0.890
	Band=V; A=0.007, B=25.10, C=0.956
	Band=I; A=0.012, B=27.68, C=1.113
NGC 6352	
Field of view	
Field	Small field
	l=341.42°; b=−7.17°
	Solid angle=0.290 square degree
Extinction law	
Diffuse extinction	0.0 mag/kpc
Discrete clouds	A_v=0.94; Distance=0pc
Selection on	
Intervals of magnitude	$15.72 \leq B \leq 25.32$
	$15.18 \leq V \leq 24.20$
	$14.53 \leq I \leq 23.52$
Photometric errors	Error function: Exponential

Table 7—Continued

	Band=B; A=0.005, B=22.31, C=0.837
	Band=V; A=0.006, B=24.13, C=0.915
	Band=I; A=0.008, B=25.71, C=1.033
NGC 6355	
Field of view	
Field	Small field
	l=359.58°; b=5.43°
	Solid angle=0.064 square degree
Extinction law	
Diffuse extinction	0.0 mag/kpc
Discrete clouds	A_v=2.26; Distance=0pc
Selection on	
Intervals of magnitude	$16.55 \leq B \leq 25.83$
	$15.50 \leq V \leq 24.20$
	$14.03 \leq I \leq 23.21$
Photometric errors	Error function: Exponential
	Band=B; A=0.004, B=23.31, C=0.864
	Band=V; A=0.004, B=22.92, C=0.869
	Band=I; A=0.005, B=24.39, C=0.992
NGC 6397	
Field of view	

Table 7—Continued

Field	Small field
	l=338.17°; b=−11.96°
	Solid angle=1.110 square degree
Extinction law	
Diffuse extinction	0.0 mag/kpc
Discrete clouds	A_v=0.54; Distance=0pc
Selection on	
Intervals of magnitude	$13.26 \leq B \leq 24.53$
	$13.08 \leq V \leq 22.74$
	$12.77 \leq I \leq 22.82$
Photometric errors	Error function: Exponential
	Band=B; A=0.005, B=21.61, C=0.849
	Band=V; A=0.004, B=21.13, C=0.838
	Band=I; A=0.009, B=26.54, C=1.121
NGC 6522	
Field of view	
Field	Small field
	l=1.02°; b=−3.93°
	Solid angle=0.064 square degree
Extinction law	
Diffuse extinction	0.0 mag/kpc

Table 7—Continued

Discrete clouds	A_v=1.61; Distance=0pc
Selection on	
Intervals of magnitude	$16.65 \leq B \leq 25.79$
	$16.23 \leq V \leq 24.47$
	$14.98 \leq I \leq 22.91$
Photometric errors	Error function: Exponential
	Band=B; A=0.006, B=21.53, C=0.796
	Band=V; A=0.008, B=22.16, C=0.840
	Band=I; A=0.014, B=25.32, C=1.032
NGC 6541	
Field of view	
Field	Small field
	l=349.48°; b=−11.09°
	Solid angle=0.450 square degree
Extinction law	
Diffuse extinction	0.0 mag/kpc
Discrete clouds	A_v=0.63; Distance=0pc
Selection on	
Intervals of magnitude	$15.53 \leq B \leq 25.53$
	$15.18 \leq V \leq 24.30$
	$14.64 \leq I \leq 23.41$

Table 7—Continued

Photometric errors	Error function: Exponential
	Band=B; A=0.006, B=22.55, C=0.841
	Band=V; A=0.005, B=22.44, C=0.848
	Band=I; A=0.005, B=22.51, C=0.898
NGC 6553	
Field of view	
Field	Small field
	l=5.25°; b=−3.03°
	Solid angle=0.064 square degree
Extinction law	
Diffuse extinction	0.0 mag/kpc
Discrete clouds	A_v=2.76; Distance=0pc
Selection on	
Intervals of magnitude	$17.08 \leq B \leq 25.31$
	$16.21 \leq V \leq 23.86$
	$14.71 \leq I \leq 22.48$
Photometric errors	Error function: Exponential
	Band=B; A=0.004, B=22.80, C=0.848
	Band=V; A=0.006, B=26.89, C=1.041
	Band=I; A=0.007, B=26.60, C=1.102
NGC 6558	

Table 7—Continued

Field of view	
Field	Small field
	l=0.20°; b=−6.02°
	Solid angle=0.064 square degree
Extinction law	
Diffuse extinction	0.0 mag/kpc
Discrete clouds	A_v=1.21; Distance=0pc
Selection on	
Intervals of magnitude	$16.64 \leq B \leq 26.26$
	$15.92 \leq V \leq 24.61$
	$15.17 \leq I \leq 23.23$
Photometric errors	Error function: Exponential
	Band=B; A=0.005, B=22.21, C=0.823
	Band=V; A=0.007, B=22.81, C=0.858
	Band=I; A=0.008, B=24.07, C=0.968
NGC 6624	
Field of view	
Field	Small field
	l=2.79°; b=−7.91°
	Solid angle=0.064 square degree
Extinction law	

Table 7—Continued

Diffuse extinction	0.0 mag/kpc
Discrete clouds	A_v=0.94; Distance=0pc
Selection on	
Intervals of magnitude	$16.30 \leq B \leq 25.44$
	$15.87 \leq V \leq 24.25$
	$14.73 \leq I \leq 23.31$
Photometric errors	Error function: Exponential
	Band=B; A=0.005, B=22.26, C=0.842
	Band=V; A=0.005, B=22.86, C=0.871
	Band=I; A=0.007, B=23.60, C=0.956
NGC 6626	
Field of view	
Field	Small field
	l=7.80°; b=−5.58°
	Solid angle=0.064 square degree
Extinction law	
Diffuse extinction	0.0 mag/kpc
Discrete clouds	A_v=1.50; Distance=0pc
Selection on	
Intervals of magnitude	$16.33 \leq B \leq 25.36$
	$15.67 \leq V \leq 23.69$

Table 7—Continued

	$14.63 \leq I \leq 22.79$
Photometric errors	Error function: Exponential
	Band=B; A=0.003, B=21.36, C=0.801
	Band=V; A=0.005, B=22.78, C=0.874
	Band=I; A=0.006, B=23.20, C=0.961
NGC 6637	
Field of view	
Field	Small field
	l=1.72°; b=−10.27°
	Solid angle=0.270 square degree
Extinction law	
Diffuse extinction	0.0 mag/kpc
Discrete clouds	A_v=0.68; Distance=0pc
Selection on	
Intervals of magnitude	$15.30 \leq B \leq 24.66$
	$14.76 \leq V \leq 23.16$
	$14.09 \leq I \leq 22.53$
Photometric errors	Error function: Exponential
	Band=B; A=0.004, B=22.40, C=0.861
	Band=V; A=0.003, B=21.74, C=0.852
	Band=I; A=0.004, B=23.30, C=0.956

Table 7—Continued

NGC 6642	
Field of view	
Field	Small field
	l=9.81°; b=−6.44°
	Solid angle=0.194 square degree
Extinction law	
Diffuse extinction	0.0 mag/kpc
Discrete clouds	A_v=1.28; Distance=0pc
Selection on	
Intervals of magnitude	$13.96 \leq B \leq 23.38$
	$13.47 \leq V \leq 21.95$
	$12.29 \leq I \leq 20.73$
Photometric errors	Error function: Exponential
	Band=B; A=0.002, B=21.83, C=0.874
	Band=V; A=0.003, B=22.85, C=0.941
	Band=I; A=0.002, B=20.68, C=0.917
NGC 6656	
Field of view	
Field	Small field
	l=9.89°; b=−7.55°
	Solid angle=0.190 square degree

Table 7—Continued

Extinction law	
Diffuse extinction	0.0 mag/kpc
Discrete clouds	A_v=1.05; Distance=0pc
Selection on	
Intervals of magnitude	$14.69 \leq B \leq 24.35$
	$14.30 \leq V \leq 23.19$
	$13.42 \leq I \leq 22.01$
Photometric errors	Error function: Exponential
	Band=B; A=0.006, B=21.32, C=0.847
	Band=V; A=0.006, B=22.88, C=0.904
	Band=I; A=0.008, B=24.26, C=1.018
NGC 6681	
Field of view	
Field	Small field
	l=2.85°; b=−12.51°
	Solid angle=0.400 square degree
Extinction law	
Diffuse extinction	0.0 mag/kpc
Discrete clouds	A_v=0.56; Distance=0pc
Selection on	
Intervals of magnitude	$15.90 \leq B \leq 25.17$

Table 7—Continued

	$15.43 \leq V \leq 24.17$
	$14.74 \leq I \leq 23.98$
Photometric errors	Error function: Exponential
	Band=B; A=0.004, B=22.00, C=0.826
	Band=V; A=0.006, B=23.99, C=0.914
	Band=I; A=0.007, B=24.79, C=0.980
NGC 6809	
Field of view	
Field	Small field
	l=8.80°; b=−23.27°
	Solid angle=2.950 square degree
Extinction law	
Diffuse extinction	0.0 mag/kpc
Discrete clouds	A_v=0.24; Distance=0pc
Selection on	
Intervals of magnitude	$14.65 \leq B \leq 25.15$
	$14.46 \leq V \leq 23.87$
	$14.19 \leq I \leq 23.03$
Photometric errors	Error function: Exponential
	Band=B; A=0.007, B=21.42, C=0.826
	Band=V; A=0.006, B=21.74, C=0.842

Table 7—Continued

Band=I; A=0.009, B=22.33, C=0.909

Table 8. Zero points to bring the photometry to the chip 2 system.

Chip	Z_B	$\Delta Y'_B$	Z_V	$\Delta Y'_V$	Z_I	$\Delta Y'_I$
1	-0.164	0.063	-0.160	0.075	-0.036	0.077
2	0.0	0.0	0.0	0.0	0.0	0.0
3	-0.107	0.005	-0.119	0.008	-0.017	0.016
4	-0.767	0.048	-0.706	0.043	-0.445	0.078
5	-0.010	0.019	0.013	0.014	0.083	0.008
6	-0.137	0.010	-0.173	0.006	-0.118	0.021
7	-0.268	0.023	-0.260	0.013	-0.185	0.052
8	-0.212	0.055	-0.169	0.042	-0.028	0.044

Table 9. Calibrating-star photometry available for the sampled clusters.

Cluster	Stetson[1]	WFPC2[2]	ACS[3]	ACS-10573[4]	*HST* missing[5]	Missing[6]
NGC6121	BVI	VI	VI	···	B	···
NGC6144	···	B	VI	···	···	···
NGC6218	BVI	BV	VI	BVI	···	···
NGC6235	···	BV	···	···	I	I
NGC6254	BVI	VI	VI	···	B	···
NGC6266	BVI	BVI	···	···	···	···
NGC6273	BVI	BV	···	···	I	···
NGC6287	BV	BVI	···	···	···	···
NGC6304	···	BV	VI	···	···	···
NGC6333	···	VI	···	BVI	···	···
NGC6342	···	BV	···	···	I	I
NGC6355	···	BV	···	···	I	I
NGC6352	BVI	VI	VI	···	B	···
NGC6397	BVI	BVI	VI	···	···	···
NGC6522	BVI	BV	···	···	I	···
NGC6541	BVI	VI	VI	···	B	···
NGC6553	···	VI	···	BVI	···	···
NGC6558	···	···	VI	···	B	B
NGC6624	···	BVI	VI	BVI	···	···
NGC6626	···	BVI	···	···	···	···
NGC6637	···	BVI	VI	BVI	···	···

Table 9—Continued

Cluster	Stetson[1]	WFPC2[2]	ACS[3]	ACS-10573[4]	*HST* missing[5]	Missing[6]
NGC6642	···	BV	VI	···	···	···
NGC6656	BVI	BVI	VI	···	···	···
NGC6681	BVI	BV	VI	···	···	···
NGC6809	BVI	···	VI	···	B	···

[1]Stetson (2000) calibrating stars observed in these specific Johnson-Cousin filters.

[2]*HST* WFPC2 photometry from archival data available in the specified filters. The filters are $f439w$, $f555w$, $f606w$, and $f814w$, and they are transformed by HSTPHOT to the Johnson-Cousins B, V, and I.

[3]*HST* ACS photometry from archival data available in the specified filters. The filters are $f606w$ and $f814w$, and they are transformed by DolPHOT to the Johnson-Cousins B, V, and I.

[4]*HST* ACS photometry from our project (SNAP 10573) available in the specified filters. The filters are $f435w$, $f555w$, and $f814w$, and they are transformed by DolPHOT to the Johnson-Cousins B, V, and I.

[5]*HST* photometry for the cluster in the filter specified is missing.

[6]*HST* photometry and Stetson calibrating stars for the cluster in the filter

specified are missing.

Table 10. Offsets applied to transform to Johnson-Cousins system photometry.

	Offset in B	Offset in V	Offset in I
Night 1			
NGC 6266	*−0.44 ± 0.02*	*−0.40 ± 0.02*	*−0.28 ± 0.02*
NGC 6273	*0.06 ± 0.02*	*−0.10 ± 0.03*	*0.00 ± 0.03*
NGC 6522	*−0.07 ± 0.03*	*−0.06 ± 0.01*	*0.04 ± 0.02*
NGC 6558	···	−0.06 ± 0.01	−0.05 ± 0.01
NGC 6624	0.01 ± 0.02	−0.03 ± 0.01	−0.04 ± 0.01
Night 2			
NGC 6144	−0.01 ± 0.02	−0.13 ± 0.02	−0.10 ± 0.02
NGC 6235	−0.10 ± 0.02	−0.05 ± 0.02	···
NGC 6304	0.02 ± 0.02	−0.02 ± 0.01	0.01 ± 0.02
NGC 6342	0.02 ± 0.02	−0.13 ± 0.03	···
NGC 6397	*0.01 ± 0.02*	*0.01 ± 0.01*	*−0.03 ± 0.01*
NGC 6541	*0.05 ± 0.04*	*0.01 ± 0.02*	*0.00 ± 0.02*
NGC 6553	0.16 ± 0.07	0.05 ± 0.03	0.06 ± 0.02
NGC 6656	*0.07 ± 0.02*	*0.02 ± 0.02*	*−0.02 ± 0.02*
NGC 6809	*0.04 ± 0.02*	*0.04 ± 0.01*	*0.05 ± 0.02*
Night 3			
NGC 6218	*0.08 ± 0.01*	*−0.06 ± 0.01*	*−0.01 ± 0.01*
NGC 6254	*−0.02 ± 0.02*	*−0.02 ± 0.01*	*−0.05 ± 0.01*
NGC 6352	*−0.05 ± 0.02*	*−0.15 ± 0.02*	*−0.15 ± 0.01*
Night 4			

Table 10—Continued

	Offset in B	Offset in V	Offset in I
NGC 6121	*-0.02 ± 0.02*	*-0.38 ± 0.02*	*-0.21 ± 0.02*
NGC 6287	*-0.14 ± 0.03*	*-0.38 ± 0.03*	-0.05 ± 0.02
NGC 6333	-0.03 ± 0.03	-0.05 ± 0.02	-0.17 ± 0.02
NGC 6355	-0.20 ± 0.02	-0.09 ± 0.02	$\cdots$
NGC 6626	-0.13 ± 0.02	-0.21 ± 0.03	-0.46 ± 0.02
NGC 6637	-0.27 ± 0.03	-0.46 ± 0.02	-0.20 ± 0.02
NGC 6642	-0.64 ± 0.03	-1.25 ± 0.02	-1.42 ± 0.02
NGC 6681	*-0.13 ± 0.01*	*-0.25 ± 0.02*	*-0.10 ± 0.02*

Note. — The numbers in italic correspond to the straight comparison between the data from Stetson (2000) and our data. The numbers in standard type correspond to the comparison between our data and the *HST* data, plus the offset between *HST* data and Stetson's data. The errors reported are the dispersions of the distributions from which the offsets were calculated, which inform about the absolute precision of the photometry of individual stars.

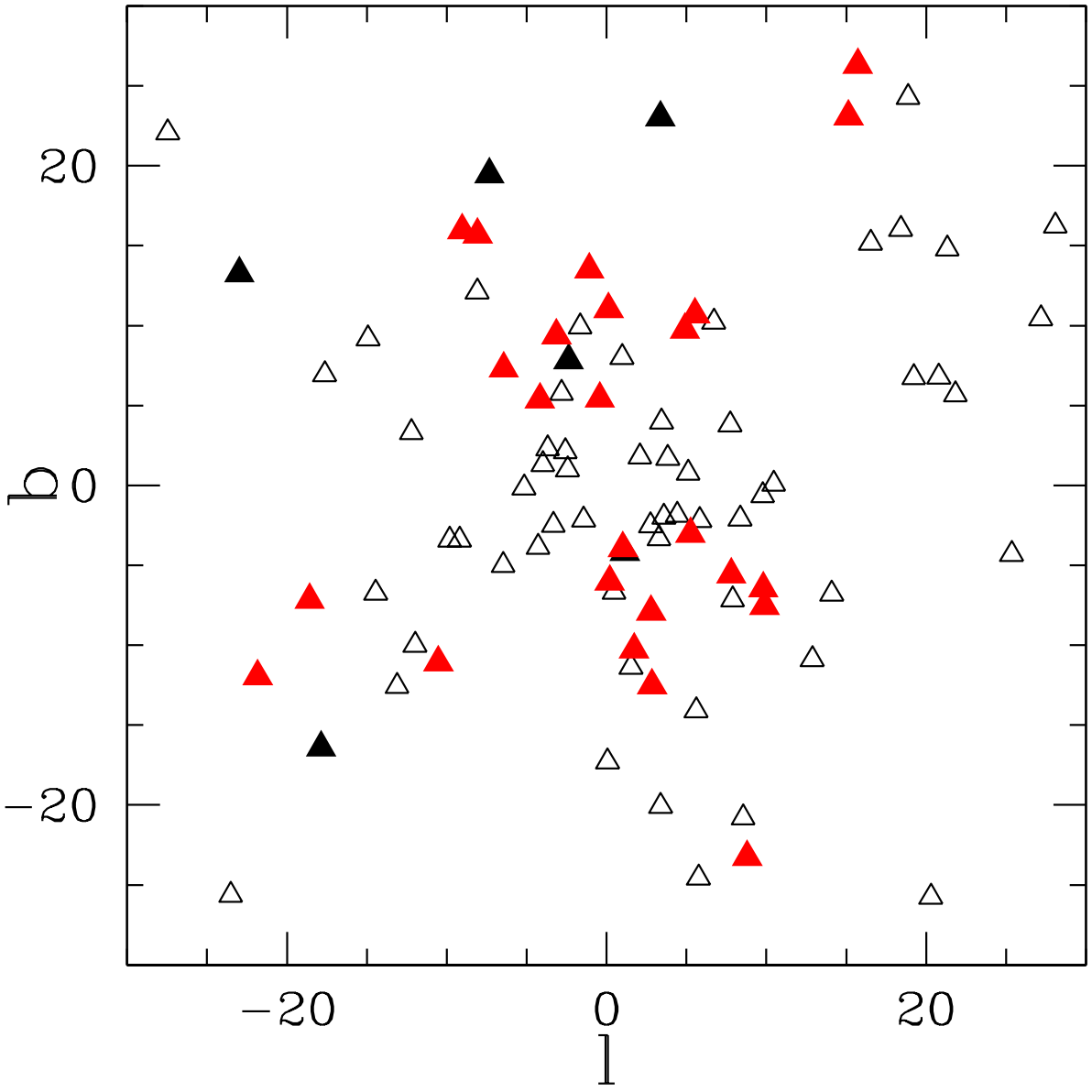

Fig. 1.— Location, in galactic coordinates, of the clusters that follow the criteria to belong to our sample (solid triangles) and the rest of the inner GGCs (open triangles). The position of the 25 GGCs that we were able to observe and comprise our final sample is in red.

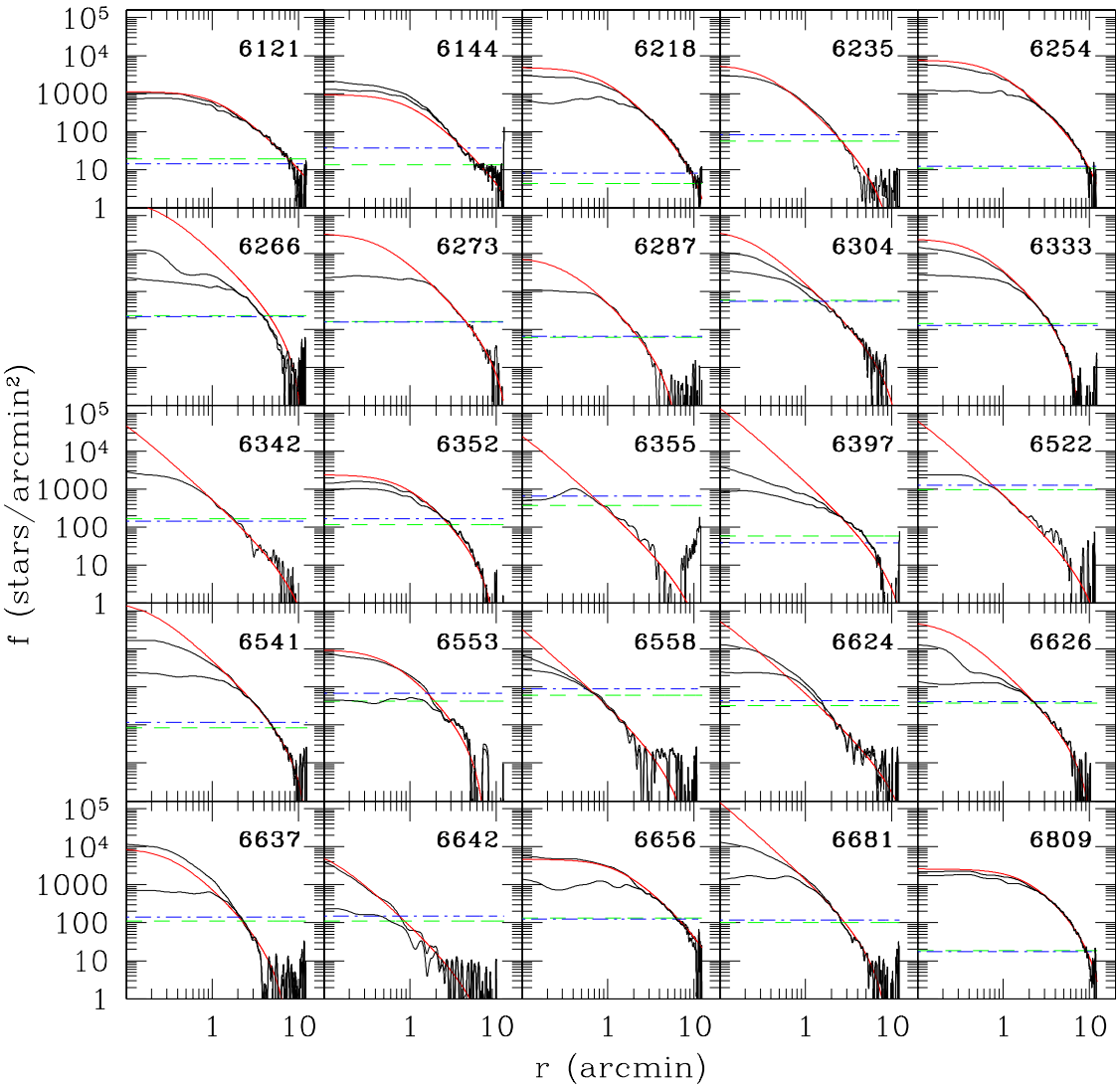

Fig. 2.— Radial density profile of the stars in the cluster from the observations (black) and from fitting a King profile (red), once the constant non-member field component has been subtracted. The straight green dashed line shows the non-member field component according to the fit. The straight blue dot-dashed line, showing the non-member field component according to the Besançon model, is plotted for comparison. The general disagreement in the inner regions between observations and models is due to the lower completeness of these regions, due to crowding effects. Whenever there are two black density profiles, one belongs to the space+ground observations, while the other corresponds to ground-only observations, and generally shows a lower completeness.

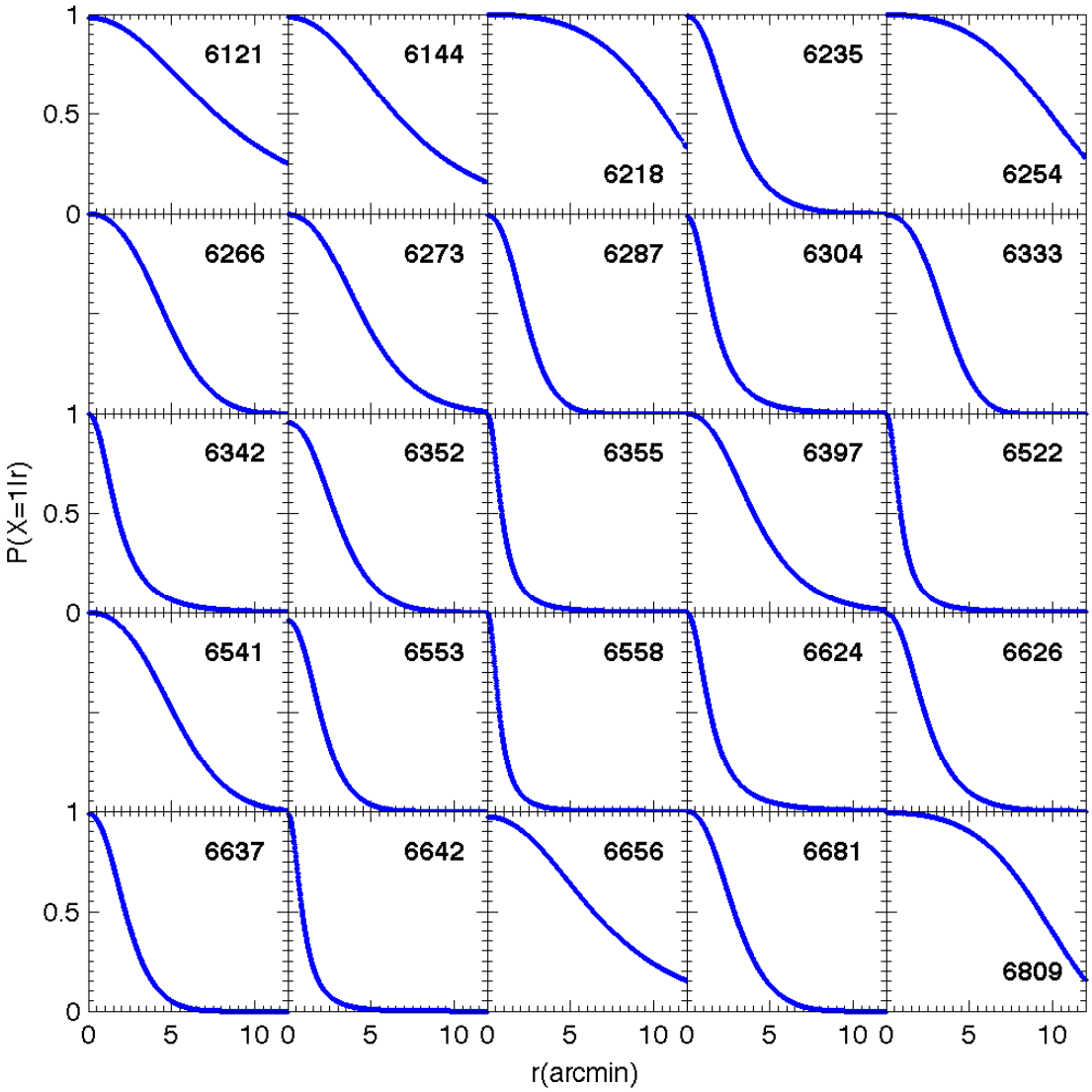

Fig. 3.— Probability to belong to the cluster as a function of distance to the center of the cluster.

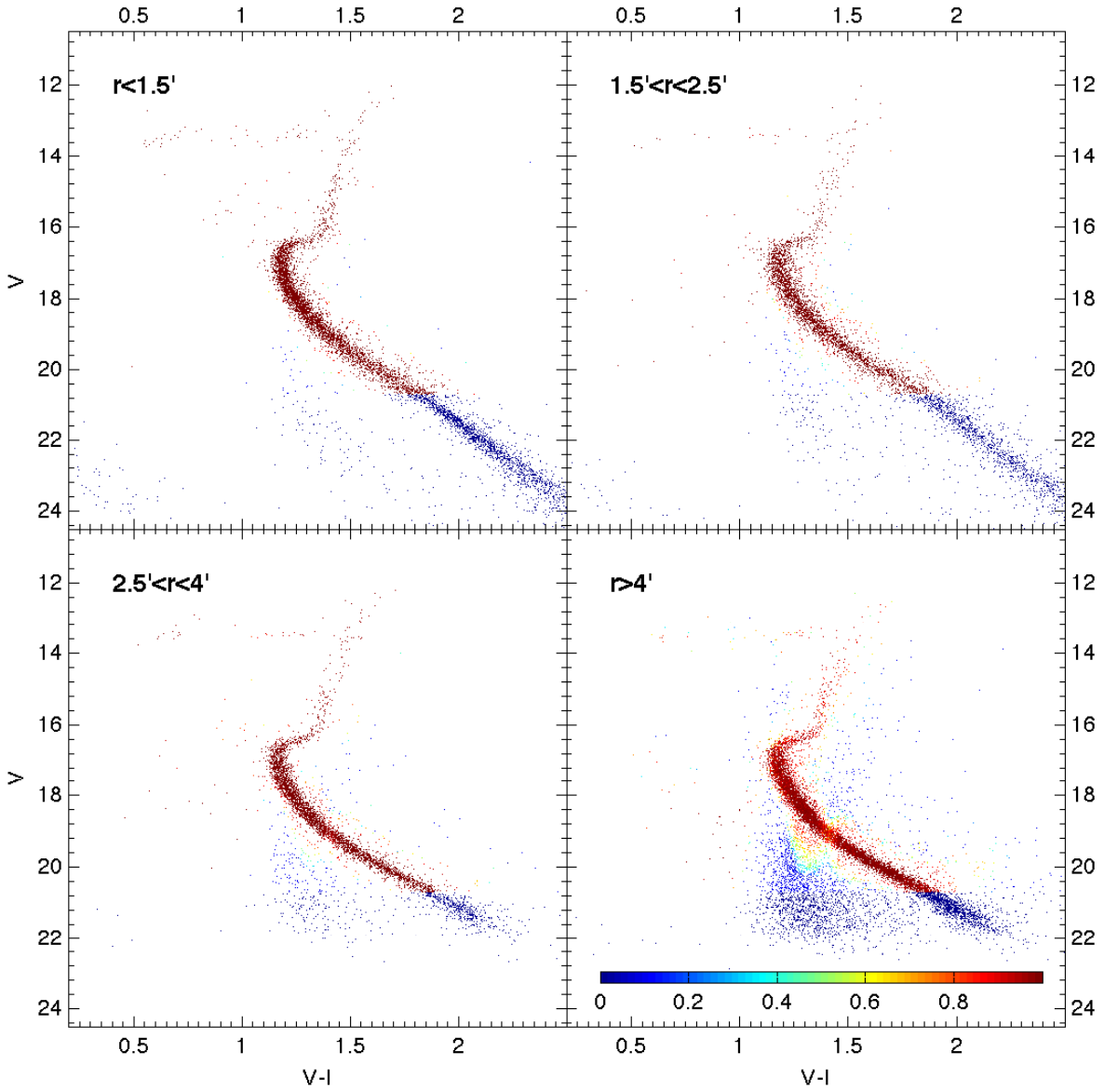

Fig. 4.— Observed dereddened CMD for M4 at four different distances from the cluster center, with the probability of every star to belong to the cluster as a function of position in the sky, color and magnitude, $P(X = 1|r, c, m)$, represented by the different colors of the stars as indicated in the color bar. Notice that we restrict our analysis to stars brighter than the completeness limit shown in Table 5.

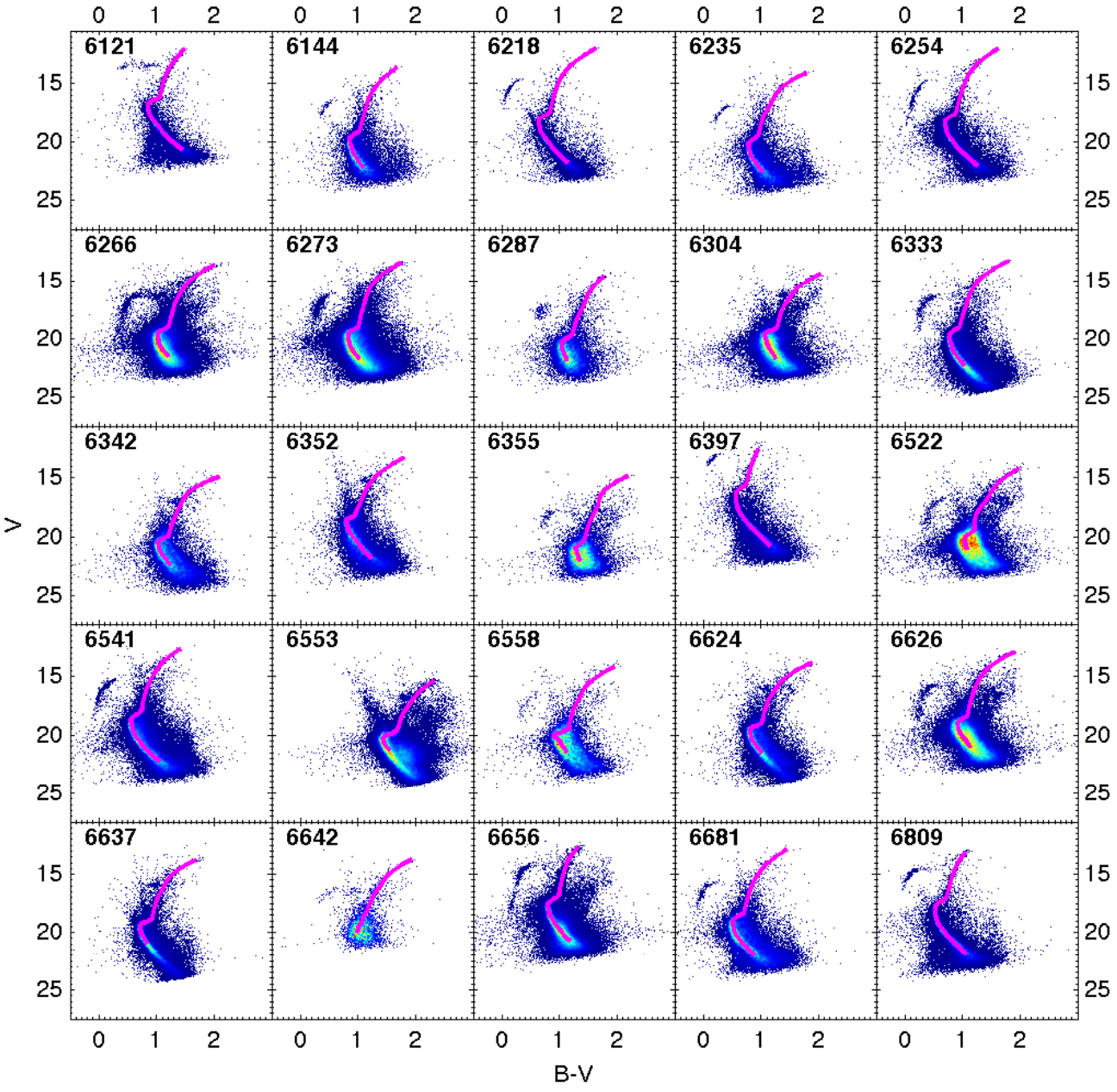

Fig. 5.— Ridgelines in the V vs. $(B-V)$ CMDs for the clusters in the sample, down to the completeness limit.

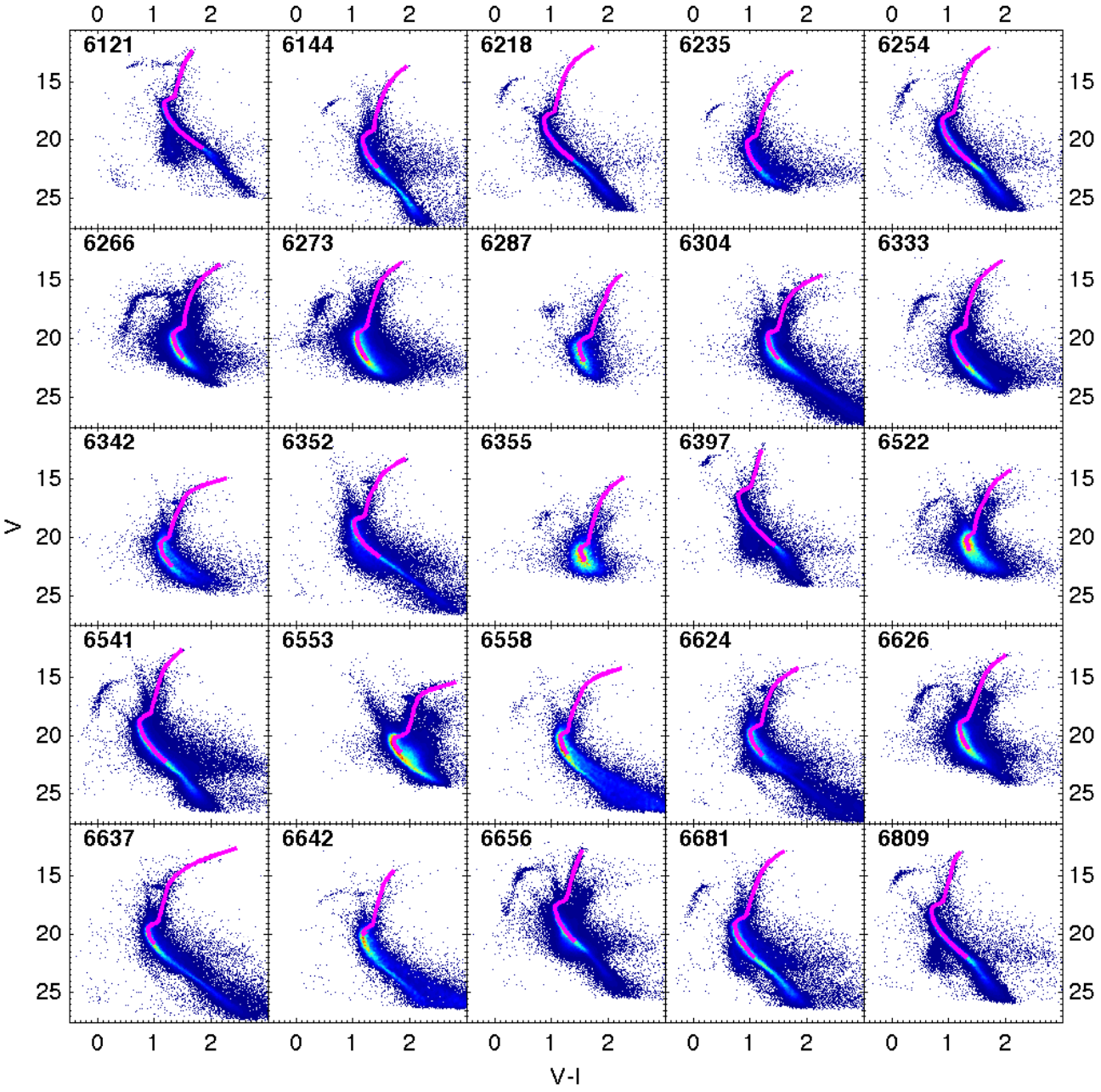

Fig. 6.— Ridgelines in the V vs. $(V-I)$ CMDs for the clusters in the sample, down to the completeness limit.

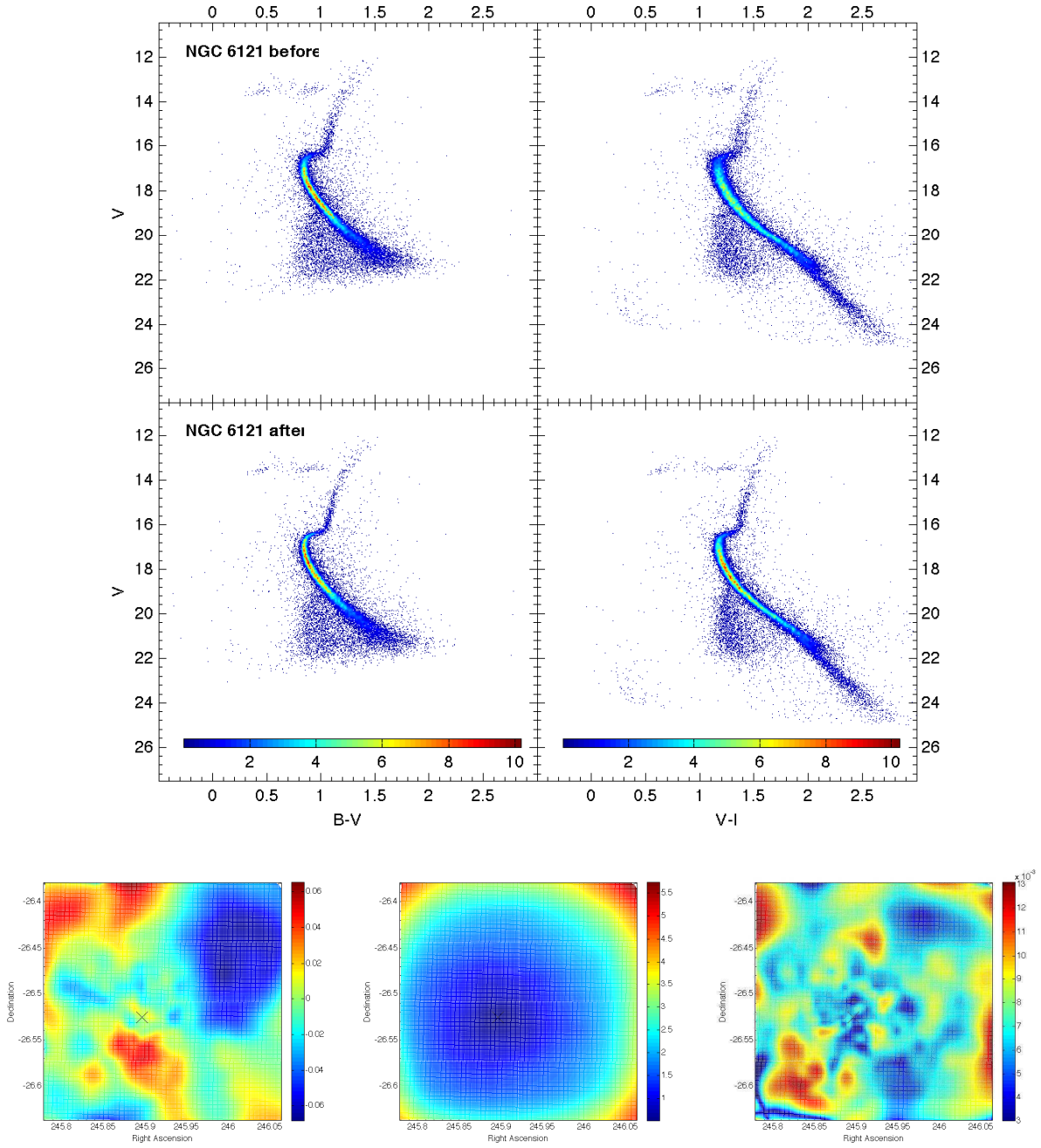

Fig. 7.— On top, CMDs of the cluster NGC 6121 - M 4, before and after being differentially dereddened. Only our Magellan photometry was used to build the $B-V$ vs. V CMD. ACS photometry (from project 10775) and Magellan photometry were used to build the $V-I$ vs. V CMD. Color bars show the range in the densities of stars in the CMD ($\times 10^4$ stars per square magnitude). On the bottom, extinction map (left) for the cluster field, along with its resolution (middle) and its precision (right), as provided by our technique. The x marks the position of the cluster center. The color code gives, respectively, the color excesses $E(B-V)$ for the extinction map, the bandwidths used in the resolution map, and the standard deviation σ of the color excesses in the precision maps.

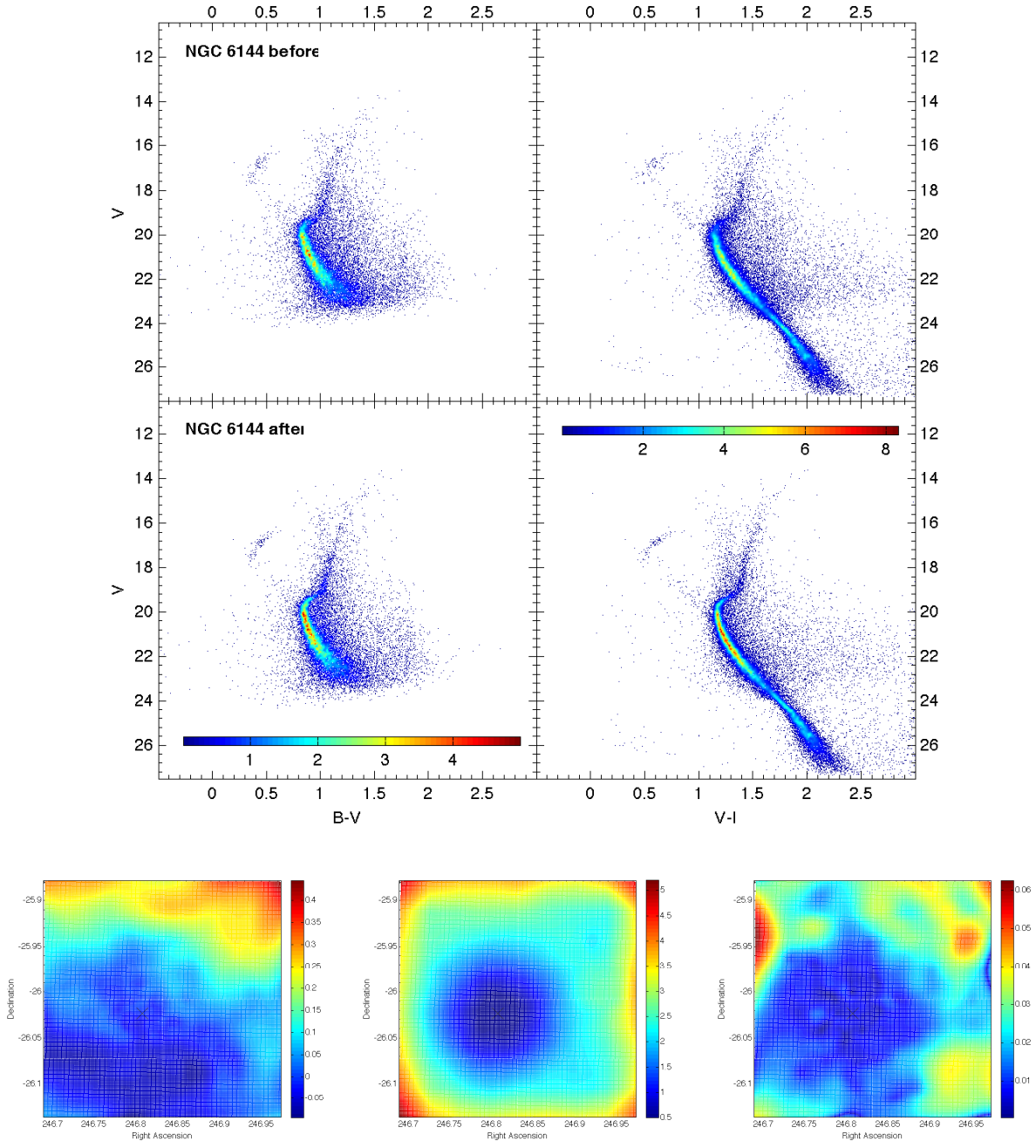

Fig. 8.— As in Figure 7, but for the cluster NGC 6144. Only our Magellan photometry was used to build the $B-V$ vs. V CMD. ACS photometry (from project 10775) and Magellan photometry were used to build the $V-I$ vs. V CMD. Notice that the $B-V$ vs. V CMD could not be correctly calibrated in color using the method described in the text because of the lack of calibrating data in the B filter.

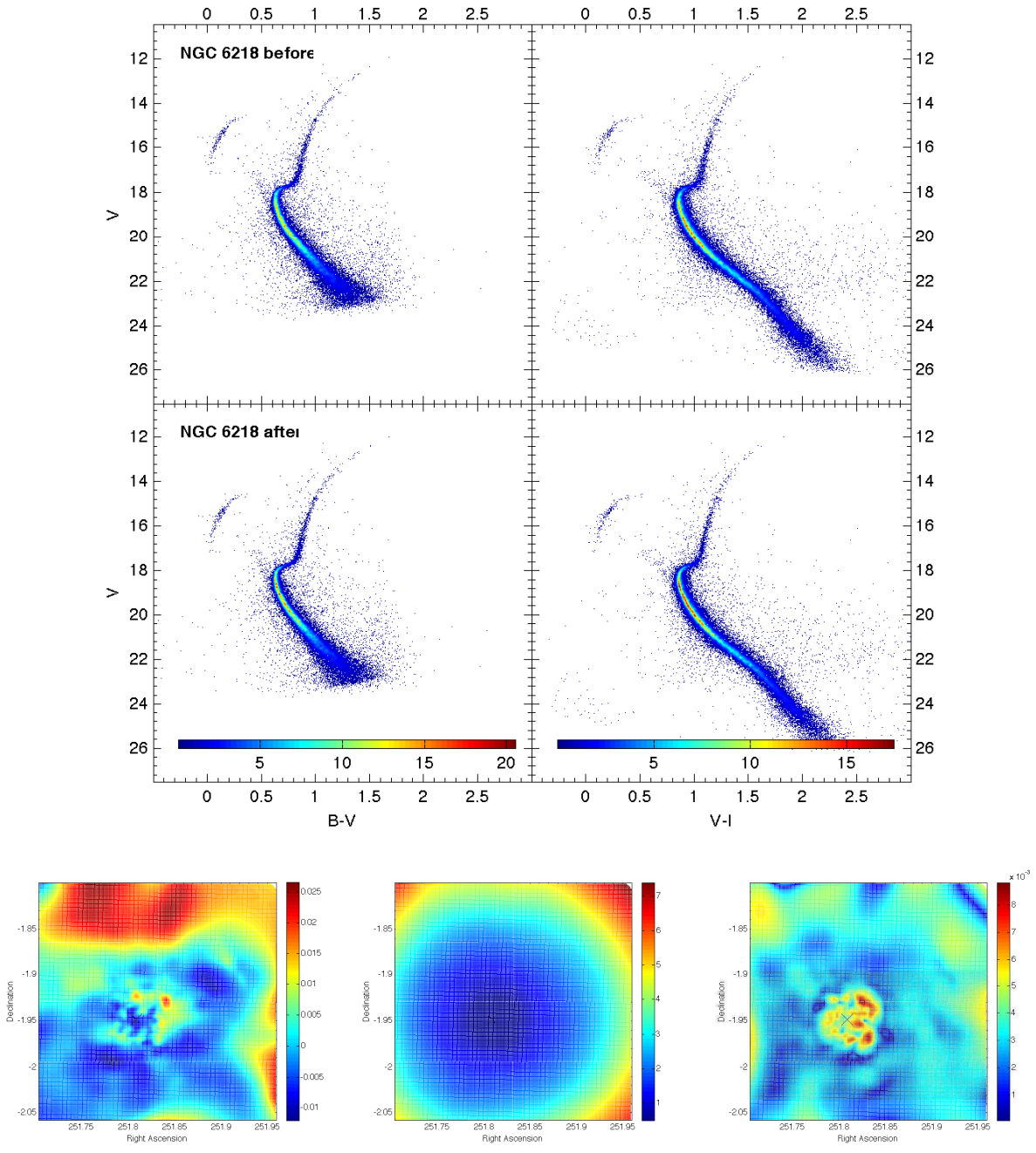

Fig. 9.— As in Figure 7, but for the cluster NGC 6218 - M 12. ACS photometry (from our project 10573) and Magellan photometry were used to build the $B-V$ vs. V CMD. ACS photometry (from project 10775) and Magellan photometry were used to build the $V-I$ vs. V CMD.

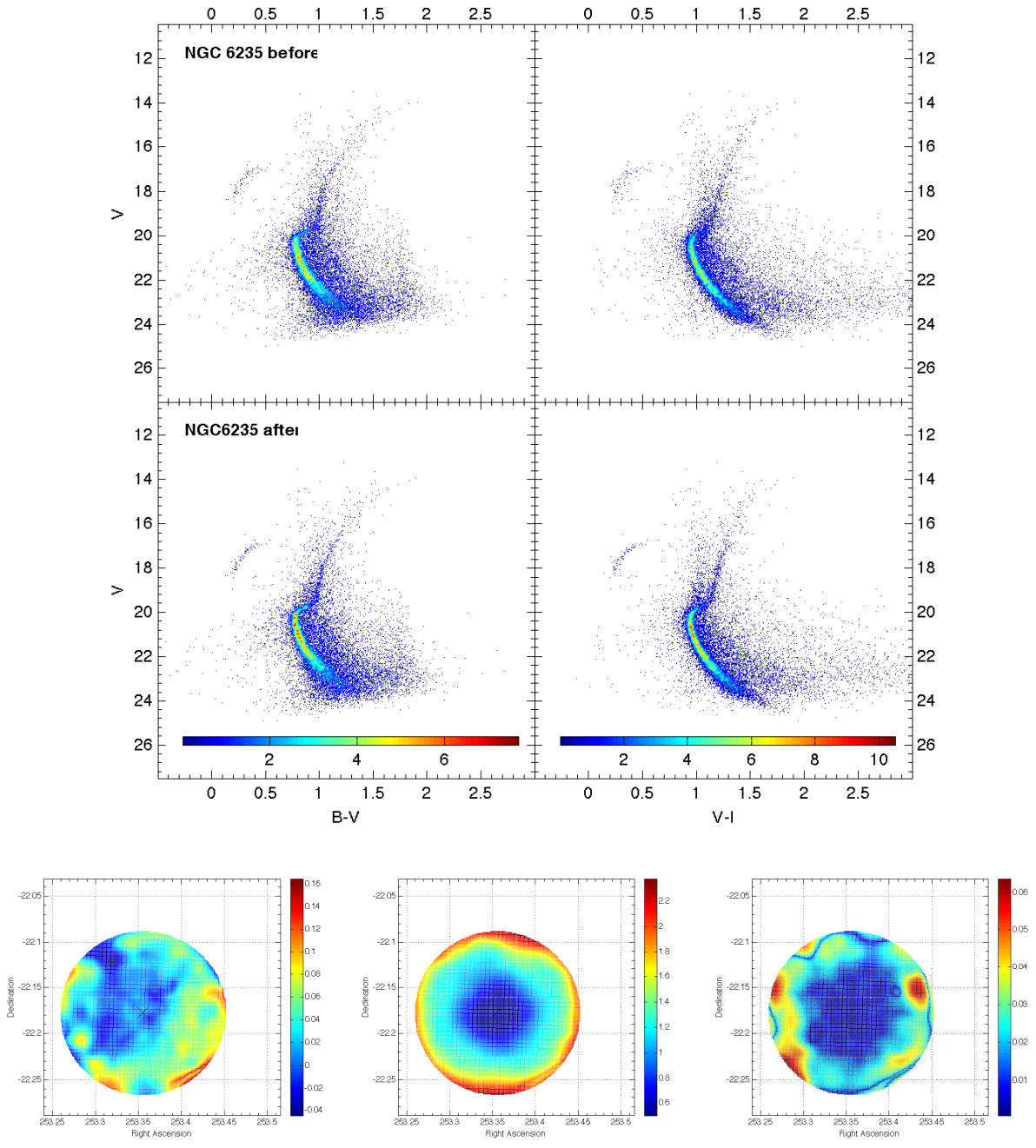

Fig. 10.— As in Figure 7, but for the cluster NGC 6235. Only our Magellan photometry was used to build the CMDs in both colors. Notice that the $V-I$ vs. V CMD could not be correctly calibrated in color using the method described in the text because of the lack of calibrating data in the I filter.

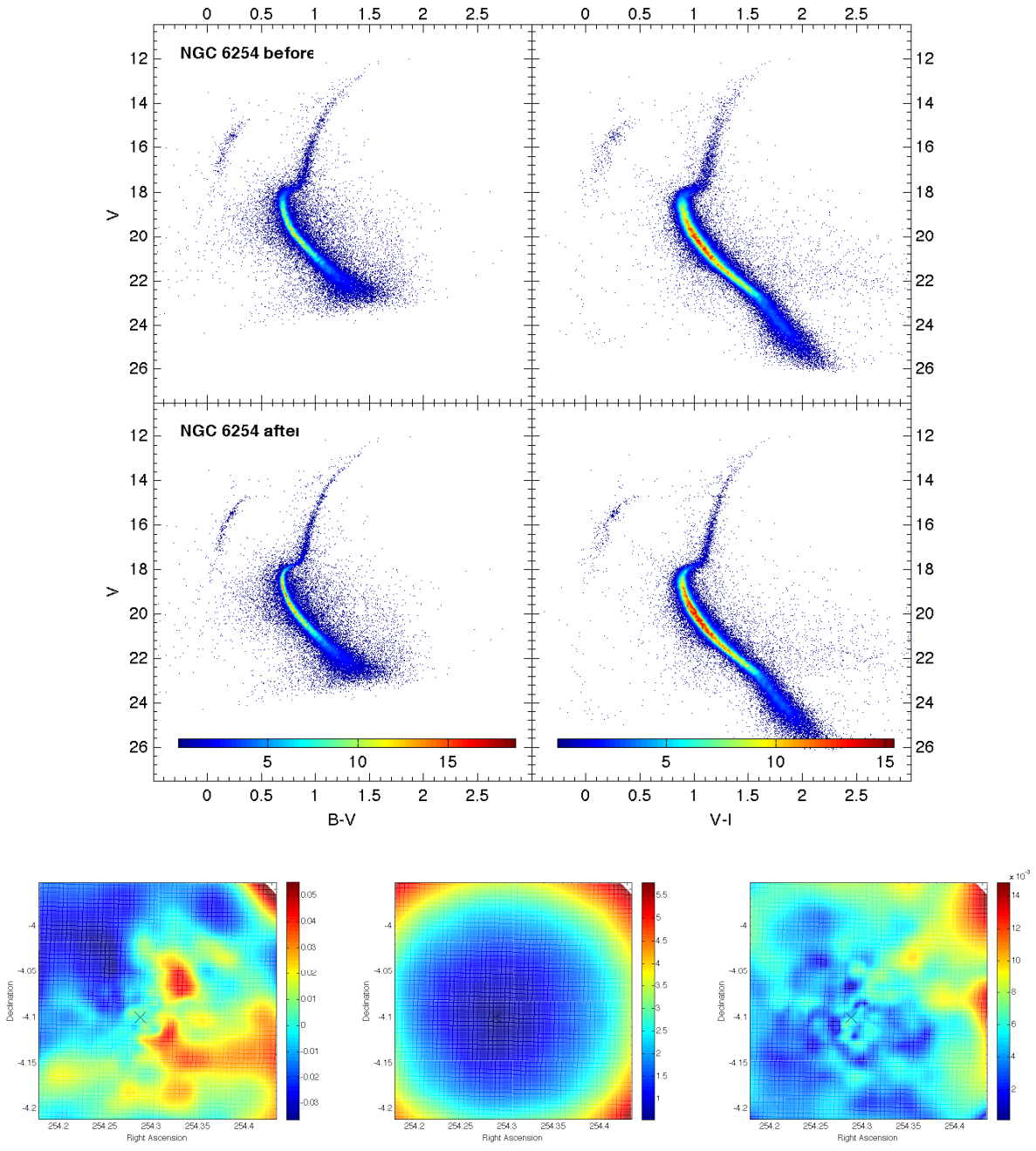

Fig. 11.— As in Figure 7, but for the NGC 6254 - M 10. Only our Magellan photometry was used to build the $B-V$ vs. V CMD. ACS photometry (from project 10775) and Magellan photometry were used to build the $V-I$ vs. V CMD.

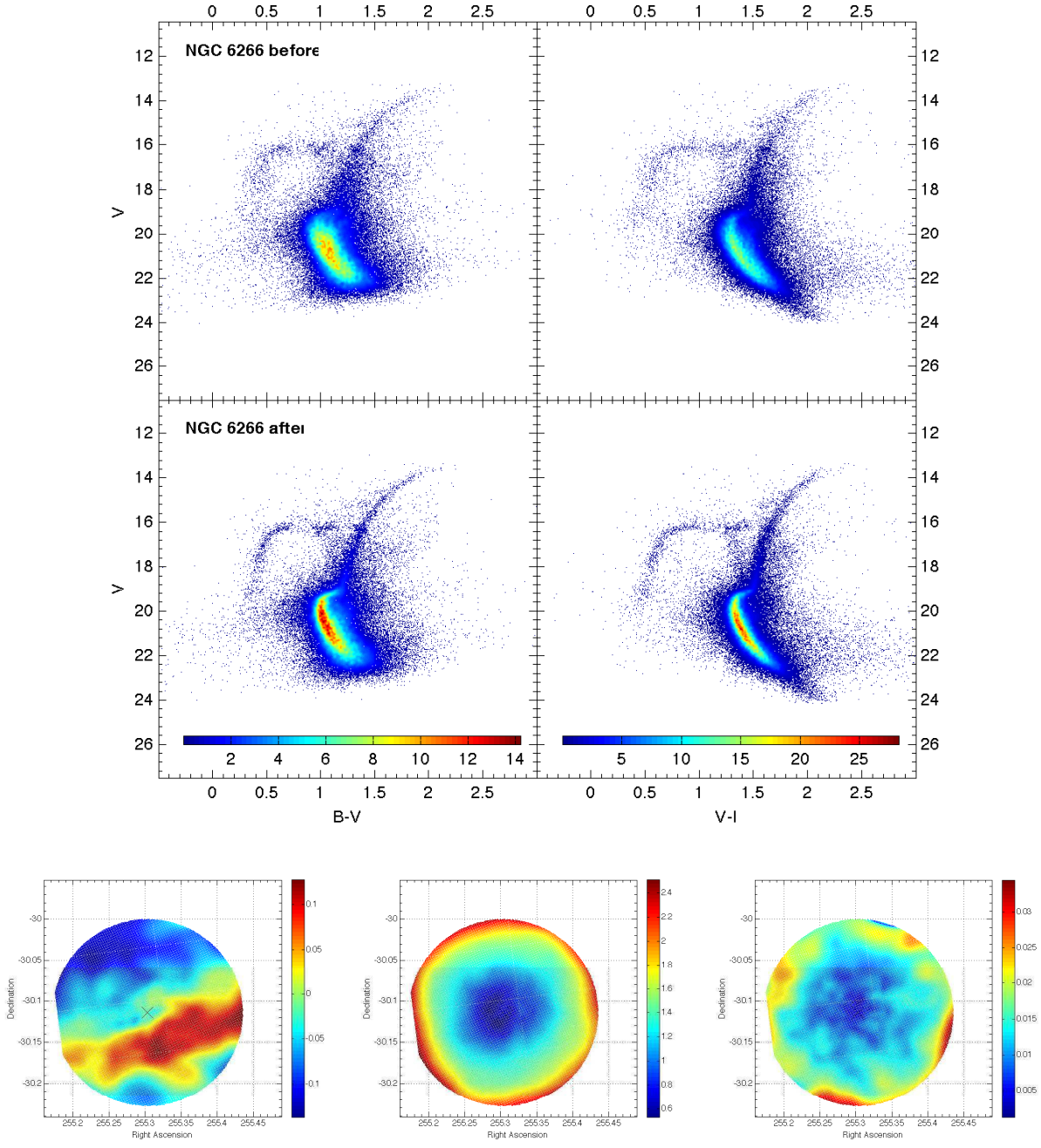

Fig. 12.— As in Figure 7, but for the cluster NGC 6266 - M 62. Only our Magellan photometry was used to build the $B-V$ vs. V CMD. WFPC2 photometry (from project 8709) and Magellan photometry were used to build the $V-I$ vs. V CMD.

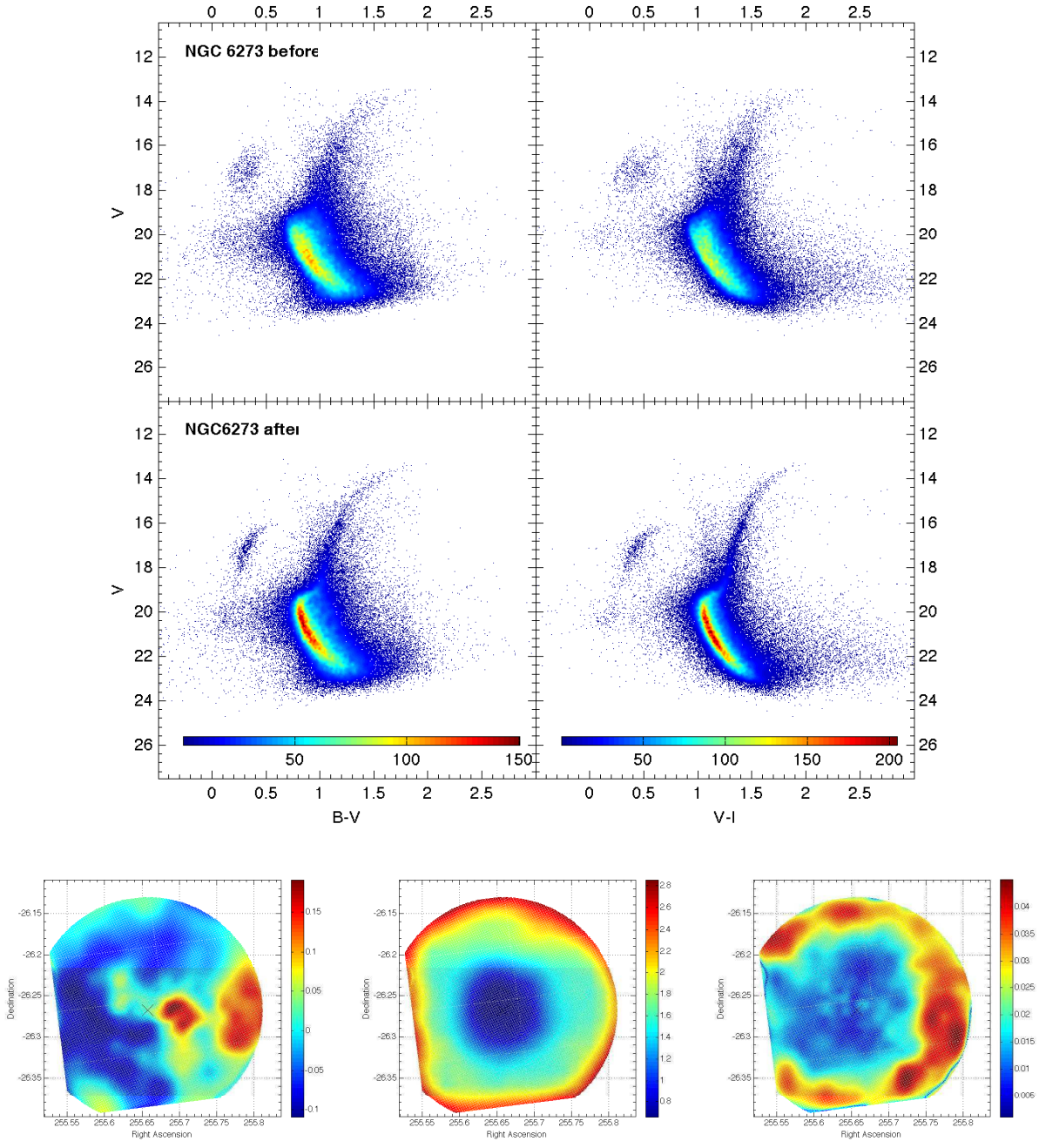

Fig. 13.— As in Figure 7, but for the cluster NGC 6273 - M 19. Only our Magellan photometry was used to build the CMDs in both colors.

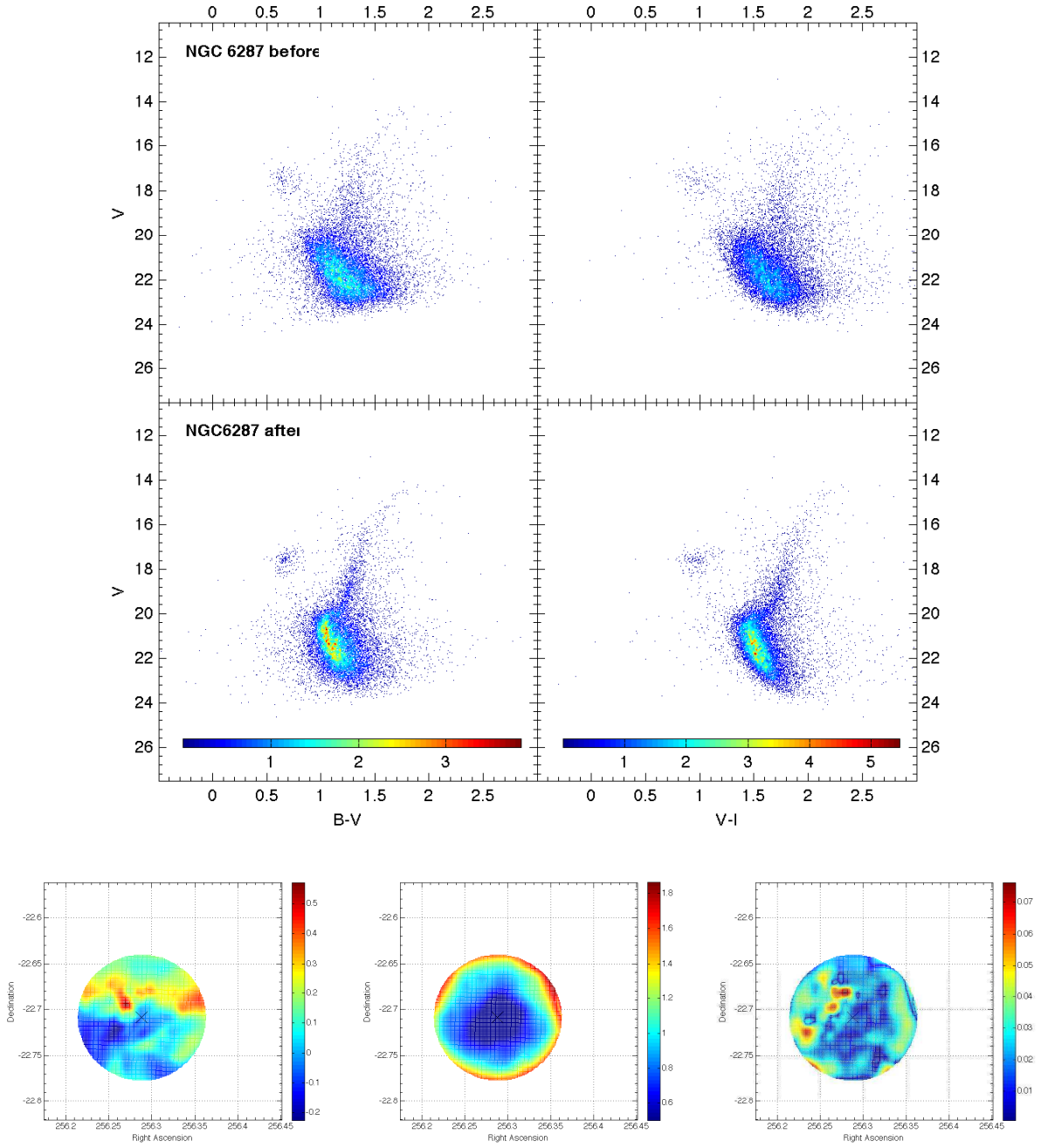

Fig. 14.— As in Figure 7, but for the cluster NGC 6287. Only our Magellan photometry was used to build the CMDs in both colors.

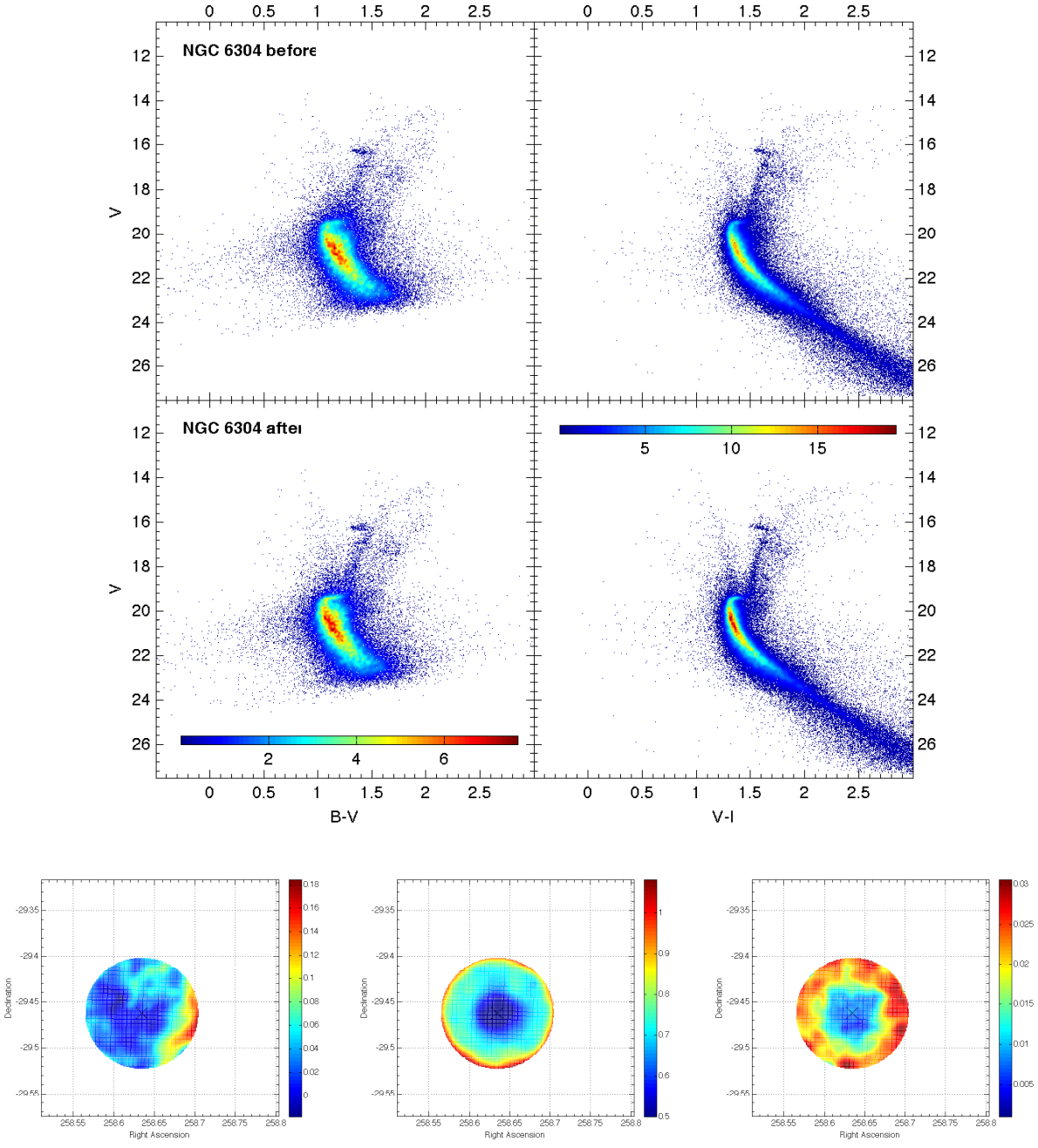

Fig. 15.— As in Figure 7, but for the cluster NGC 6304. Only our Magellan photometry was used to build the $B-V$ vs. V CMD. ACS photometry (from project 10775) and Magellan photometry were used to build the $V-I$ vs. V CMD.

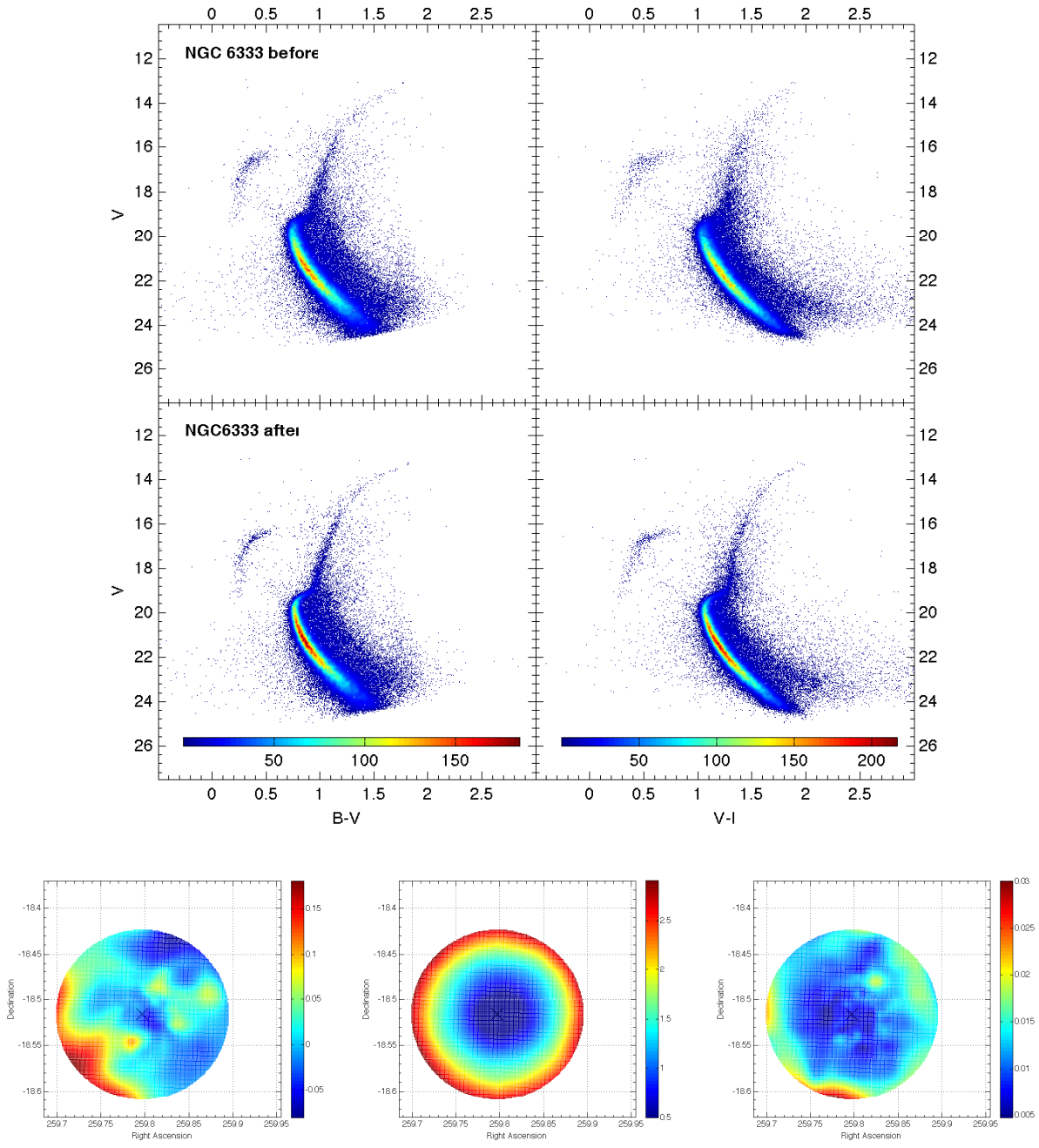

Fig. 16.— As in Figure 7, but for the cluster NGC 6333 - M 9. ACS photometry (from our project 10573) and our Magellan photometry were used to build the CMDs in both colors.

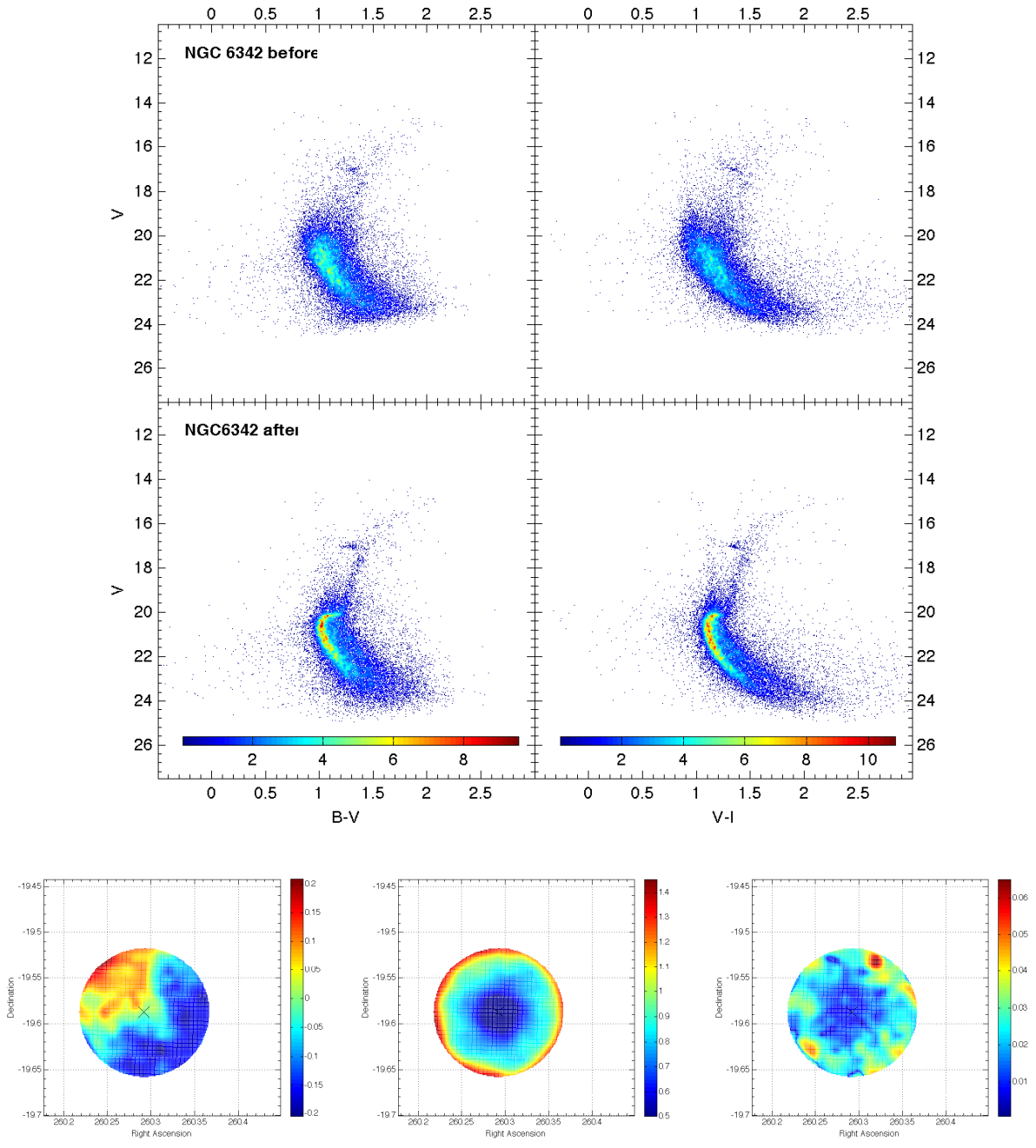

Fig. 17.— As in Figure 7, but for the cluster NGC 6342. Only our Magellan photometry was used to build the CMDs in both colors. Notice that the $V-I$ vs. V CMD could not be correctly calibrated in color using the method described in the text because of the lack of calibrating data in the I filter.

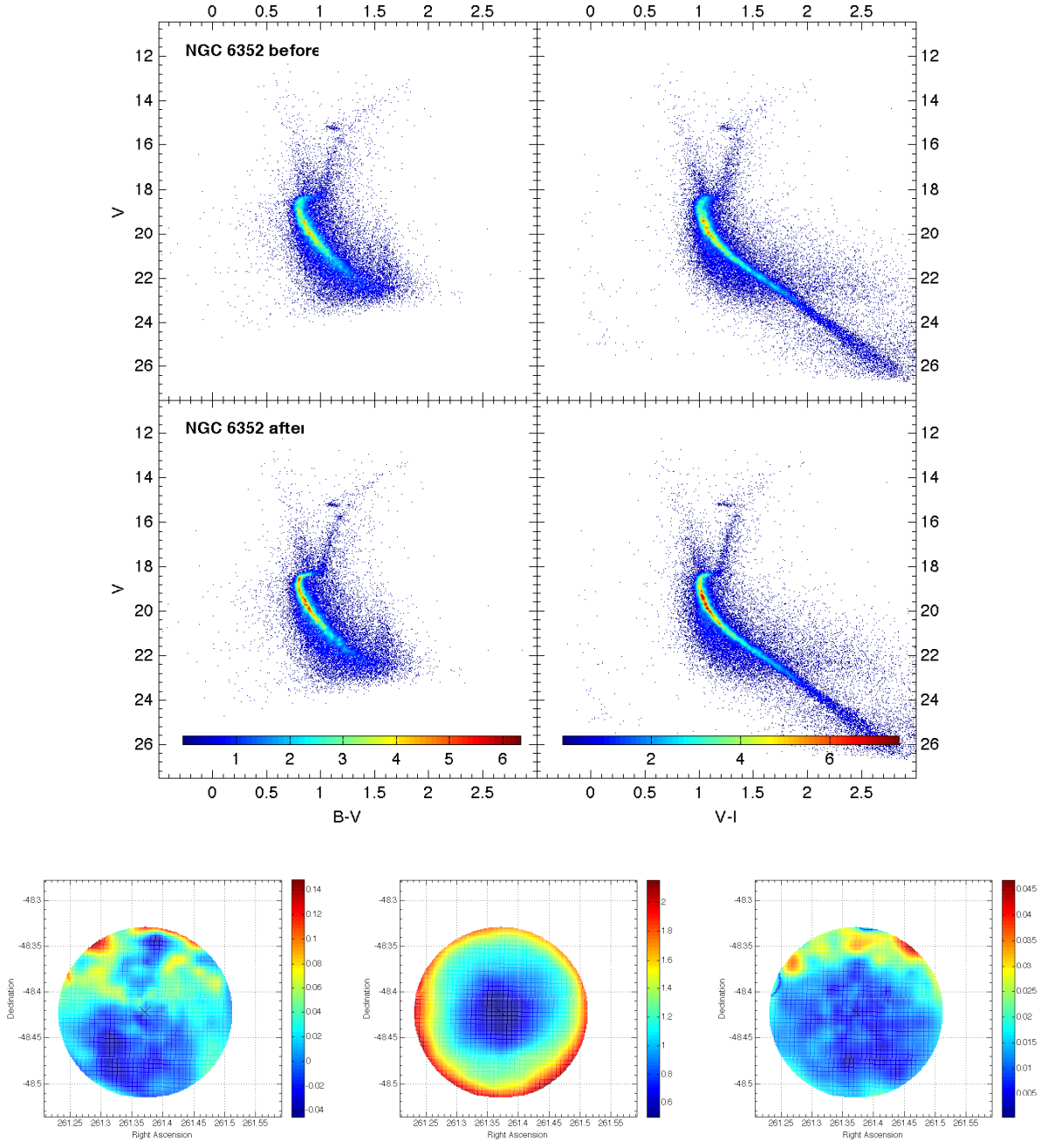

Fig. 18.— As in Figure 7, but for the cluster NGC 6352. Only our Magellan photometry was used to build the $B-V$ vs. V CMD. ACS photometry (from project 10775) and Magellan photometry were used to build the $V-I$ vs. V CMD.

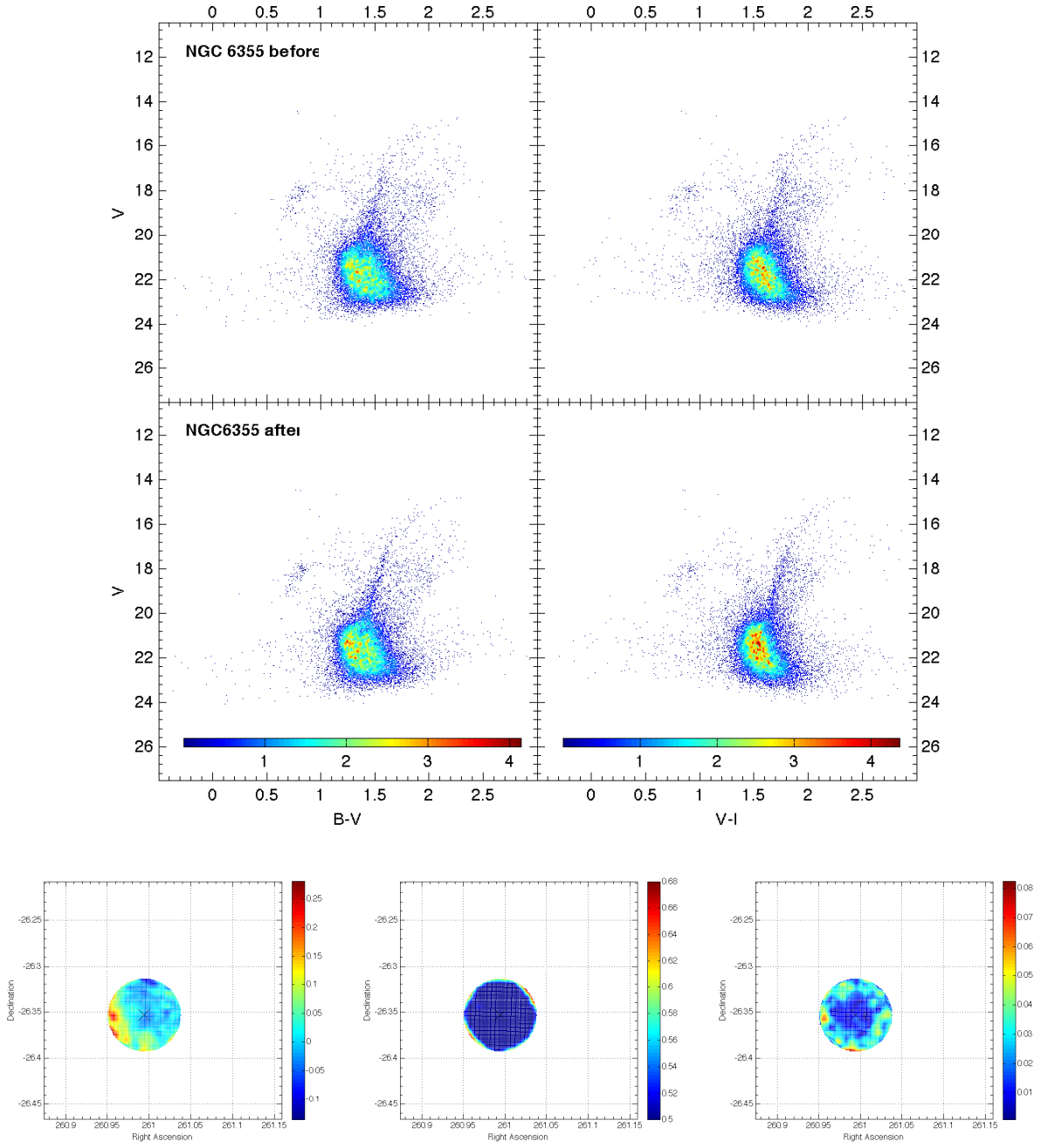

Fig. 19.— As in Figure 7, but for the cluster NGC 6355. Only our Magellan photometry was used to build the CMDs in both colors. Notice that the $V-I$ vs. V CMD could not be correctly calibrated in color using the method described in the text because of the lack of calibrating data in the I filter.

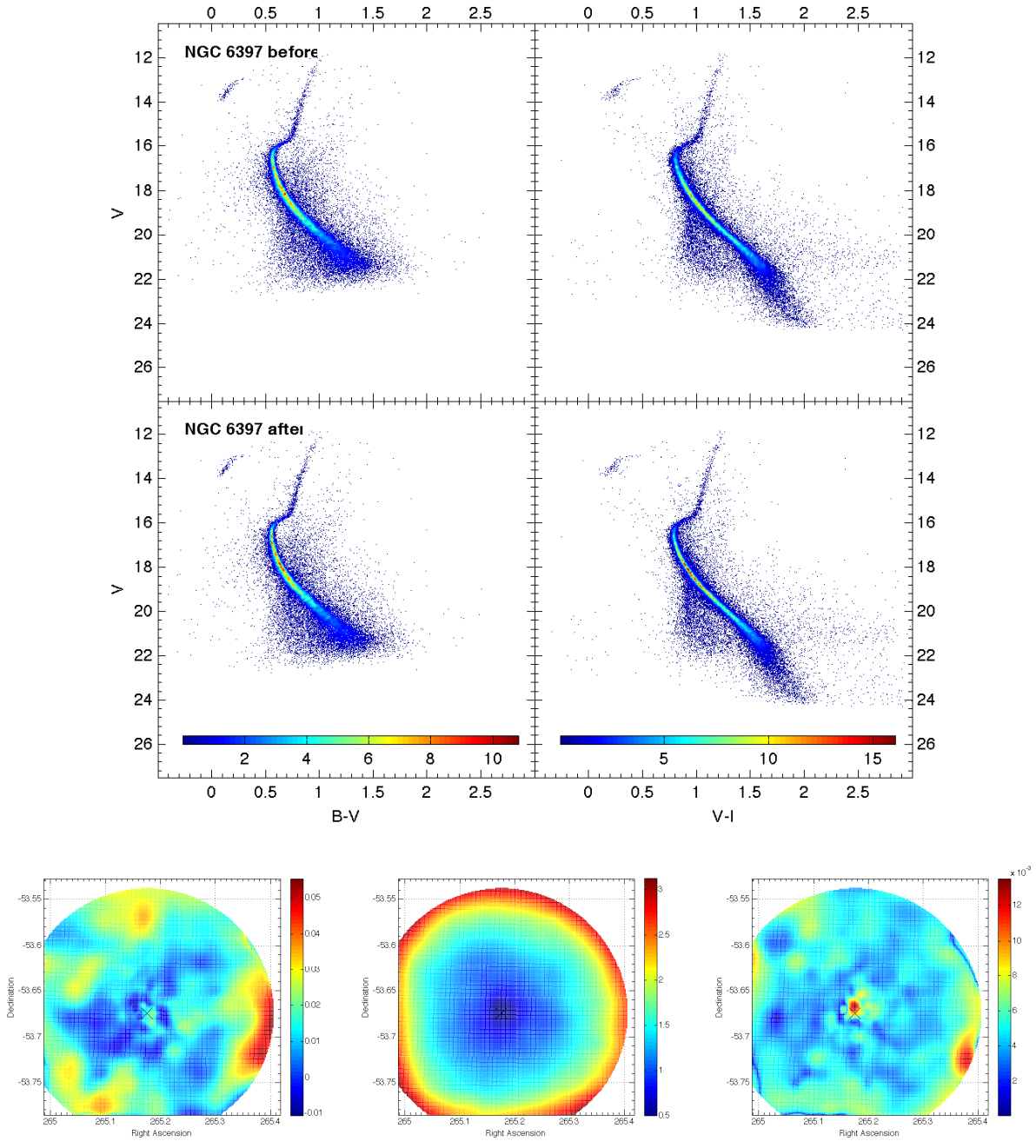

Fig. 20.— As in Figure 7, but for the cluster NGC 6397, before and after being differentially dereddened. Only our Magellan photometry was used to build the $B-V$ vs. V CMD. ACS photometry (from project 10775) and Magellan photometry were used to build the $V-I$ vs. V CMD.

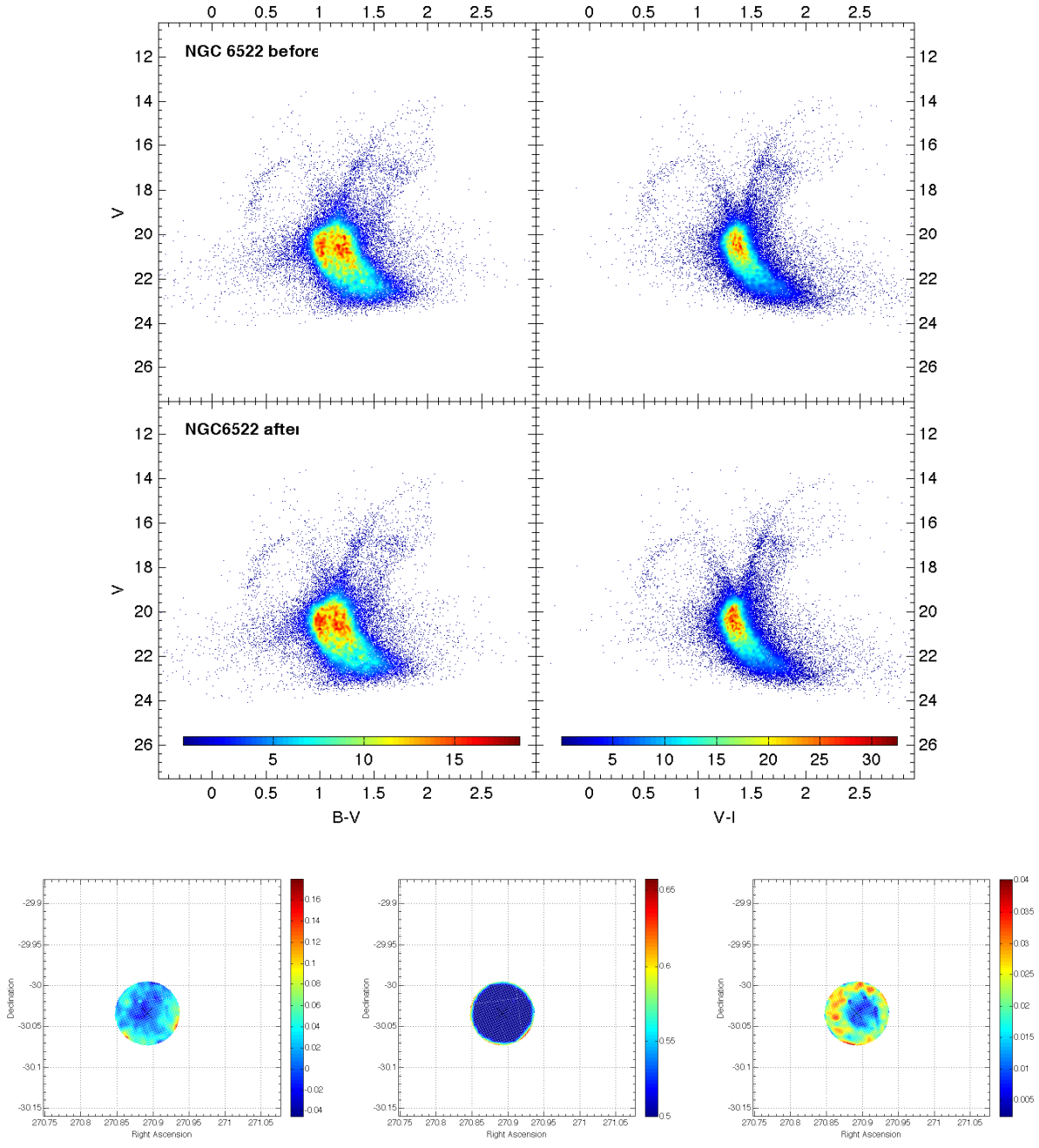

Fig. 21.— As in Figure 7, but for the cluster NGC 6522. Only our Magellan photometry was used to build the CMDs in both colors.

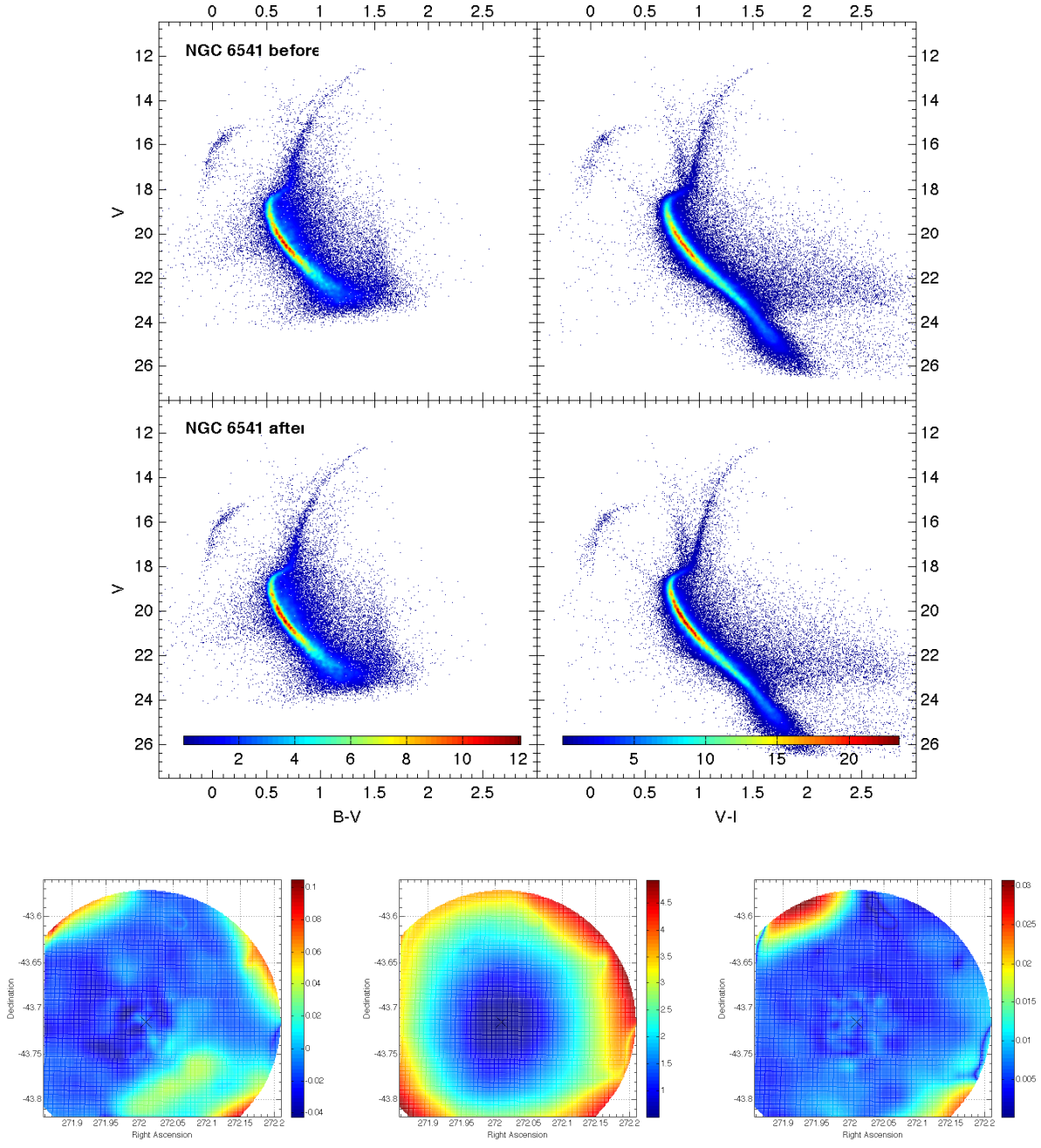

Fig. 22.— As in Figure 7, but for the cluster NGC 6541. Only our Magellan photometry was used to build the $B-V$ vs. V CMD. ACS photometry (from project 10775) and Magellan photometry were used to build the $V-I$ vs. V CMD.

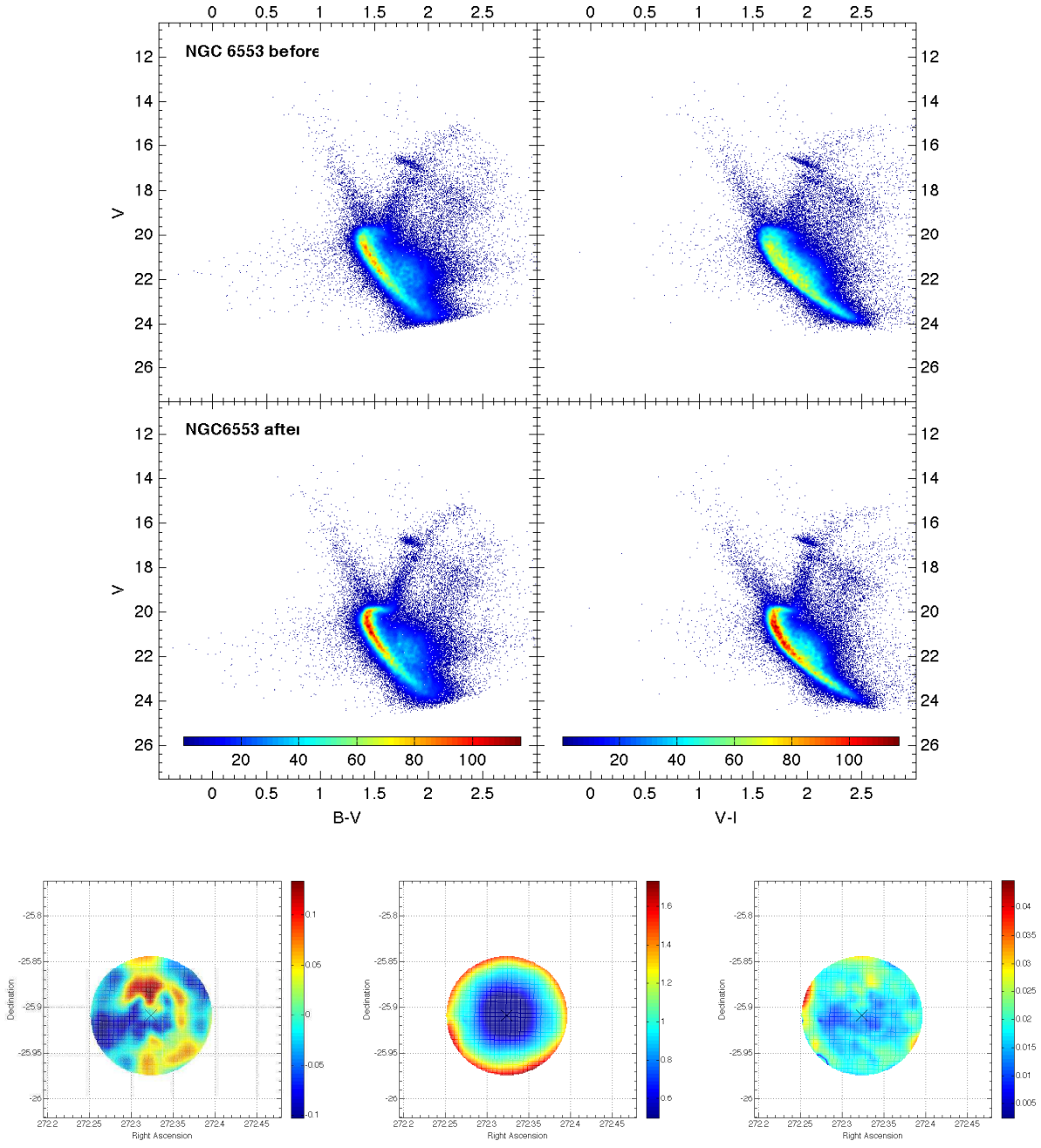

Fig. 23.— As in Figure 7, but for the cluster NGC 6553. ACS photometry (from our project 10573) and our Magellan photometry were used to build the CMDs in both colors.

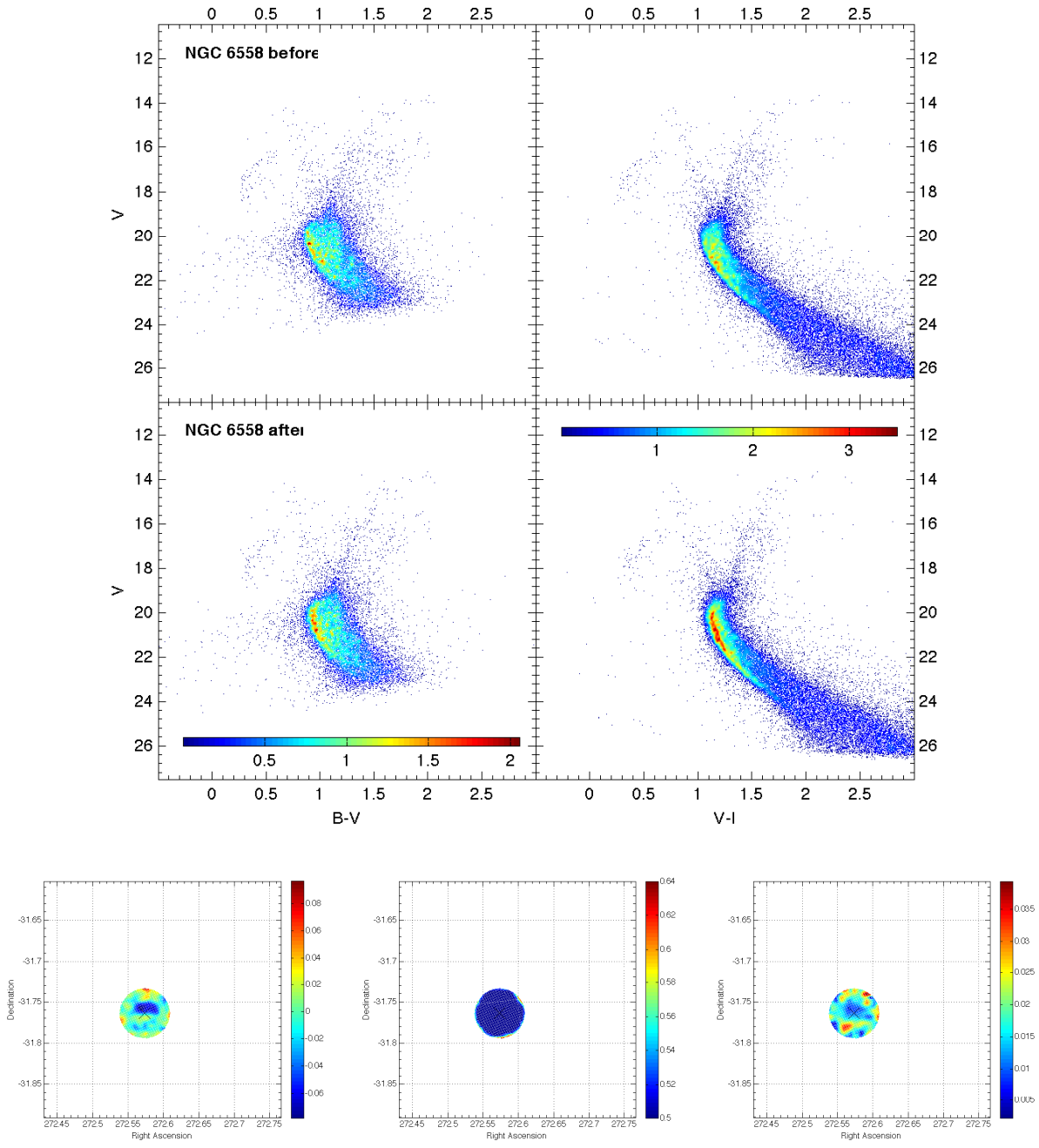

Fig. 24.— As in Figure 7, but for the cluster NGC 6558. Only our Magellan photometry was used to build the $B-V$ vs. V CMD. ACS photometry (from project 9799) and Magellan photometry were used to build the $V-I$ vs. V CMD. Notice that the $B-V$ vs. V CMD could not be correctly calibrated in color using the method described in the text because of the lack of calibrating data in the B filter.

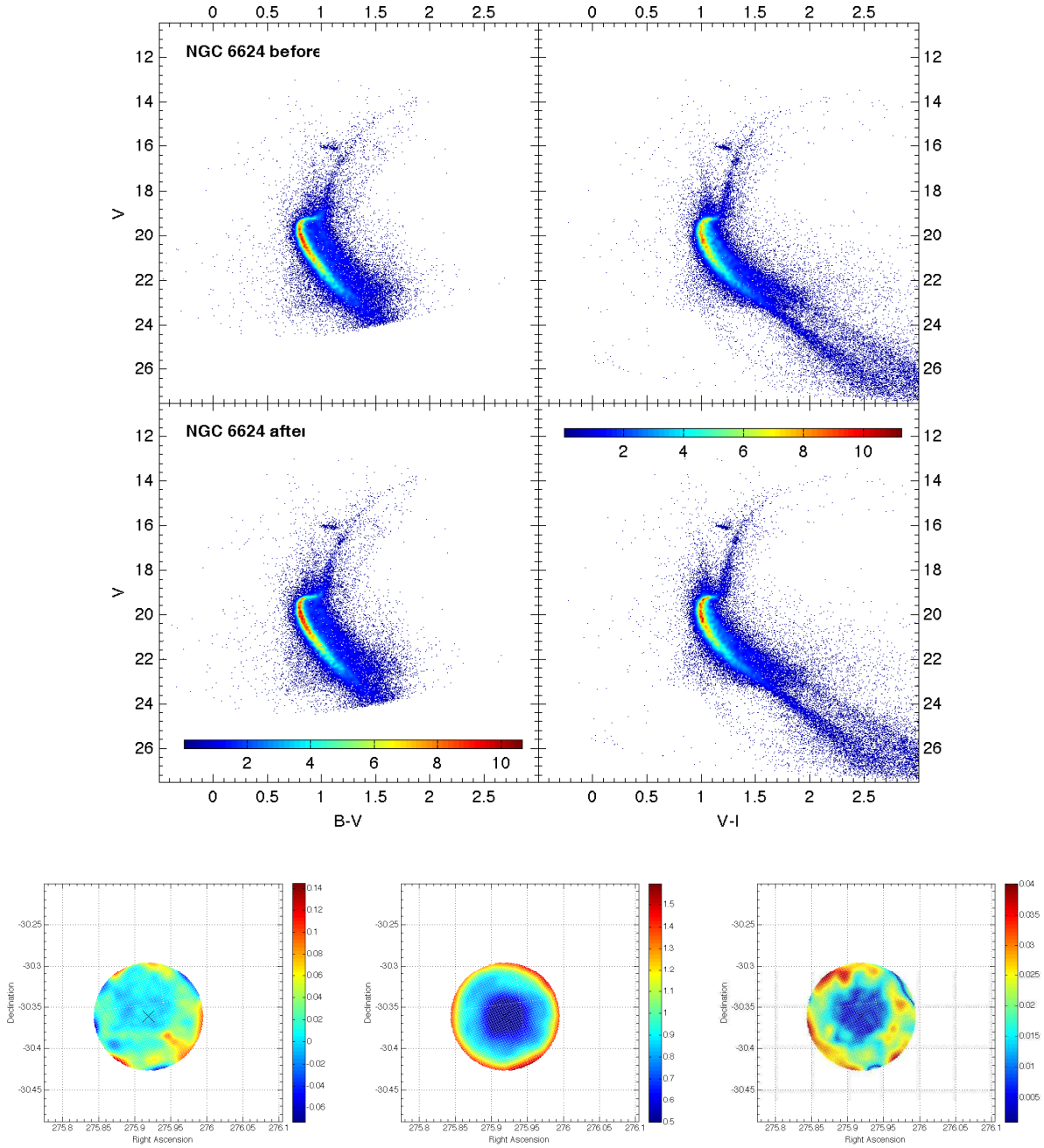

Fig. 25.— As in Figure 7, but for the cluster NGC 6624. ACS photometry (from our project 10573) and Magellan photometry were used to build the $B-V$ vs. V CMD. ACS photometry (from project 10775) and Magellan photometry were used to build the $V-I$ vs. V CMD.

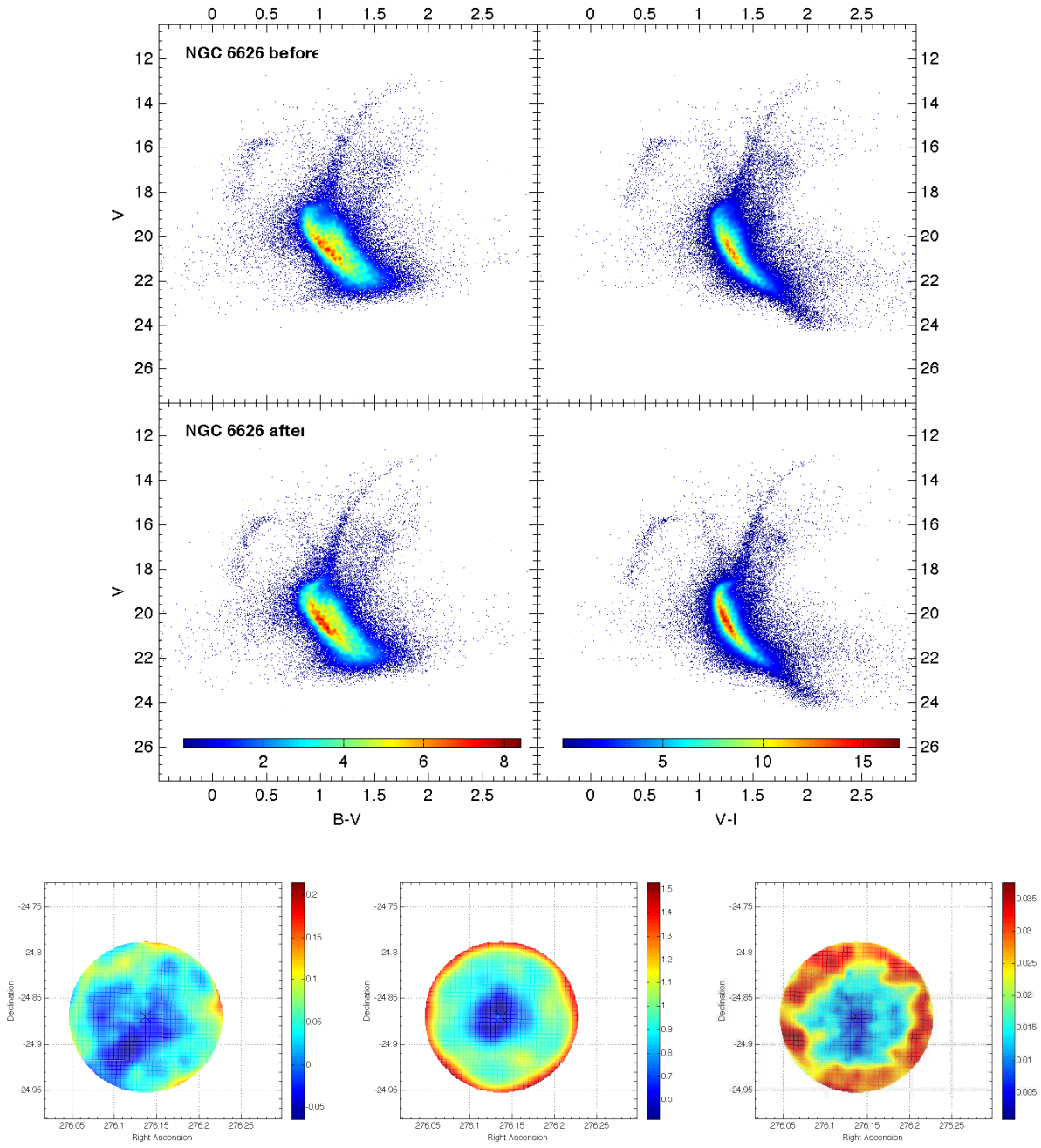

Fig. 26.— As in Figure 7, but for the cluster NGC 6626 - M 28. Only our Magellan photometry was used to build the $B-V$ vs. V CMD. WFPC2 photometry (from project 6779) and Magellan photometry were used to build the $V-I$ vs. V CMD. Notice that the $B-V$ vs. V CMD could not be correctly calibrated in color using the method described in the text because of the lack of calibrating data in the B filter.

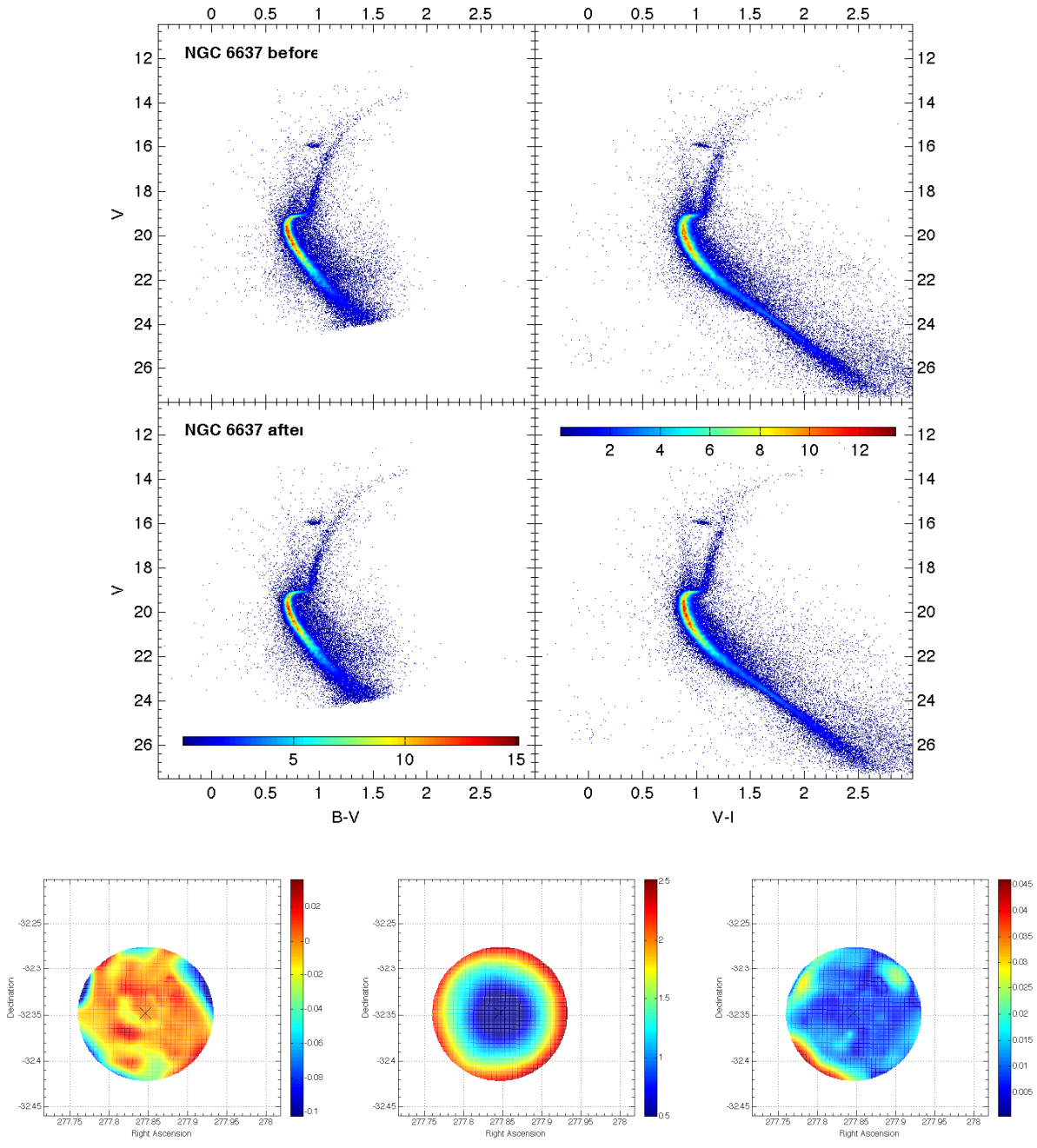

Fig. 27.— As in Figure 7, but for the cluster NGC 6637 - M 69. ACS photometry (from our project 10573) and Magellan photometry were used to build the $B-V$ vs. V CMD. ACS photometry (from project 10775) and Magellan photometry were used to build the $V-I$ vs. V CMD.

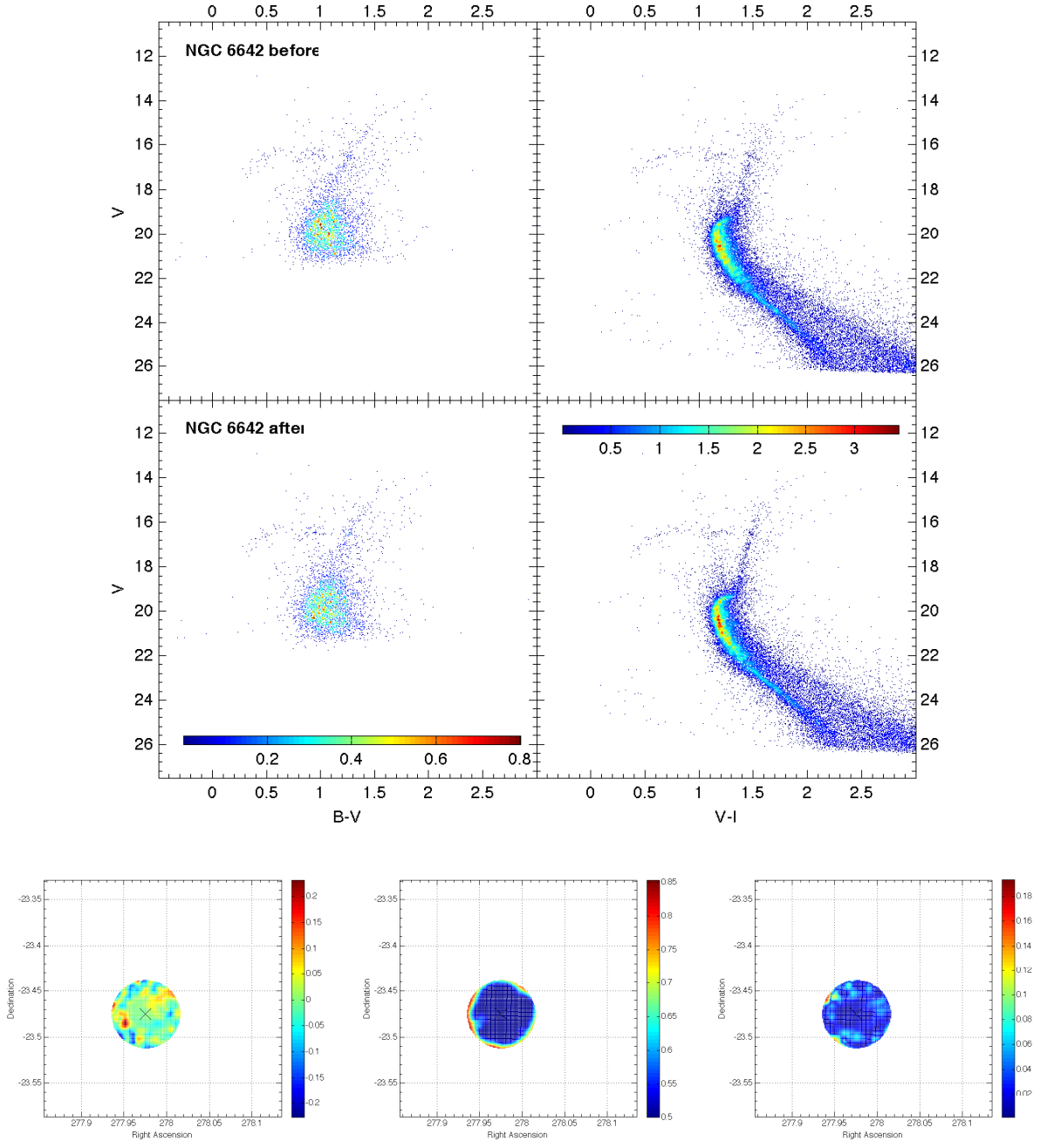

Fig. 28.— As in Figure 7, but for the cluster NGC 6642. Only our Magellan photometry was used to build the $B-V$ vs. V CMD. ACS photometry (from project 10775) and Magellan photometry were used to build the $V-I$ vs. V CMD.

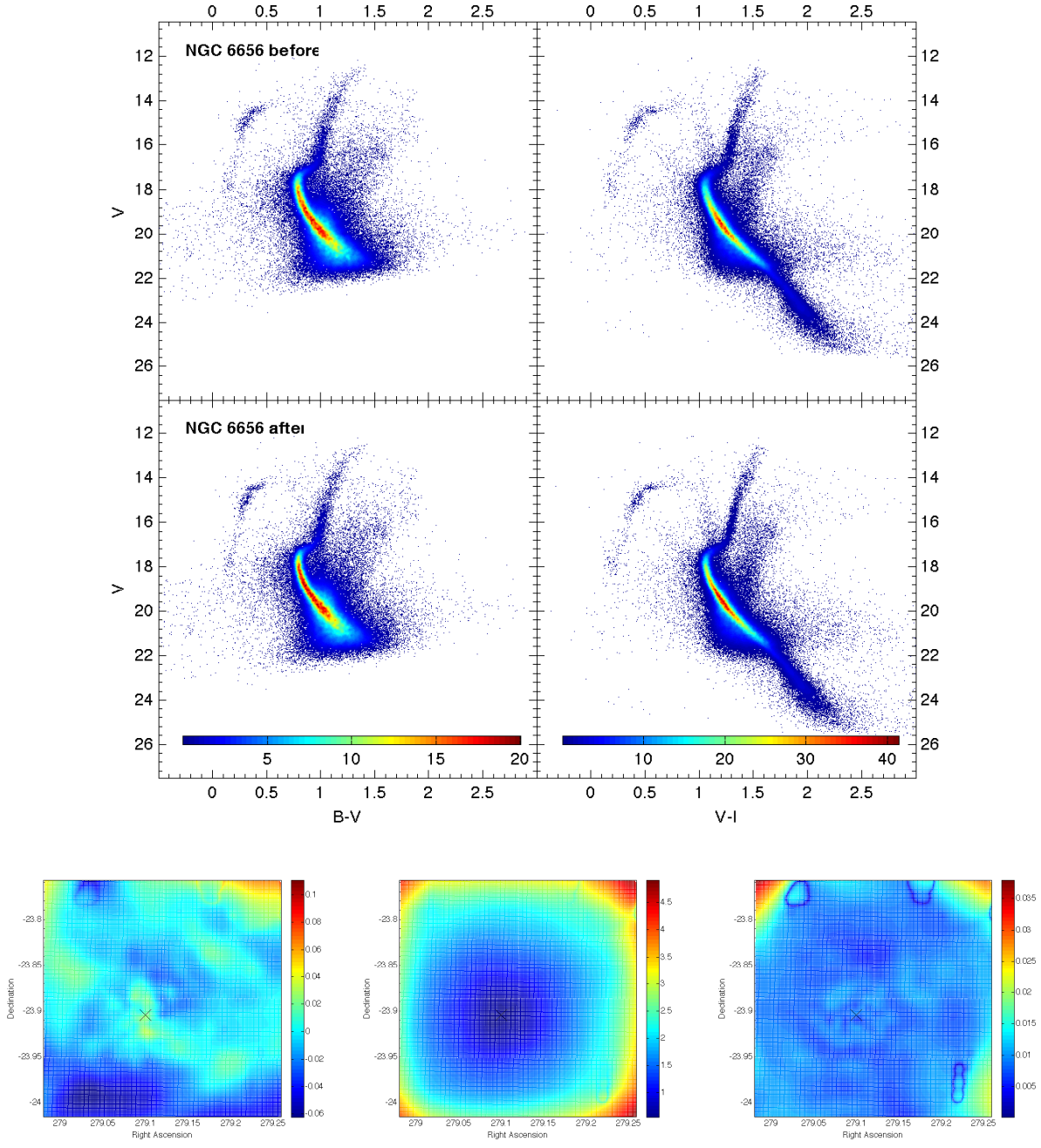

Fig. 29.— As in Figure 7, but for the cluster NGC 6656 - M 22. Only our Magellan photometry was used to build the $B-V$ vs. V CMD. ACS photometry (from project 10775) and Magellan photometry were used to build the $V-I$ vs. V CMD.

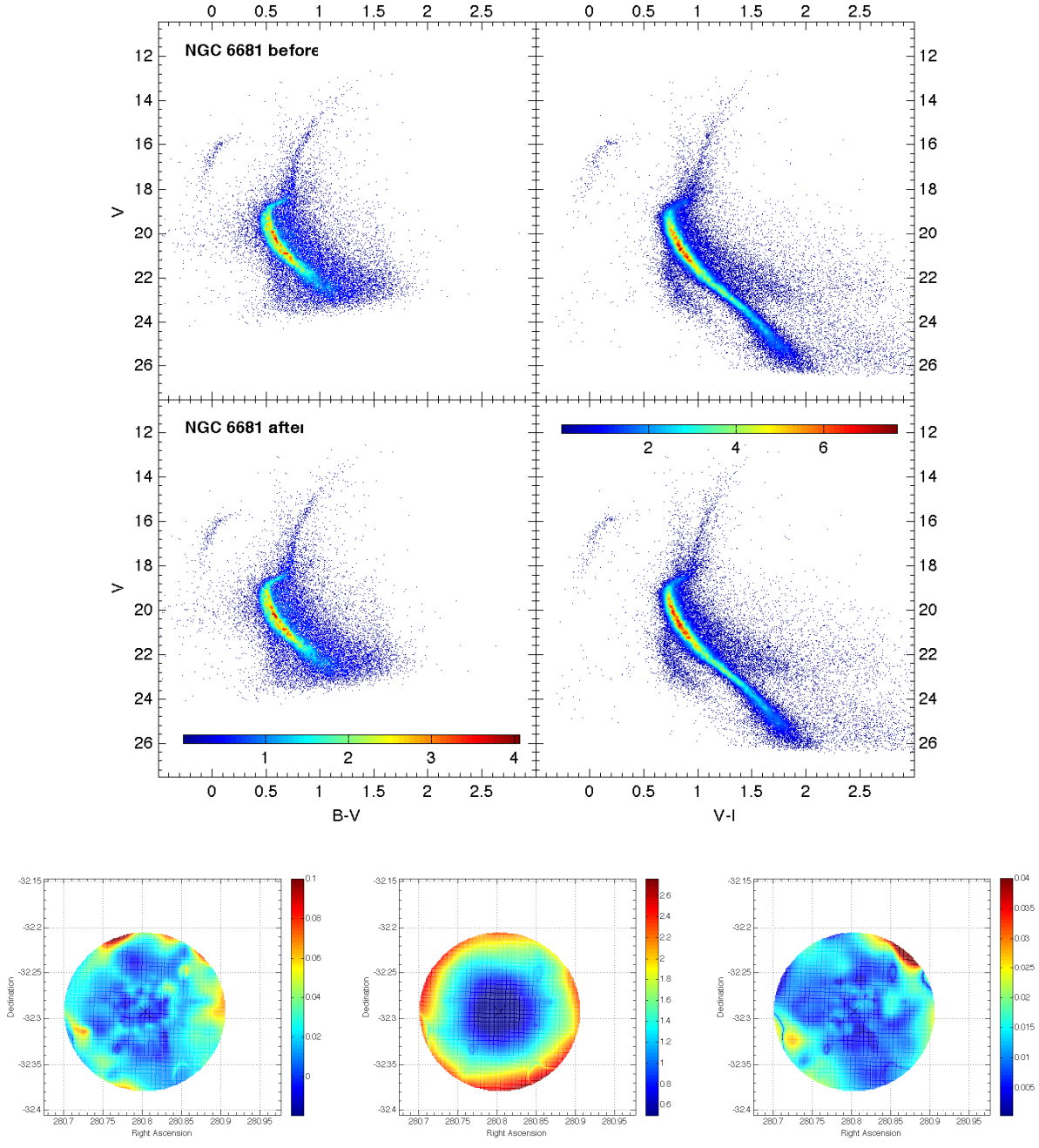

Fig. 30.— As in Figure 7, but for the cluster NGC 6681 - M 70. Only our Magellan photometry was used to build the $B-V$ vs. V CMD. ACS photometry (from project 10775) and Magellan photometry were used to build the $V-I$ vs. V CMD.

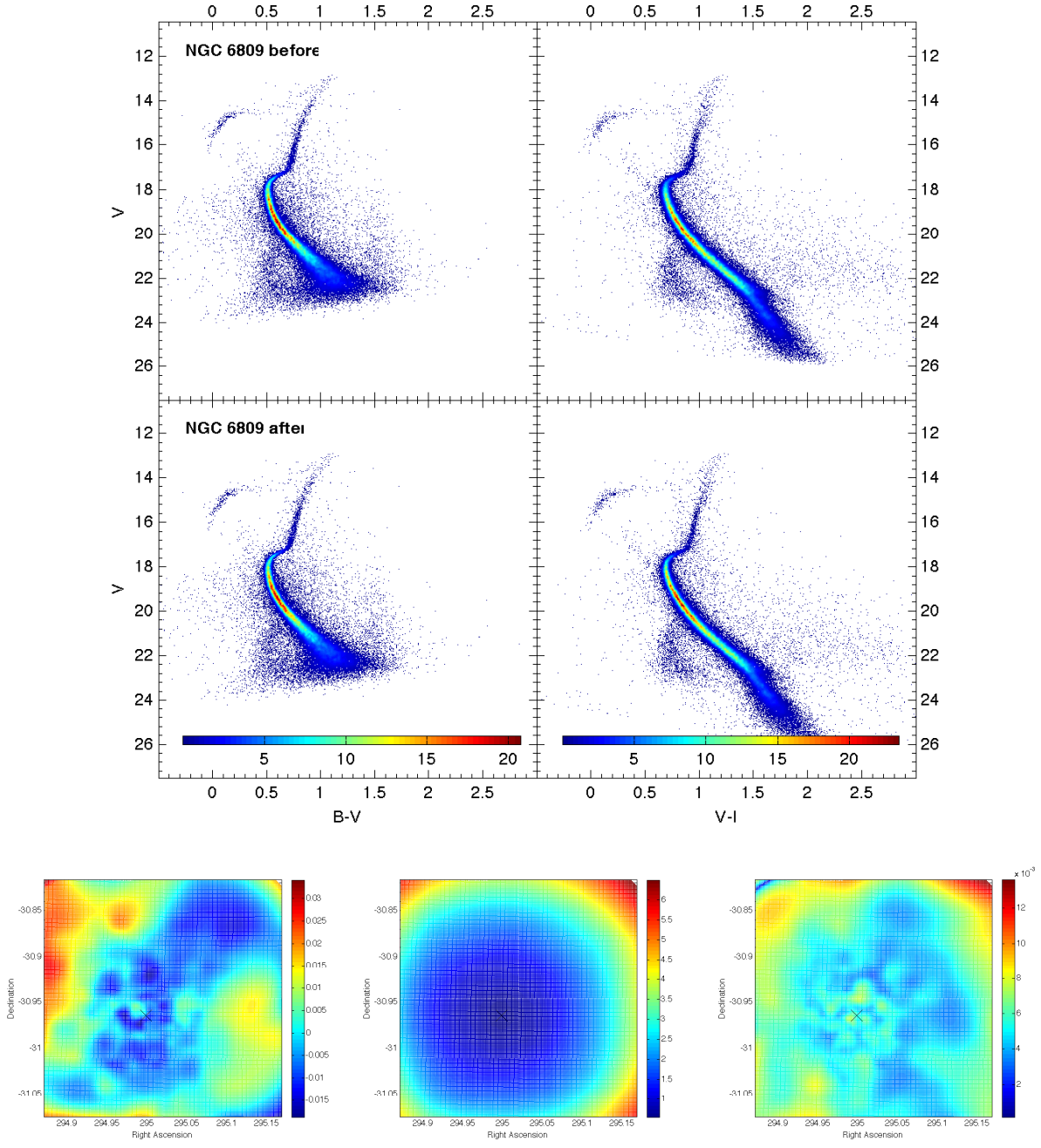

Fig. 31.— As in Figure 7, but for the cluster NGC 6809 - M 55. Only our Magellan photometry was used to build the $B-V$ vs. V CMD. ACS photometry (from project 10775) and Magellan photometry were used to build the $V-I$ vs. V CMD.

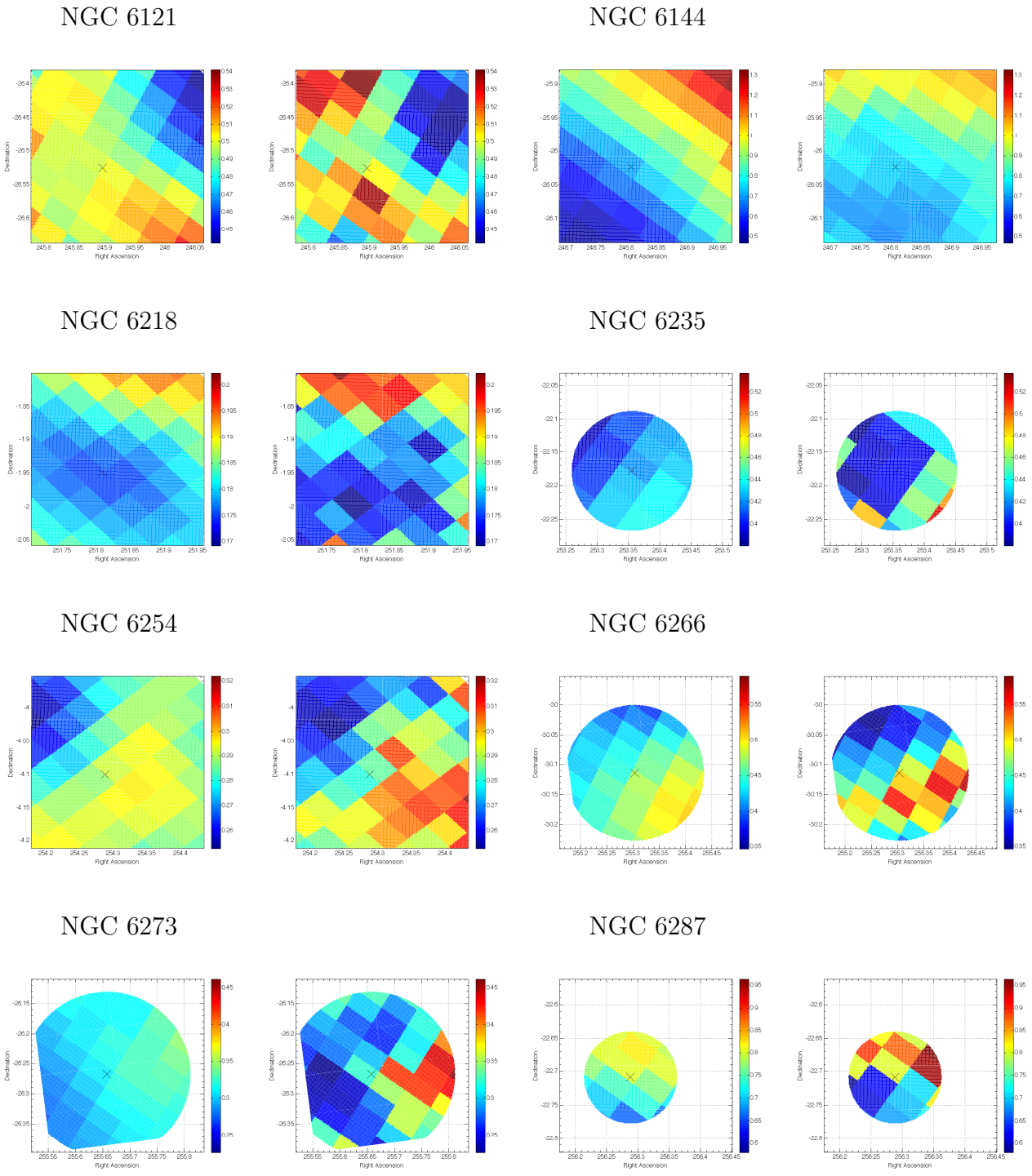

Fig. 32.— Comparison of the E(B-V) extinction maps provided by our technique (left) with the SFD maps (right). We have lowered the resolution of our maps (see text) to compare them more easily with the SFD maps. From the comparison of both maps for every GC we have obtained a reddening zero point for our map, that we have added to facilitate the comparison.

NGC 6304

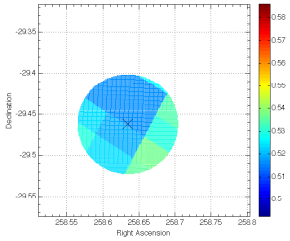
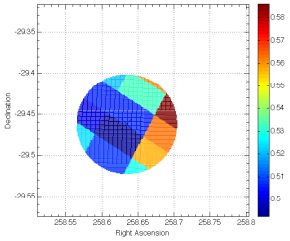

NGC 6333

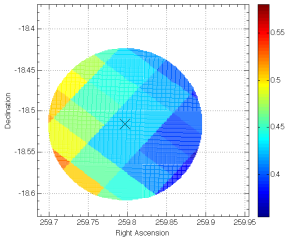
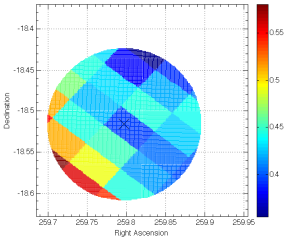

NGC 6342

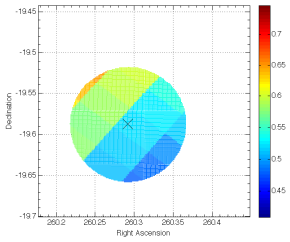
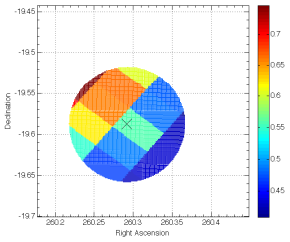

NGC 6352

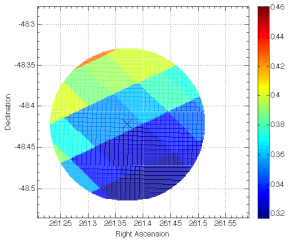
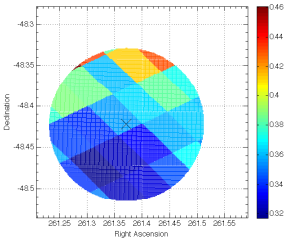

NGC 6355

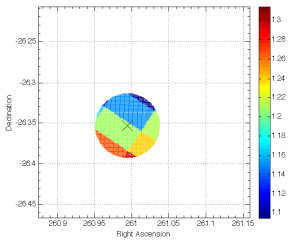
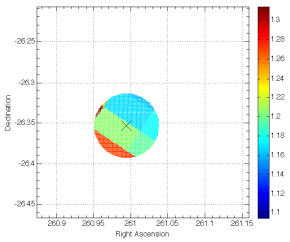

NGC 6397

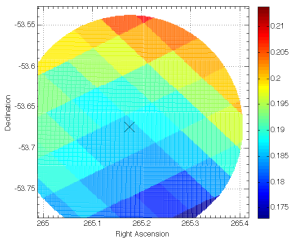
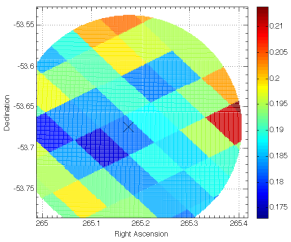

NGC 6522

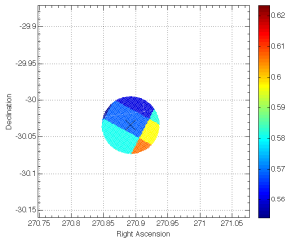
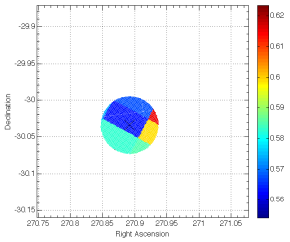

NGC 6541

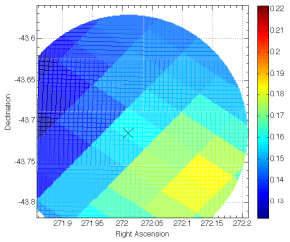
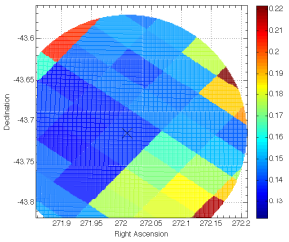

NGC 6553

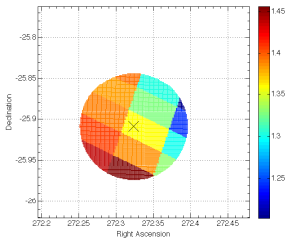
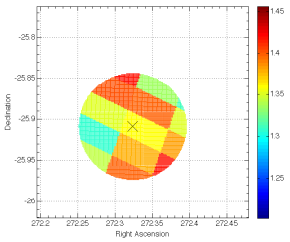

NGC 6558

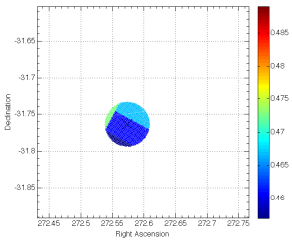
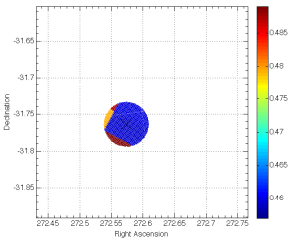

NGC 6624

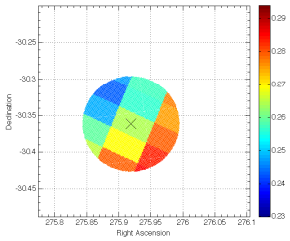

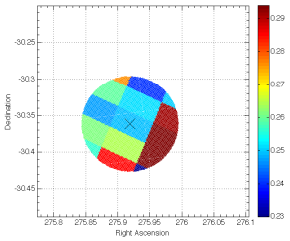

NGC 6626

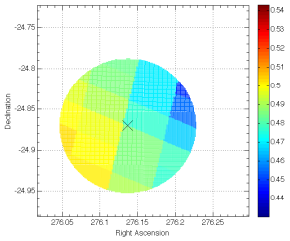

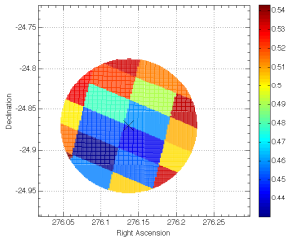

NGC 6637

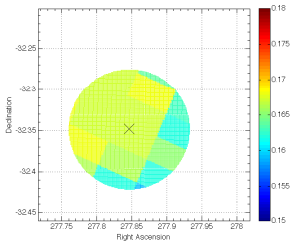

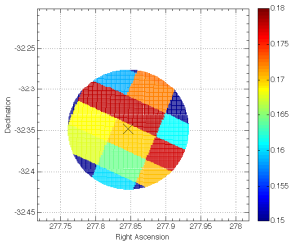

NGC 6642

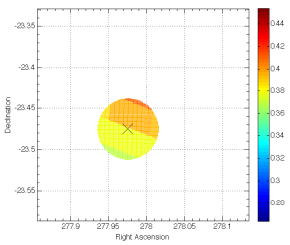

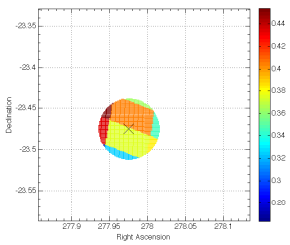

NGC 6656

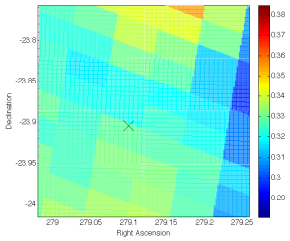

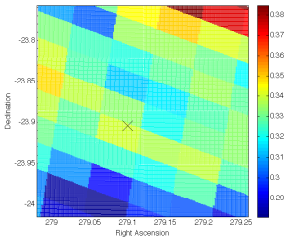

NGC 6681

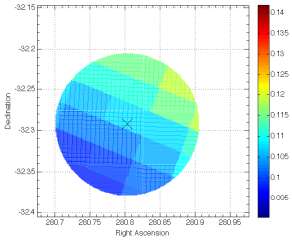

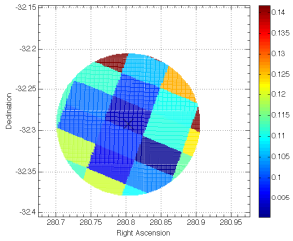

NGC 6809

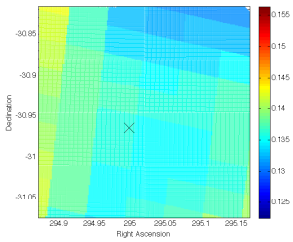

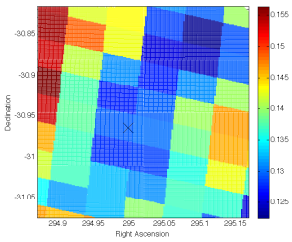

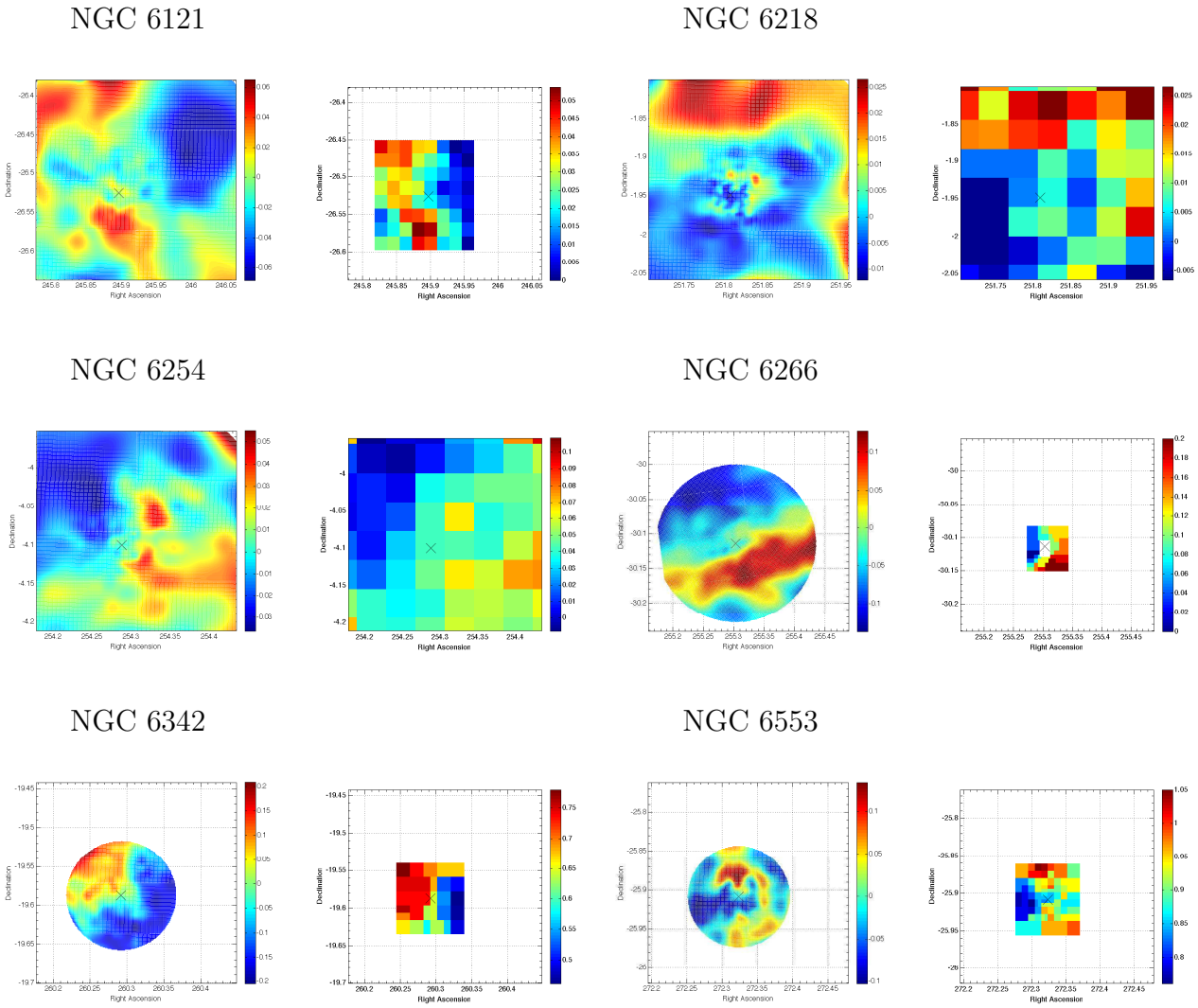

Fig. 33.— Comparison of the E(B-V) extinction maps provided by our technique (left) with the extinction maps (right) provided by Mochejska et al. (2002) for NGC 6121, by von Braun et al. (2002) for NGC 6218 and NGC 6254, by Gerashchenko & Kadla (2004) for NGC 6266, and by Heitsch & Richtler (1999) for NGC 6342 and NGC 6553. All the maps from the literature show relative differential extinctions with respect to the extinction zero point of a fiducial region, except for NGC 6342 and NGC 6553, that show absolute extinctions. Notice that the extinction zero points between our maps and those from the literature can differ.

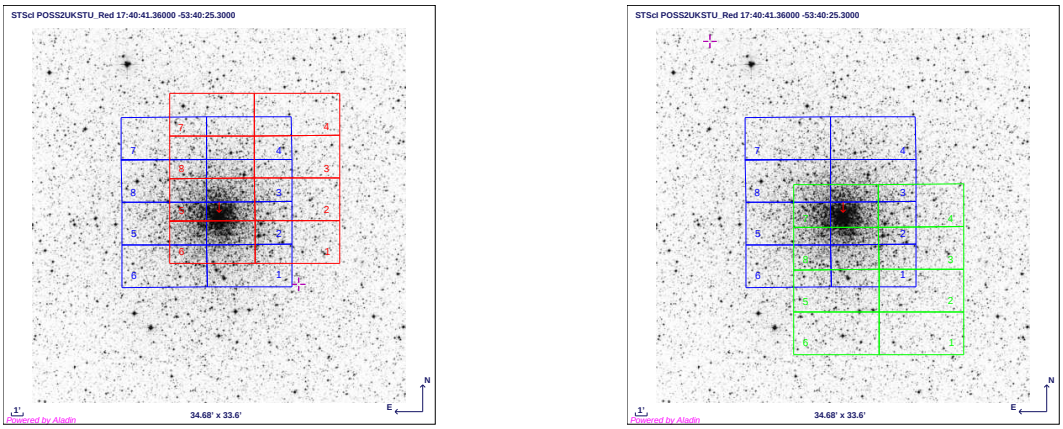

Fig. 34.— Pointings used to make the instrumental calibration, bringing the photometry from the different chips to the chip2 system. We chose these pointings because they allowed us to observe stars in common between chip2 and all the other chips in just 3 pointings (chips 1, 5 and 6 have stars in common with chip 2 in the left configuration and chips 3, 4, 7, and 8 have stars in common with chip2 in the right configuration). We used stars from the cluster NGC6397, one of the clusters in our sample, to do this calibration. The blue pointing was the same as the one originally used in our observing run. That way we were able to compare the photometries of our original observing run and the calibrating run for all the chips in the camera and take care of any effect produced by a change in the sensitivity of the chips (see text).

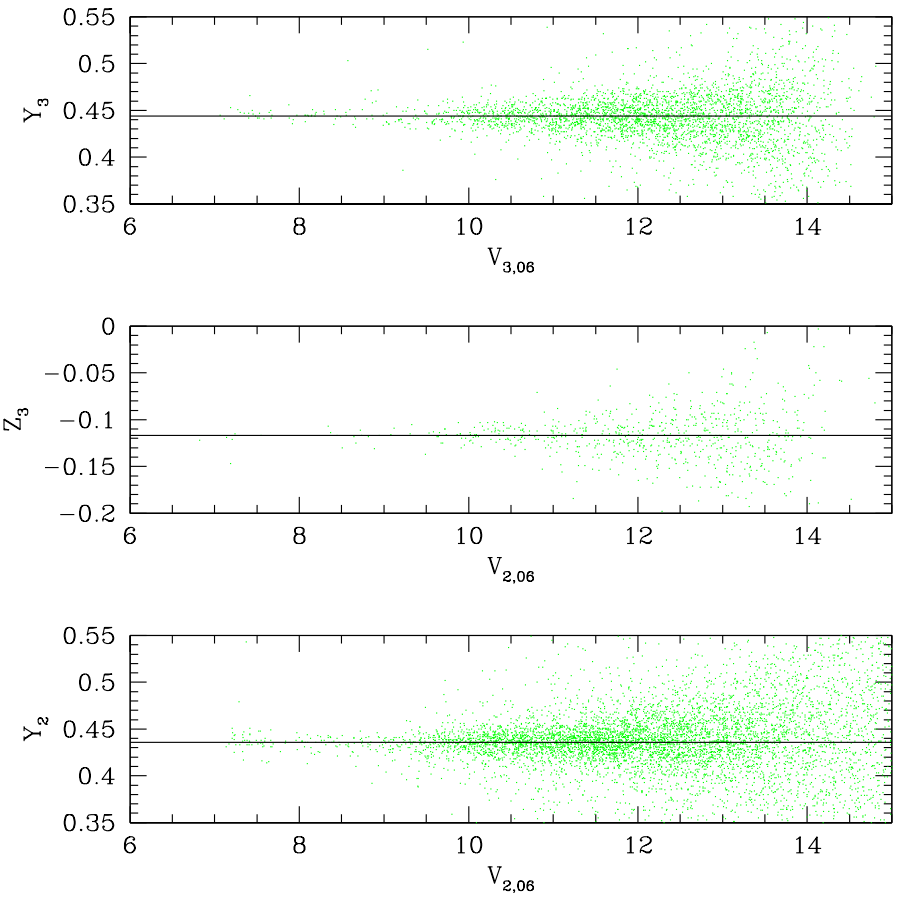

Fig. 35.— Calculation of the zero points to bring the photometry to the chip2 system. In this figure we have plotted, as an example of the technique, the different zero points that we have to obtain to move the V photometry from the chip3 to the chip2 reference system (see equations in the text). The solid lines show the final average values adopted.

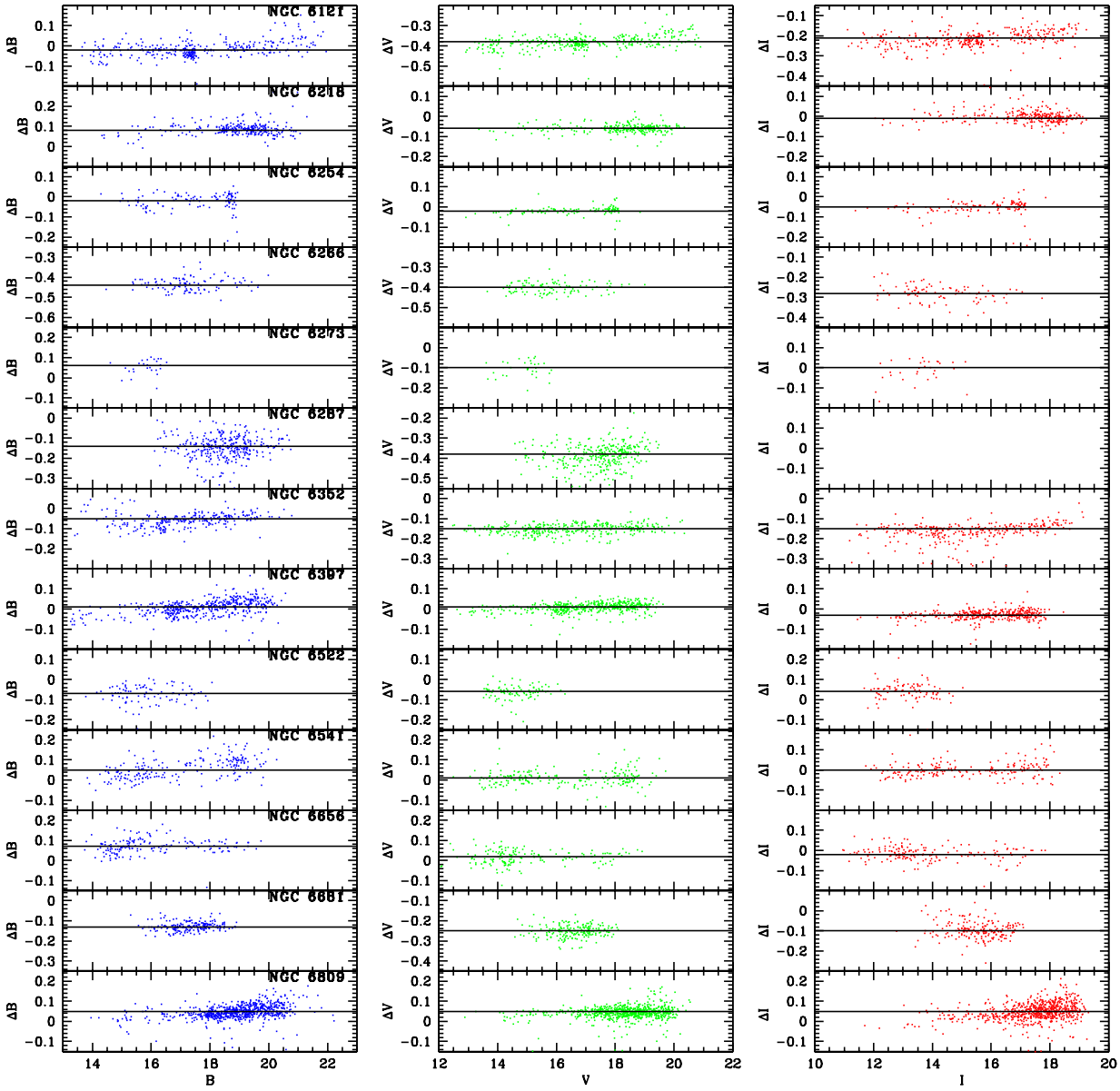

Fig. 36.— Comparison of our raw ground-based photometry with the Stetson (2000) calibrating stars for the clusters and filters available. We plot the magnitudes of the stars in our photometry for the different filters versus Stetson's values minus ours. The lines show where the average offsets lie.

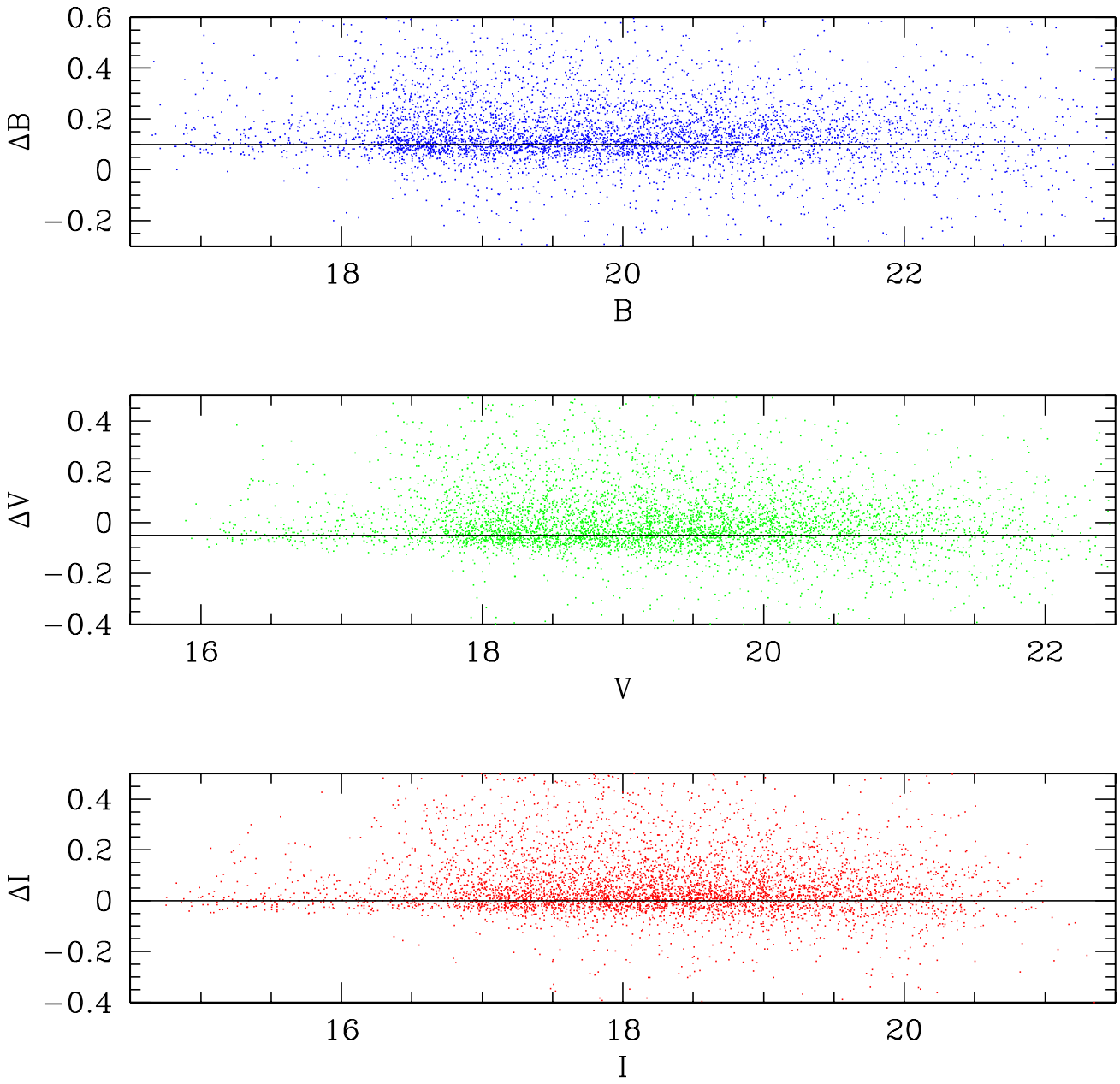

Fig. 37.— Comparison of our raw ground-based photometry with the *HST* photometry. In this figure we show the steps to calculate the offsets in NGC 6218, as an example of the technique. We plot the magnitudes obtained from our ground-based observations versus the *HST* photometry minus our ground-based photometry. We can observe the existence of the spread mentioned and explained in the text. The average offsets, shown by the lines, are calculated using a clipped weighted average (see text).

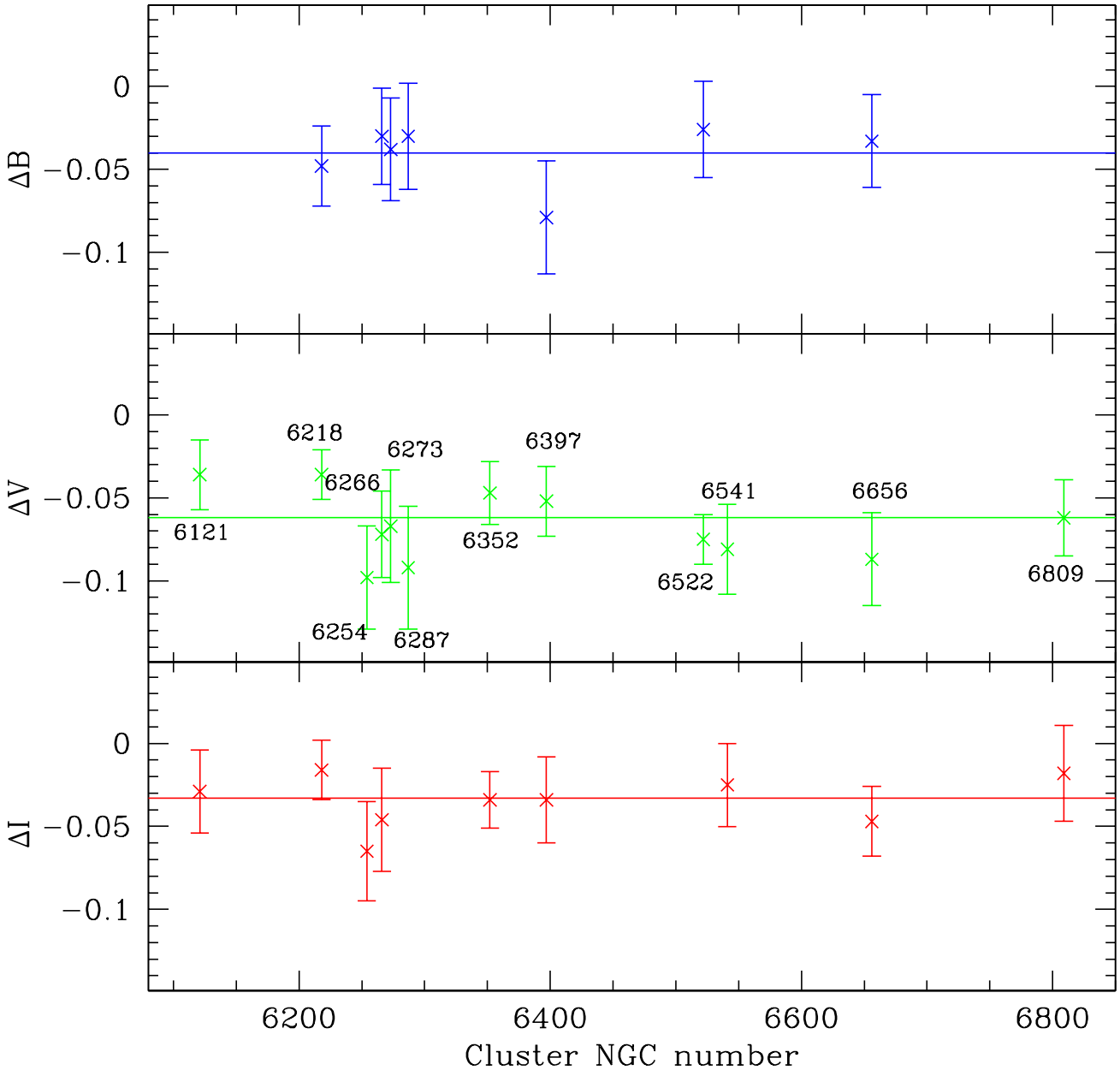

Fig. 38.— Comparison of our photometry corrected with the available *HST* offsets, with the Stetson (2000) calibrating stars. We plot the average differences of Stetson's values minus ours, for every cluster and filter. The lines show the weighted average offsets for every filter.